

L. E. HUGHES

**FLECHT SEASET Program
NRC/EPRI/Westinghouse Report No.8
NUREG/CR-1533
EPRI NP-1460
WCAP-9729**

**ANALYSIS OF THE FLECHT SEASET
UNBLOCKED BUNDLE STEAM COOLING
AND BOILOFF TESTS**

JANUARY 1981

Program Jointly Sponsored by USNRC, EPRI and

Westinghouse Under Contract Number

NRC-04-77-127 and EPRI RP959-1

FLECHT SEASET Program
NRC/EPRI/Westinghouse Report No. 8
NUREG/CR-1533
EPRI NP-1460
WCAP-9729

**ANALYSIS OF THE FLECHT SEASET
UNBLOCKED BUNDLE STEAM COOLING
AND BOILOFF TESTS**

January 1981

S. Wong
L. E. Hochreiter

prepared for
United States Nuclear Regulatory Commission
Washington, DC 20555

Electric Power Research Institute
3412 Hillview Avenue
Palo Alto, California 94303

and

Westinghouse Electric Corporation
Nuclear Energy Systems
P. O. Box 355
Pittsburgh, Pennsylvania 15230

by

Westinghouse Electric Corporation

under

Contract No. NRC-04-77-127, EPRI Project No. RP959-1

Program Management Group
NRC - L. H. Sullivan
EPRI - K. H. Sun
Westinghouse - L. Chajson

LEGAL NOTICE

This report was prepared as an account of work sponsored by the U.S. Nuclear Regulatory Commission, the Electric Power Research Institute, Inc., and the Westinghouse Electric Corporation. Neither the United States government nor any agency thereof, nor the Institute or members thereof, nor the Westinghouse Electric Corporation, nor any of their employees, makes any warranty, expressed or implied, or assumes any legal liability or responsibility for any third party's use or the results of such use of any information, apparatus, product, or process disclosed in this report or represents that its use by such third party would not infringe privately owned rights.

ABSTRACT

A series of forced convection steam cooling tests at low Reynolds numbers and bundle boiloff tests were conducted in the unblocked bundle task of the FLECHT SEASET program. The COBRA-IV-I computer code was utilized to simulate the steam cooling tests, so that the effects of the housing, disconnected heater rods in the bundle, and subchannel mixing were accurately accounted for. After careful data screening, a steady-state forced convection steam cooling heat transfer correlation was developed using the measured heater rod power, heater rod surface temperatures calculated from the measured cladding inner surface temperature by an inverse conduction code, and the vapor temperatures at various subchannels calculated by the COBRA-IV-I code. The new correlation was found to give higher heat transfer than the conventional Dittus-Boelter correlation in the low Reynolds number region. At higher Reynolds numbers, the data begin to merge with the Dittus-Boelter correlation.

The significant data scatter shown by the results of the bundle boiloff tests prevented correlation of the heat transfer data. However, comparisons were made with the Yeh void fraction model; agreement was shown. Comparing the Reynolds and Grashof numbers with other literature indicated that the flow in the rod bundle was always in a forced convection mode even at very low Reynolds numbers, well within the laminar regime.

ACKNOWLEDGMENTS

The authors wish to acknowledge the help of D. P. Kitzmiller in reduction and analysis of the data, and also in development of the data analysis program; K. M. Beatty in development of the data reduction methods; N. Lee with the COBRA code; H. C. Yeh for his analysis of the boiloff void fraction data, and R. P. Vijuk for his review and comments on this report.

TABLE OF CONTENTS

Section	Title	Page
1	INTRODUCTION	1-1
2	TEST DESCRIPTION	2-1
	2-1. Introduction	2-1
	2-2. Test Facility Description	2-1
	2-3. Test Procedure	2-5
	2-4. Test Matrix	2-6
3	DATA REDUCTION	3-1
	3-1. Steam Cooling Tests Data Reduction Methods	3-1
	3-2. Problem Description	3-2
	3-3. Input Data	3-3
	3-4. Hydraulic Diameter	3-3
	3-5. Vapor Physical Properties	3-4
	3-6. Vapor Mass Flow Rate	3-4
	3-7. Wall Heat Flux and Heater Rod Power	3-5
	3-8. Wall Temperature	3-7
	3-9. Vapor Temperature	3-8
	3-10. Geometric Distortion and Bad Instrumentation Locations	3-14
	3-11. Summary of Data Selection Methods and Data Analyzed	3-17
	3-12. Subchannel Mixing and Effects of Unpowered Zone	3-19
	3-13. Boiloff Tests Data Reduction Methods	3-19
	3-14. Data Averaging	3-19
	3-15. Rod-to-Rod Variation of Wall Heat Flux	3-19
	3-16. Determination of Rod Dryout Time and Froth Level	3-22
	3-17. Mass Flow Rate Above Froth Level	3-31
	3-18. Void Fraction	3-34
	3-19. Determination of Froth Level by Pressure Drop Data	3-39

TABLE OF CONTENTS (cont)

Section	Title	Page
4	DATA ANALYSIS AND CORRELATION DEVELOPMENT	4-1
4-1.	Introduction	4-1
4-2.	Comparisons of Rod-Centered Subchannel Energy Balance and COBRA-IV-I-Analysis	4-1
4-3.	Effect of Elevation and Grid Spacers on Heat Transfer for Steam Cooling Tests	4-2
4-4.	Data-Based Heat Transfer Correlation in Rod Bundles	4-2
4-5.	Recommended Correlation for Steam Cooling in Rod Bundles	4-8
4-6.	Effects of Free Convection in Boiloff Tests	4-10
4-7.	Comparison of Void Fraction and Pressure Drop Data With Yeh Void Fraction Correlation	4-11
5	CONCLUSIONS	5-1
5-1.	Steam Cooling Tests	5-1
5-2.	Boiloff Tests	5-1
APPENDIX A	SUMMARY OF DATA SCREENING AND CALCULATED HEAT TRANSFER RESULTS FOR EIGHT STEAM COOLING TESTS	A-1
APPENDIX B	ERROR ANALYSIS OF CALCULATED HEAT TRANSFER RESULTS FOR EIGHT STEAM COOLING TESTS	B-1
APPENDIX C	SUMMARY OF DRYOUT TIMES FOR BOILOFF TESTS	C-1

LIST OF ILLUSTRATIONS

Figure	Title	Page
2-1	Bundle Cross Section	2-2
2-2	Cosine Axial Power Profile	2-3
2-3	FLECHT SEASET Test Configuration (Unblocked Bundle Task)	2-4
3-1	Rod-Centered Subchannel	3-3
3-2	Rise in Wall Temperature at End of Steam Cooling Test (2 sheets)	3-9
3-3	Wall Temperature at Steady State (2 sheets)	3-11
3-4	Comparison of Vapor Temperature Data With Data Calculated by Rod-Centered Subchannel Energy Balance and COBRA-IV-I Code	3-13
3-5	Unpowered Rods in Runs 36160 Through 37170 and Runs 35557 Through 35759	3-15
3-6	Unpowered Rods in Runs 32652 Through 33056	3-16
3-7	FLECHT SEASET 161-Rod Unblocked Bundle Subchannel Simulation by COBRA-IV-I Code	3-18
3-8	Vapor Temperature at Various Subchannels Calculated by COBRA-IV-I Code for Run 36160, 1.52 m (60 in.) Elevation	3-20
3-9	Vapor Mass Flow Rate at Various Subchannels Calculated by COBRA-IV-I Code for Run 36160, 1.52 m (60 in.) Elevation	3-21
3-10	Wall Heat Flux, Run 35557 at 3.05 m (120 in.), 70 Seconds After Beginning of Test	3-23
3-11	Wall Heat Flux, Run 35557 at 3.05 m (120 in.) 145 Seconds After Beginning of Test	3-24
3-12	Wall Heat Flux, Run 35557 at 3.05 m (120 in.), 220 Seconds After Beginning of Test	3-25
3-13	Wall Temperature History, Run 35557, Rod 8E, 2.44 m (96 in.) Elevation	3-26
3-14	Wall Temperature History, Run 35557, Rod 8E, 2.59 m (102 in.) Elevation	3-27
3-15	Dryout Time and Froth Level, Run 35557	3-28

LIST OF ILLUSTRATIONS (cont)

Figure	Title	Page
3-16	Dryout Time and Froth Level, Run 35658	3-29
3-17	Dryout Time and Froth Level, Run 35759	3-30
3-18	Pressure Drop Measurements at Carryover Tank, Run 35557	3-32
3-19	Pressure Drop Measurements at Steam Separator Drain Tank, Run 35557	3-33
3-20	Overall Pressure Drop Data, Run 35557, 0 to 3.05 m (0 to 120 in.)	3-35
3-21	Calculated Mass Flow Rate Above Froth Level, Run 35557	3-36
3-22	Pressure Drop Between 0.61 and 0.91 m (24 and 36 in.), Run 35557, Showing a Quasi-Steady-State Period	3-37
3-23	Pressure Drop Between 2.74 and 3.05 m (108 and 120 in.), Run 35557, Showing No Distinct Quasi-Steady-State Period	3-38
4-1	Comparison of Calculated Nusselt and Reynolds Numbers by Rod-Centered Subchannel Energy Balance and COBRA-IV-I Analysis	4-3
4-2	Effect of Elevation on Heat Transfer, Run 32753	4-4
4-3	Effect of Elevation on Heat Transfer, Run 36160	4-4
4-4	Effect of Elevation on Heat Transfer, Run 36261	4-5
4-5	Effect of Elevation on Heat Transfer, Run 36362	4-5
4-6	Effect of Elevation on Heat Transfer, Run 36463	4-6
4-7	Effect of Elevation on Heat Transfer, Run 36564	4-6
4-8	Effect of Elevation on Heat Transfer, Run 36766	4-7
4-9	Effect of Elevation on Heat Transfer, Run 36867	4-7

LIST OF ILLUSTRATIONS (cont)

Figure	Title	Page
4-10	Data-Based Nusselt Number Versus Reynolds Number for Eight Steam Cooling Tests	4-9
4-11	Effects of Free Convection in Boiloff Tests, Run 35557	4-12
4-12	Effects of Free Convection in Boiloff Tests, Run 35658	4-13
4-13	Effects of Free Convection in Boiloff Tests, Run 35759	4-14
4-14	Comparison of Steady-State Void Fraction Data With Yeh Correlation, Run 35557	4-15
4-15	Comparison of Steady-State Void Fraction Data With Yeh Correlation, Run 35658	4-16
4-16	Comparison of Steady-State Void Fraction Data With Yeh Correlation, Run 35759	4-17
4-17	Comparison of Pressure Drop Data With Yeh Correlation, Run 35557	4-19
4-18	Comparison of Pressure Drop Data With Yeh Correlation, Run 35658	4-20
4-19	Comparison of Pressure Drop Data With Yeh Correlation, Run 35759	4-21

LIST OF TABLES

Table	Title	Page
2-1	FLECHT SEASET Unblocked Bundle Steam Cooling and Boiloff Test Matrix	2-7

SECTION 1

INTRODUCTION

The FLECHT SEASET reflood and natural circulation heat transfer program⁽¹⁾ is designed to provide both experimental and analysis information which is useful for a large-break loss-of-coolant accident (LOCA). However, after the Three Mile Island accident, the FLECHT SEASET program was reexamined to see what additional data and analysis could be obtained from the FLECHT SEASET facilities to examine small-break LOCA situations. Two such areas were identified by the FLECHT SEASET Program Management Group (PMG). They were forced convection steam cooling tests at low Reynolds numbers and bundle boiloff tests. These tests would provide forced convection steam cooling data in rod bundles at low Reynolds numbers and would fill a needed gap in the heat transfer area. A brief review of the literature indicated that no data exist on steam flow through rod bundles at these Reynolds numbers.

The forced convection heat transfer data obtained in the FLECHT SEASET program permitted development of an improved heat transfer correlation for the low Reynolds number region for rod bundle geometries. The data obtained also permitted comparisons of rod bundle geometry data with conventional forced convection heat transfer correlations which have been derived from conventional pipe flow heat transfer experiments.

1. Conway, C. E., et al., "PWR FLECHT Separate Effects and Systems Effects Test (SEASET) Program Plan," NRC/EPRI/Westinghouse-1, December 1977.

SECTION 2

TEST DESCRIPTION

2-1. INTRODUCTION

The FLECHT SEASET unblocked bundle was originally designed as a reflood test facility. With a few minor changes, the facility was converted such that some limited steam cooling tests could be performed. The main limitation on the unblocked test facility was the temperature limit on the heater rod seals, the upper plenum, and associated downstream piping. The temperature limitation of the components limited the maximum vapor temperature in the test to less than 204°C (400°F). This limitation was not necessary for normal reflood tests, since the entrained liquid maintained the downstream components within their temperature limits.

2-2. TEST FACILITY DESCRIPTION

The test facility is described in detail in NRC/EPRI/Westinghouse Report No. 3;⁽¹⁾ a brief description follows.

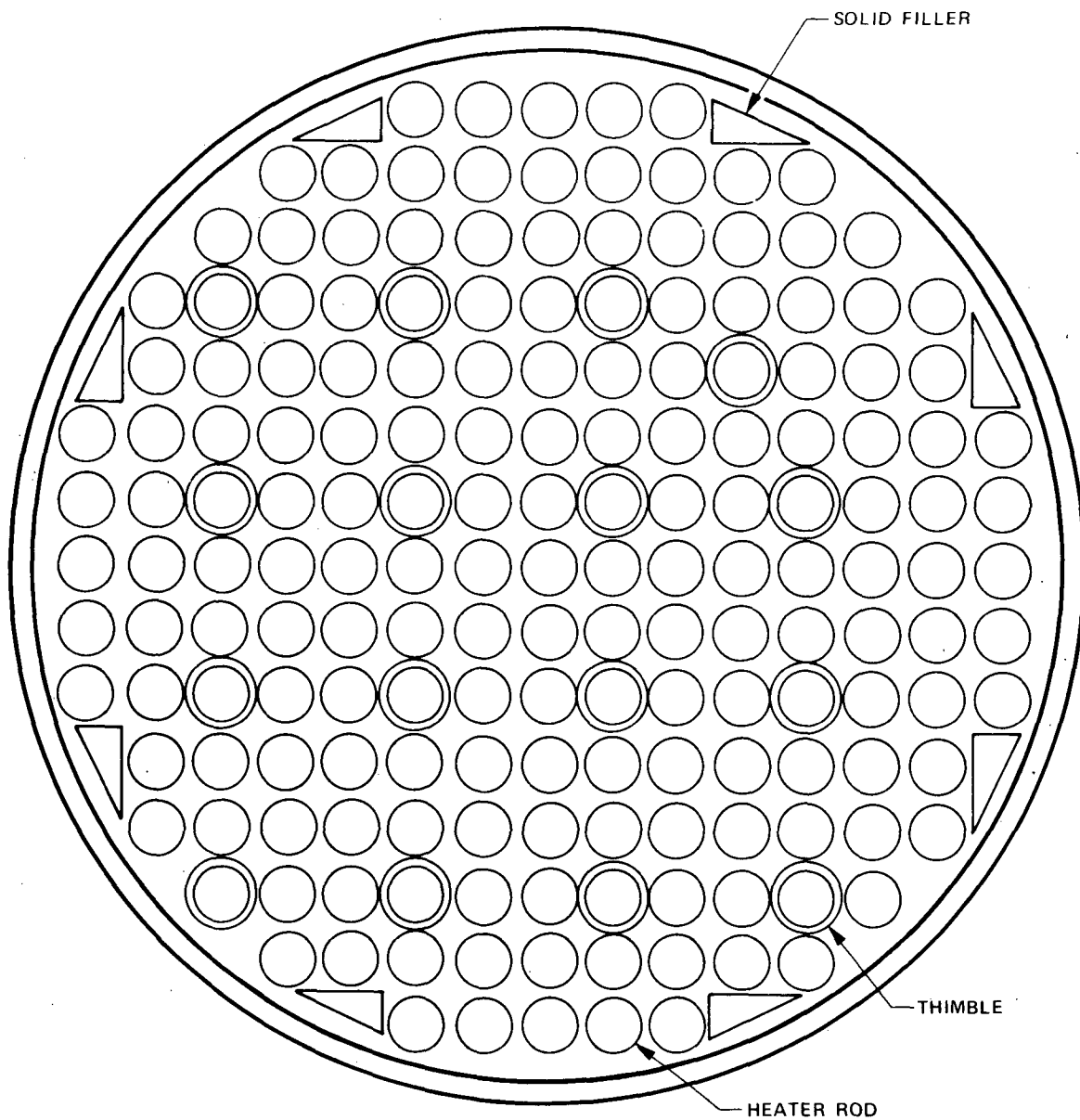
The unblocked test facility is a once-through reflood heat transfer facility which utilizes electrically heated fuel rod simulators arranged on a square pitch to simulate a portion of a PWR fuel assembly. The rod bundle consists of 161 heater rods, 16 guide tube thimbles, and 8 filler rods enclosed in a circular stainless steel housing.

The cross section and dimensions of the rod bundle are shown in figure 2-1. The heater rods used are boron nitride filled, stainless steel clad electrical heaters which utilize a Kanthal heating element to generate a cosine axial power profile. Details of the heater rod design are given in NRC/EPRI/Westinghouse Report No. 3. The heater rods have a 1.66 chopped axial cosine shape (figure 2-2). The tests were run with no radial power gradient so that the flow would be nearly one-dimensional.

The test loop is shown in figure 2-3. The test bundle shown in this figure was configured for reflood tests. The major changes to the facility for the steam cooling tests were as follows:

- The water injection system was isolated from the test bundle inlet plenum.

1. Hochreiter, L. E., et al., "PWR FLECHT SEASET Unblocked Bundle Forced and Gravity Reflood Task: Task Plan Report," NRC/EPRI/Westinghouse-3, March 1978.



BUNDLE STATISTICS

HOUSING INSIDE DIAMETER	194.0 mm	7.625 in.
HOUSING WALL THICKNESS	5.08 mm	0.200 in.
ROD DIAMETER	9.50 mm	0.374 in.
THIMBLE DIAMETER	12.0 mm	0.474 in.
ROD PITCH	12.6 mm	0.496 in.
CROSS-SECTIONAL FLOW AREA	15476 mm ²	23.989 in. ²
FILLER DIMENSIONS	19.43 mm X 8.64 mm	0.765 IN. X 0.340 in.
161 HEATER RODS	-	-
16 THIMBLES	-	-
8 FILLERS	-	-

Figure 2-1. Bundle Cross Section

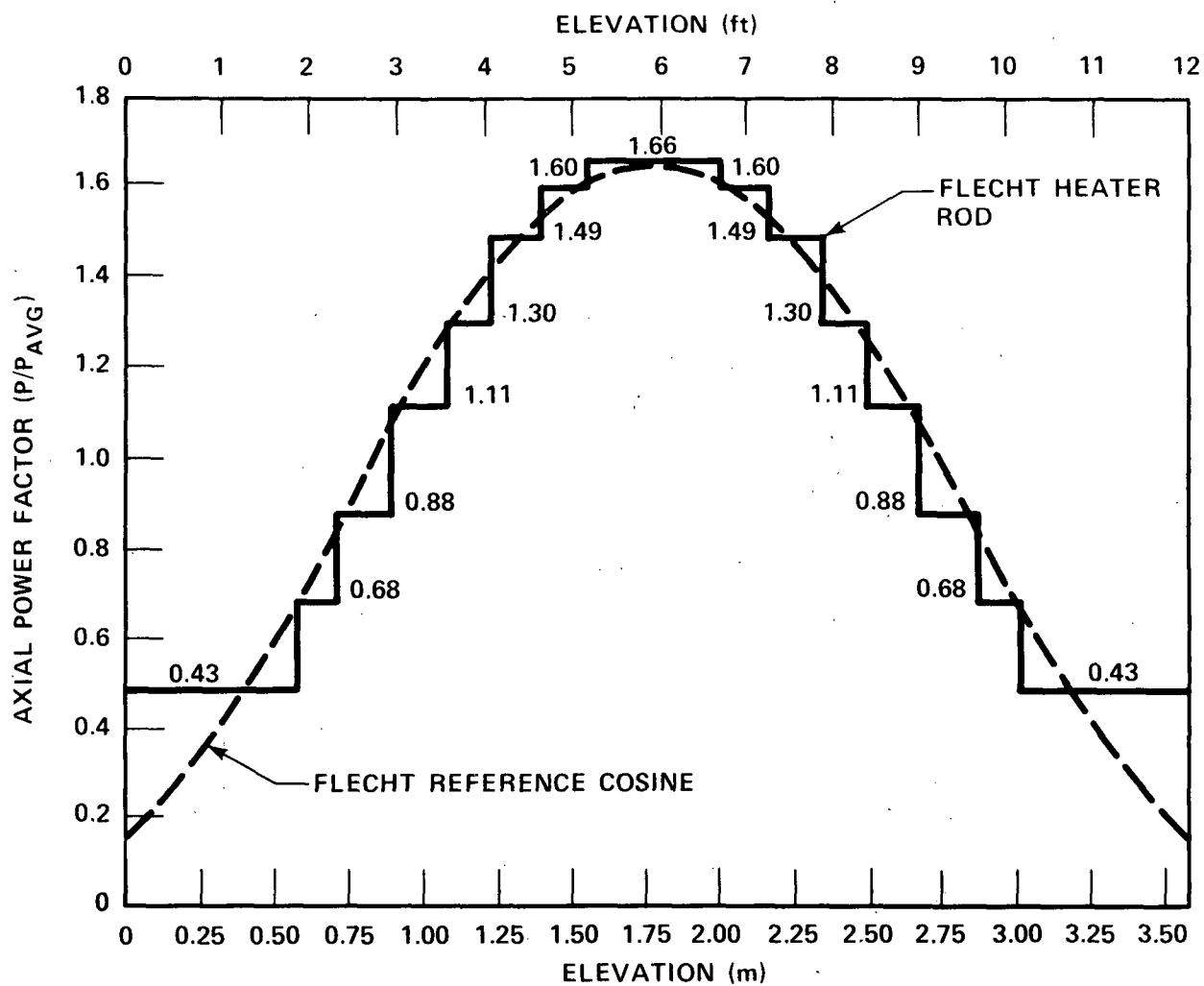


Figure 2-2. Cosine Axial Power Profile

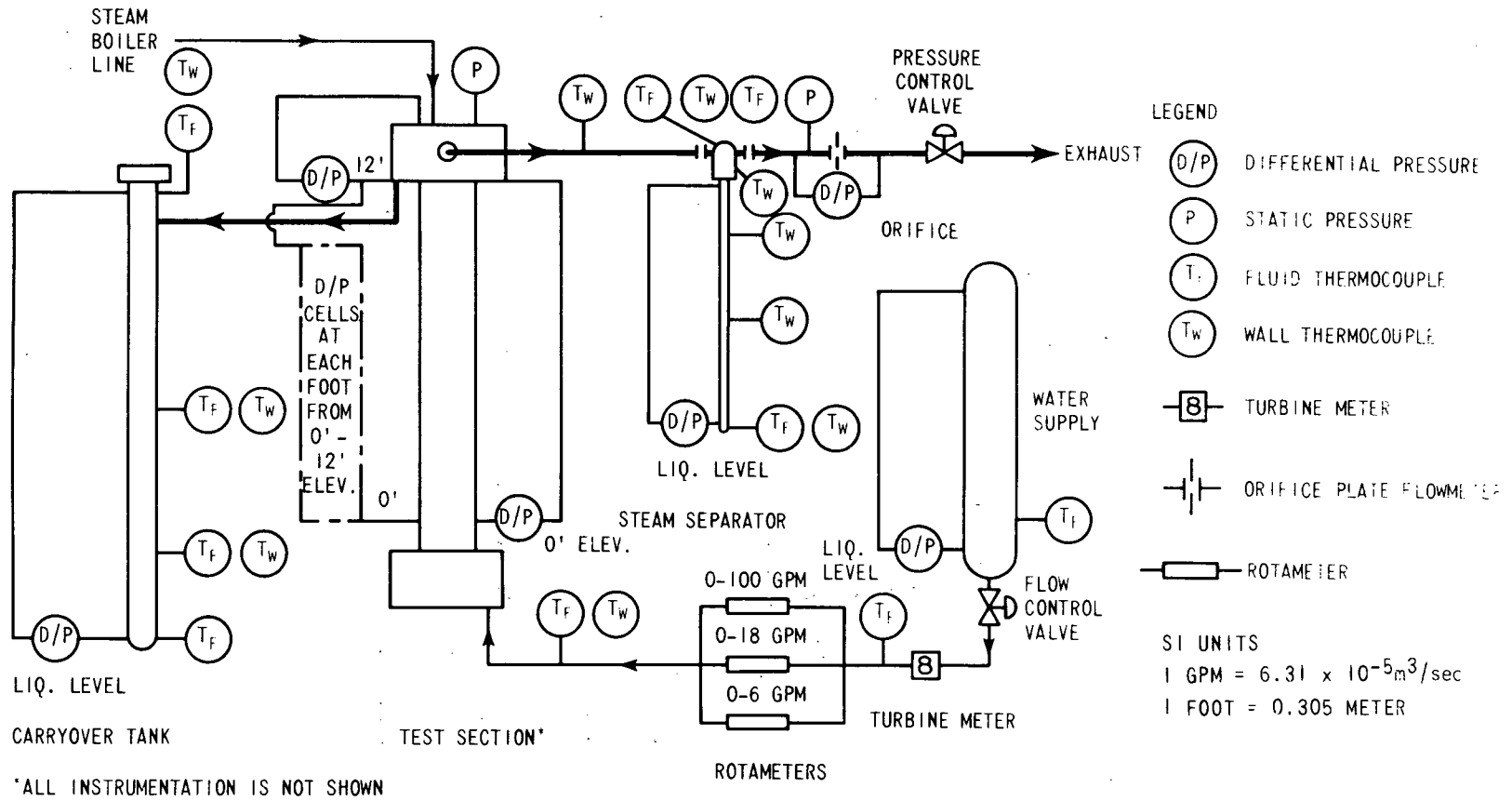


Figure 2-3. FLECHT SEASET Test Configuration (Unblocked Bundle Task)

- A steam line was connected from the steam generator separate effects test facility (described in NRC/EPRI/Westinghouse Report No. 3) to the inlet of the unblocked bundle lower plenum. The steam generator separate effects test facility boiler was capable of a steam flow of about 0.45 kg/sec (3600 lbm/hr) of saturated steam at 0.69 MPa (100 psia).
- After test 33056, all three power zones for the rod bundle were interconnected to one SCR power supply so that more accurate low power measurements could be achieved.
- A thermocouple was placed in a machined hole in the top seal flange of the rod bundle and was connected to a strip chart recorder. This thermocouple gave an indication of the temperature that the heater rod O-ring seals would be exposed to, and was used to help protect the seals from an overtemperature condition. Fluid temperatures in the upper plenum were also recorded to help identify the steam temperature environment to which the seals were exposed.

The facility as constituted for the boiloff tests was very similar to that for the reflood tests (NRC/EPRI/Westinghouse Report No. 3). For these tests, the bundle was pressurized and filled with water at the saturation temperature for the test pressure. Once the bundle had been filled, the accumulator was isolated from the test section. The rod bundle power was then turned on to the preset value and the water in the test section was boiled away. In the boiloff tests, the steam probes which exited the bundle from the bottom were turned off so that no water could escape from the bundle. Only the upper-elevation steam probes were operational.

The instrumentation used in both the steam cooling and boiloff tests was the same as that described in NRC/EPRI/Westinghouse Report No. 3. A total of 256 channels of instrumentation were recorded on the data computer.

2-3. TEST PROCEDURE

The forced convection steam flow tests were initiated by pressurizing and preheating the rod bundle and associated piping with steam from the steam generator separate effects test boiler. Since the boiler produced saturated steam at 0.69 MPa (100 psia), the steam pressure was reduced across a central valve so that slightly superheated steam entered the test section. Once the test section had been heated above the saturation temperature, the rod power was turned on to a preset value and the rods were heated up to steady-state or near-steady-state conditions.

Data were obtained as the rods heated up to the steady-state conditions. The duration of the test was limited by the maximum number of data scans which could be recorded by the data acquisition computer storage disk; tests typically lasted 1400 seconds. As discussed later in this report, 1400 seconds was not always sufficient for a true steady state to be achieved. After the test was complete, the power was turned off. The recorded data were processed onto computer tape, and the power and flow were reset for the next test.

The boiloff test procedure was somewhat similar to that for a reflood test, except that no bundle flooding rate was used. Once the bundle had been filled with saturated water at the test pressure and pressurized, the rod power was turned on to its preset value and the bundle was allowed to boil essentially dry. The rod bundle was protected against overtemperature by setting the screen temperature for the heater rods at 1093°C (2000°F). The tests were then repeated at different bundle pressures.

2-4. TEST MATRIX

The test matrix for the steam cooling and boiloff tests is given in table 2-1. It should be noted that heater rods were disconnected for some of these tests because of rod failures. The loss of these rods was compensated for by increasing the power, to provide a more typical power-to-flow ratio for the experiments.

TABLE 2-1
FLECHT SEASET UNBLOCKED BUNDLE STEAM COOLING AND BOILOFF TEST MATRIX

Run Conditions									
Test No.	Run No.	Upper Plenum Pressure [MPa (psia)]	Rod Initial $T_{wall}^{(a)}$ [$^{\circ}$ C ($^{\circ}$ F)]	Rod Peak Power [kw/m (kw/ft)]	Inlet Flow Rate [kg/sec (lb/sec)]	Coolant Temperature [$^{\circ}$ C ($^{\circ}$ F)]	Inlet Bundle Reynolds Number	Bundle Radial Power Profile	Disconnected Rod Locations
STEAM COOLING TESTS									
52	32652	0.28 (40)	130 (266)	0.023 (0.0071)	0.0472 (0.104)	131 (268)	2212	Uniform	4G, 5G
53	32753	0.28 (40)	135 (275)	0.205 (0.0625)	0.36 (0.80)	132 (269)	17017	Uniform	4G, 5G
54	32854	0.28 (40)	132 (269)	0.0735 (0.0224)	0.14 (0.30)	132 (269)	6382	Uniform	4G, 5G
55	32955	0.28 (40)	131 (268)	0.123 (0.0375)	0.23 (0.50)	131 (268)	10636	Uniform	4G, 5G
56	33056	0.28 (40)	157 (316)	1.6 (0.50)	0.36 (0.80)	132 (269)	17017	Uniform	4G, 5G
60	36160	0.27 (39)	143 (289)	0.16 (0.049)	0.37 (0.81)	144 (292)	16410	Uniform	4G, 5G, 11IJK, 12IJK, 13JK
61	36261	0.27 (39)	140 (283)	0.13 (0.039)	0.297 (0.655)	142 (287)	13349	Uniform	4G, 5G, 11IJK, 12IJK, 13JK
62	36362	0.27 (39)	142 (287)	0.79 (0.024)	0.18 (0.40)	138 (280)	8236	Uniform	4G, 5G, 11IJK, 12IJK, 13JK
63	36463	0.28 (40)	131 (268)	0.479 (0.0146)	0.110 (0.243)	134 (273)	5059	Uniform	4G, 5G, 11IJK, 12IJK, 13JK
64	36564	0.28 (40)	146 (296)	0.039 (0.012)	0.0853 (0.188)	133 (271)	3938	Uniform	4G, 5G, 11IJK, 12IJK, 13JK
65	36665	0.28 (40)	174 (345)	0.03 (0.009)	0.674 (0.148)	131 (267)	3109	Uniform	4G, 5G, 11IJK, 12IJK, 13JK
66	36766	0.28 (40)	180 (356)	0.02 (0.007)	0.054 (0.12)	131 (267)	2521	Uniform	4G, 5G, 11IJK, 12IJK, 13JK
67	36867	0.27 (39)	174 (346)	0.02 (0.006)	0.0531 (0.117)	131 (267)	2458	Uniform	4G, 5G, 11IJK, 12IJK, 13JK
68	Invalid								
69	37069	0.27 (39)	143 (289)	0.059 (0.018)	0.137 (0.303)	131 (267)	6366	Uniform	4G, 5G, 11IJK, 12IJK, 13JK
70	37170	0.28 (40)	131 (268)	0.098 (0.030)	0.230 (0.508)	139 (282)	10447	Uniform	4G, 5G, 11IJK, 12IJK, 13JK

a. Rod location 7J, channel 59, 1.83 m (72 in.) elevation

TABLE 2-1 (cont)
FLECHT SEASET UNBLOCKED BUNDLE STEAM COOLING AND BOILOFF TEST MATRIX

Run Conditions									
Test No.	Run No.	Upper Plenum Pressure [MPa (psia)]	Rod Initial $T_{wall}^{(a)}$ [$^{\circ}$ C ($^{\circ}$ F)]	Rod Peak Power [kw/m (kw/ft)]	Inlet Flow Rate [kg/sec (lb/sec)]	Coolant Temperature [$^{\circ}$ C ($^{\circ}$ F)]	Initial Water Level [m(ft)]	Bundle Radial Power Profile	Disconnected Rod Locations
BOILOFF									
57	35557	0.41 (60)	135 (275)	1.38 (0.422)	0 (0)	139 (281) ^(b)	3.054 (10.02)	Uniform	4G, 5G, 11IJK, 12IJK, 13JK
58	35658	0.14 (20)	104 (220)	1.38 (0.422)	0 (0)	108 (227) ^(b)	3.063 (10.05)	Uniform	4G, 5G, 11IJK, 12IJK, 13JK
59	35759	0.28 (40)	122 (251)	1.38 (0.422)	0 (0)	123 (254) ^(b)	3.00 (9.85)	Uniform	4G, 5G, 11IJK, 12IJK, 13JK

- a. Rod location 7J, channel 59, 1.83 m (72 in.) elevation
b. 1.83 m (72 in.) steam probe temperature

SECTION 3 DATA REDUCTION

3-1. STEAM COOLING TESTS DATA REDUCTION METHODS

The steam cooling tests performed in the 161-rod bundle were much more difficult to analyze than tests performed in a pipe. The effects of the bundle geometry, the relatively cold housing and disconnected heater rods, the mixing and variation of flow and temperature among subchannels, and the rod-to-rod variation of power had to be addressed. The problem was further complicated by the low-flow and low-power conditions of the tests; because the temperature difference between the wall and steam was small, both the wall and steam temperatures had to be determined quite accurately to calculate a reliable heat transfer coefficient or Nusselt number.

Severe bundle distortion was observed⁽¹⁾ from the disassembled bundle after all tests were complete. To ensure that the reduced data were applicable to rod bundle geometry, only data taken from instrumentation locations where the geometry was intact were utilized. Because of the low-flow and low-power conditions of the tests, the change of vapor and wall temperatures during the transients was small. Also, because of the slow rate of change of the wall temperatures, an attempt to use an inverse conduction code to analyze the transient data generally gave undesirable fluctuations in the calculated wall heat flux during the transient period. Reducing the transient data would not expand the range of testing conditions, but would greatly increase the uncertainty of the reduced data. Therefore, transient data were not utilized, and only steady-state data were reduced.

An early attempt to calculate the subchannel vapor temperatures used a rod-centered subchannel energy balance approach. It was found that, because subchannel mixing was neglected, the calculated vapor temperatures were consistently overpredicted. The COBRA-IV-I computer code⁽²⁾ was then used to simulate the steam cooling tests in the 161-rod bundle; the effects of the housing, disconnected rods, and subchannel mixing were correctly accounted for, and the calculated subchannel vapor temperatures were used to calculate the corresponding heat transfer coefficients and to develop a heat transfer correlation.

-
1. Loftus, M. J., et al., "PWR FLECHT SEASET Unblocked Bundle, Forced and Gravity Reflood Task: Data Report," NRC/EPRI/Westinghouse Report No. 7, to be published.
 2. Wheeler, C. L., et al., "COBRA-IV-I: An Interim Version of COBRA for Thermal Hydraulic Analysis of Rod Bundle Nuclear Fuel Elements and Cores," BNWL-1962, March 1976.

Detailed data reduction methods are described below. The reduced data were used to develop a forced convection heat transfer correlation in rod bundles under steady-state steam cooling conditions, as described in section 4.

3-2. Problem Description

The goal of the FLECHT SEASET steam cooling experiments is to develop data-based heat transfer correlations in rod bundles under steady-state conditions. To this end, it is necessary to determine the local Nusselt and Reynolds numbers at various instrumentation locations inside the FLECHT SEASET 161-rod unblocked bundle test section. Namely,

$$Re = \frac{GD_h}{\mu} \quad (3-1)$$

$$Nu = \frac{hD_h}{k} \quad (3-2)$$

where

- Re = vapor Reynolds number
- G = vapor mass flux (kg/m²-sec)
- μ = vapor viscosity (kg/m-sec)
- D_h = hydraulic diameter (ft)
- Nu = Nusselt number
- h = heat transfer coefficient (kw/m²-°K)
- k = vapor conductivity (kw/m²-°K)

The heat transfer coefficient is given by

$$h = \frac{\dot{q}_w''}{T_w - T_v} \quad (3-3)$$

where

\dot{q}_w'' = wall heat flux (kw/m²)

T_w = wall surface temperature (°C)

T_v = vapor temperature (°C)

3-3. Input Data

The methods used to determine G, geometric factors and physical properties (D_h , μ , k), \dot{q}_w'' , T_w , and T_v are described in detail below. The determinations show that, in reduction of the steam cooling data, care has been taken to ensure that the data satisfy steady-state conditions and that the rod bundle geometry was intact in the neighborhood of the instrumentation locations.

3-4. Hydraulic Diameter — The hydraulic diameter is defined by

$$D_h = \frac{4 \text{ (flow area)}}{\text{heated perimeter}} \quad (3-4)$$

In the present analysis, the hydraulic diameter is defined by a rod-centered subchannel (figure 3-1):

$$D_h = \frac{4[\text{pitch}^2 - 0.25 \pi (\text{rod diameter})^2]}{\pi (\text{rod diameter})} \quad (3-5)$$

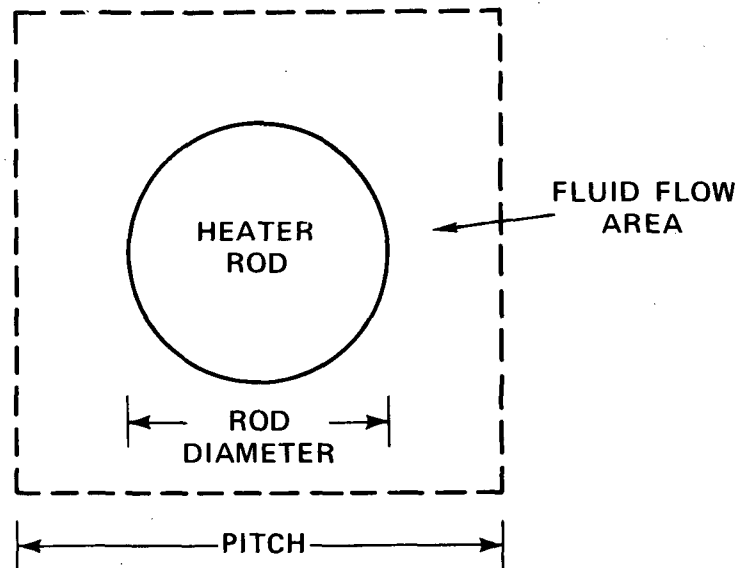


Figure 3-1. Rod-Centered Subchannel

Other definitions are possible (for example, one could define the hydraulic diameter to include the effect of the thimble), but the differences among them are small. It should be noted that the angular position of the heater rod thermocouple within the subchannel is not known. Therefore, throughout the present analysis, the hydraulic diameter defined by equation (3-5) was used.

3-5. Vapor Physical Properties — The vapor physical properties (μ , k) are commonly evaluated at a reference temperature (T_{ref}) which is between the wall and bulk vapor temperature:

$$T_{ref} = \epsilon T_v + (1-\epsilon) T_w \quad (3-6)$$

where

$$0 \leq \epsilon \leq 1$$

In the present steam cooling experiments, the wall to vapor temperature difference is small [typically between 5°C and 28°C (10°F and 50°F)]. Hence it makes little difference how T_{ref} is defined. Throughout the present analysis, ϵ is defined to be 0.5, and T_{ref} is equal to the film temperature.

3-6. Vapor Mass Flow Rate — The total vapor mass flow rate in the bundle test section taken from the vortex meter (located downstream of the boiler) is listed in table 2-1 for all the steady-state steam cooling tests. The vapor mass flows recorded (except for run 36968 where the steam flow was too small to be measured by the vortex meter) were generally very steady and the fluctuations were less than ± 1 percent shortly after the beginning of the tests. Because the steam flow for run 36968 was out of the range of the vortex meter for rate measurement, the data for this run have not been used for developing the heat transfer correlation.

In an early attempt to calculate the Reynolds number and Nusselt number by a rod-centered sub-channel mass and energy balance, the mass flux G was assumed to be constant in the entire bundle test section:

$$G = \frac{\dot{M}_v}{A} \quad (3-7)$$

where

$$\begin{aligned} \dot{M}_v &= \text{test section vapor flow rate (kg/sec)} \\ A &= \text{test section flow area (m}^2\text{)} \end{aligned}$$

In reality, the vapor mass flux was distributed unevenly in different subchannels. The effects of cross flows and subchannel variation of vapor properties were analyzed using the COBRA-IV-I computer code; the subchannel analysis by COBRA is described in more detail in paragraph 3-12.

3-7. Wall Heat Flux and Heater Rod Power — In the present analysis, only steady-state data, for which the heater wall temperature was a constant (see paragraph 3-8), have been analyzed. Under such conditions, the wall heat flux can easily be calculated from the heater rod power:

$$q''_{w} \text{ (i-th rod, } z) = R_i F_{zi} \frac{\bar{q}'}{\pi d} \quad (3-8)$$

where

R_i = ratio of the power of the i-th rod to the average power of the connected (powered) rods in the test section

F_{zi} = axial power factor of the i-th rod at z

\bar{q}' = average linear power (kw/m) of the connected (powered) rods in the test section

d = diameter of heater rod (m)

The average linear power, \bar{q}' , was calculated from

$$\bar{q}' = \frac{P}{NL} \quad (3-9)$$

where

P = steady-state power supply (kw)

N = total number of rods receiving power from P

L = heater rod length (m)

As in the high-temperature reflood experiments, the 159 connected heater rods for runs 32652 through 33056 were grouped into three different power zones. Power for each heater rod group or power zone was supplied by a different SCR (silicon current rectifier) channel. In such cases, P in equation (3-9) was the power supply to the heater rod group of interest, and N was the number of connected heater rods in the group. Also, because of the much lower power density utilized in the low-temperature steam cooling tests than in the high-temperature reflood tests, power readings recorded directly from the SCR channels were not very accurate. Therefore, for runs 32652 through 33056, a more accurate Yew meter was used to measure the power supplied to the three different power zones at the beginning of the tests. However, power data from the SCR channels showed that the steady-state power at the end of the tests was generally slightly different from the power recorded at the beginning of the tests. The Yew meter readings were hence corrected to give a more accurate steady-state power to be used in equation (3-9):

$$P = Y_o \frac{SCR_e}{SCR_o} \quad (3-10)$$

where

Y_o = Yew meter reading recorded at beginning of test (kw)

SCR_o = SCR channel reading recorded at beginning of test (kw)

SCR_e = SCR channel reading recorded at end of test (kw)

In view of the problems encountered in obtaining an accurate power reading for the first five steam cooling tests, a change of test procedure was deemed necessary. For runs 36160 through 37170, only one SCR channel was used to supply electric power to all the 151 connected heater rods in the test section. Because of the much higher power supply when only one channel was used, power readings recorded directly from the SCR channels were accurate and were used in equation (3-9).

For a few of the steam cooling tests, data were taken even after the power supply was turned off. To avoid using these bad data points, the power data from channel 227 were scanned from the beginning of the test to detect any abrupt drop in power. Whenever the power drop was greater than 2 kw/sec, the scanning stopped, and the steady-state power was defined as the average of the previous 50 consecutive power data points (data were taken at 1-second intervals). All the power data have been examined carefully and this criterion was found sufficient to detect all bad data at the end of all steam cooling tests. If the power data were steady throughout the entire test, then the steady-state power was defined to be the average of the last 50 data points of the test. The same time period (50 seconds) was then used to define the steady-state values for other data, such as the heater rod wall temperatures.

Finally, it should be mentioned that the heater rod heat flux calculated by equation (3-8) using steady-state power has been compared to that calculated by the DATARH inverse conduction code. The comparisons were excellent and the differences were less than 2 percent. Also, it was shown in an error analysis (appendix B) that the contribution to the estimated error of the calculated heat transfer coefficient (or Nusselt number) due to the power supply was negligible relative to that due to the temperature measurements. Hence, using the steady-state power to calculate the heater rod heat flux is justified.

3-8. Wall Temperature — At steady-state conditions, the heater rod temperature is a constant. A careful review of the steam cooling heater rod temperature data, however, revealed that for many runs steady-state conditions were not attained. Also, for nearly all the runs, the measured heater rod temperatures for many of the rods at high elevations [2.13 m (84 in.) and above] were still rising steadily at the end of the test (figure 3-2). These plots have a very fine temperature scale; because the data computer resolution is 0.5°C (1°F), step changes in the temperature can be observed in these figures as the rod approaches steady state.

It should also be noted that the typical temperature difference between wall and vapor for the steam cooling tests, depending on elevation, rod power, and mass flow rate, ranged from approximately 5°C to 28°C (10°F to 50°F). A few degrees error in either the wall or vapor temperature can cause a large error in the heat transfer coefficient or Nusselt number given in equations (3-2) and (3-3). This small temperature difference makes the data analysis extremely difficult, and some of the data cannot be used with confidence. Since most of the data at the upper elevations do not reflect steady-state conditions by the end of the test, these data were not used to develop a heat transfer correlation.

Also, the upper-elevation data could have been affected by the bundle geometric distortion between 1.68 and 2.13 m (66 and 84 in.) discussed in paragraph 3-10. Only data below the 1.52 m (60 in.) elevation which satisfied steady-state conditions were used to develop the heat transfer correlation.

Determining whether the heater rod temperatures had attained steady-state conditions required some judgment. Figure 3-2, for example, shows that the wall temperature could remain constant for time intervals of 50 to 100 seconds, but the entire curves show clearly that the wall temperature was still rising. Figure 3-3, on the other hand, shows that the wall temperature had attained steady-state conditions, to within about 0.5°C or 1°C (1°F or 2°F). Note that the data computer resolution is 0.5°C (1°F), hence spikes of 0.5°C (1°F) were observed in the figures. It could be misleading to conclude that the wall temperature was steady when it remained constant for a certain time interval (note that 100 seconds contain 100 data points). All wall temperature data plots were examined carefully, and only those data that behaved similarly to the figure 3-3 data were considered steady-state and were analyzed. Finally, the wall surface temperatures were calculated from the measured cladding inner surface temperatures by an inverse conduction code.

3-9. Vapor Temperature — The vapor temperature can be obtained either from steam probe measurements or from energy balance calculations. Steam probe data are available only at limited elevations and locations. As mentioned before, because of the small temperature difference between the heated walls and the vapor, accurate subchannel vapor temperatures are required for the analysis. The steam probe data were reviewed and found to give lower temperatures than those obtained in the energy balance calculations. In some cases, the steam probe data did not show a consistent axial behavior such that steam temperature at a higher elevation was lower than that at a lower elevation. A possible explanation for this behavior is that condensation became trapped in the steam probe as the bundle was preheated; this condensation wetted the steam probe thermocouple and the interior of the steam probe. Since low superheats were used in the steam cooling tests, it was more difficult to dry out the steam probes in these tests than in the higher-temperature reflood tests. A typical comparison of the steam probe data with the COBRA-IV-I and single-channel energy balance calculations is shown in figure 3-4. Since there was additional uncertainty in the steam probe data because the probes were not perfectly dry, only the energy balance and COBRA-IV-I calculated vapor temperatures were used to analyze the data.

Vapor temperature calculations by rod-centered energy balance are described below COBRA-IV-I analyses are described in paragraph 3-12.

Consider the flow area associated with each rod as defined in figure 3-1. Assuming that the channel is isolated from the surroundings such that no subchannel mixing can occur, the vapor temperature in the channel at an elevation z can readily be calculated from an energy balance:

$$T_v(z) = \frac{\int_0^z \dot{q}'(\xi) d\xi}{GAC_p} + T_o \quad (3-11)$$

RUN 32652
 PRESSURE = 0.28 MPa (40 psia)
 PEAK POWER = 0.023 kw/m (0.0071 kw/ft)
 INLET FLOW RATE = 0.0472 kg/sec (0.104 lb/sec)
 INLET FLOW TEMPERATURE = 131°C (268°F)

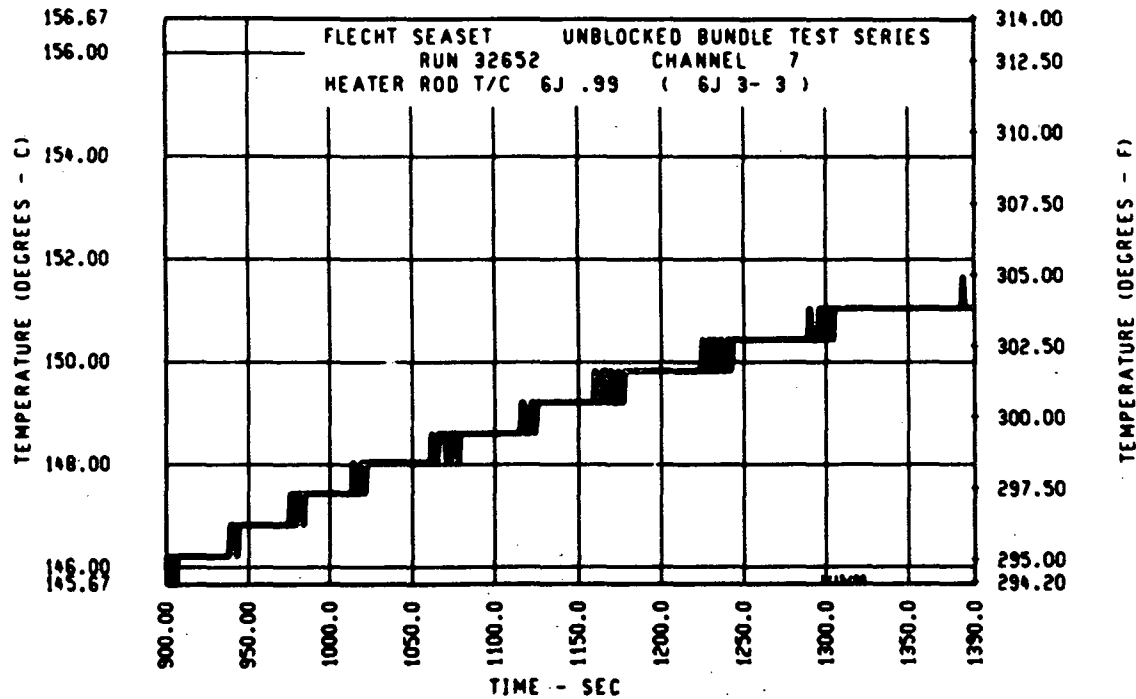


Figure 3-2. Rise in Wall Temperature at End of Steam Cooling Test (sheet 1 of 2)

RUN 32652
 PRESSURE = 0.28 MPa (40 psia)
 PEAK POWER = 0.023 kw/m (0.0071 kw/ft)
 INLET FLOW RATE = 0.0472 kg/sec (0.104 lb/sec)
 INLET FLOW TEMPERATURE = 131°C (268°F)

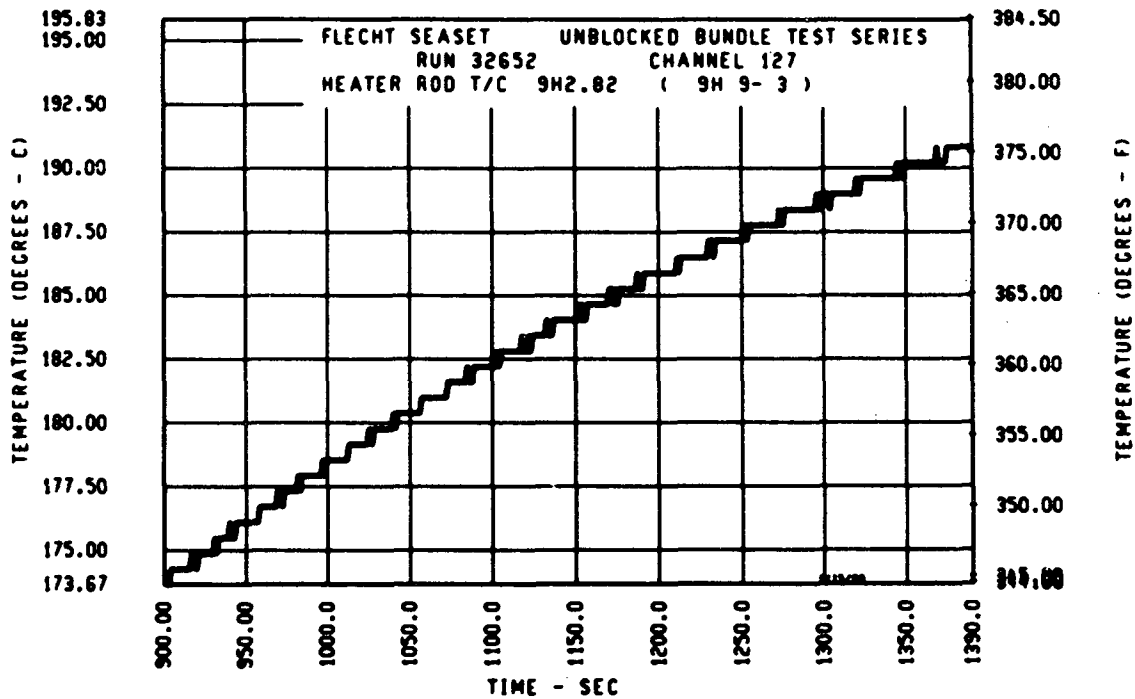


Figure 3-2. Rise in Wall Temperature at End of Steam Cooling Test (sheet 2 of 2)

RUN 36160
PRESSURE = 0.28 MPa (40 psia)
PEAK POWER = 0.16 kw/m (0.049 kw/ft)
INLET FLOW RATE = 0.37 kg/sec (0.81 lb/sec)
INLET FLOW TEMPERATURE = 144°C (292°F)

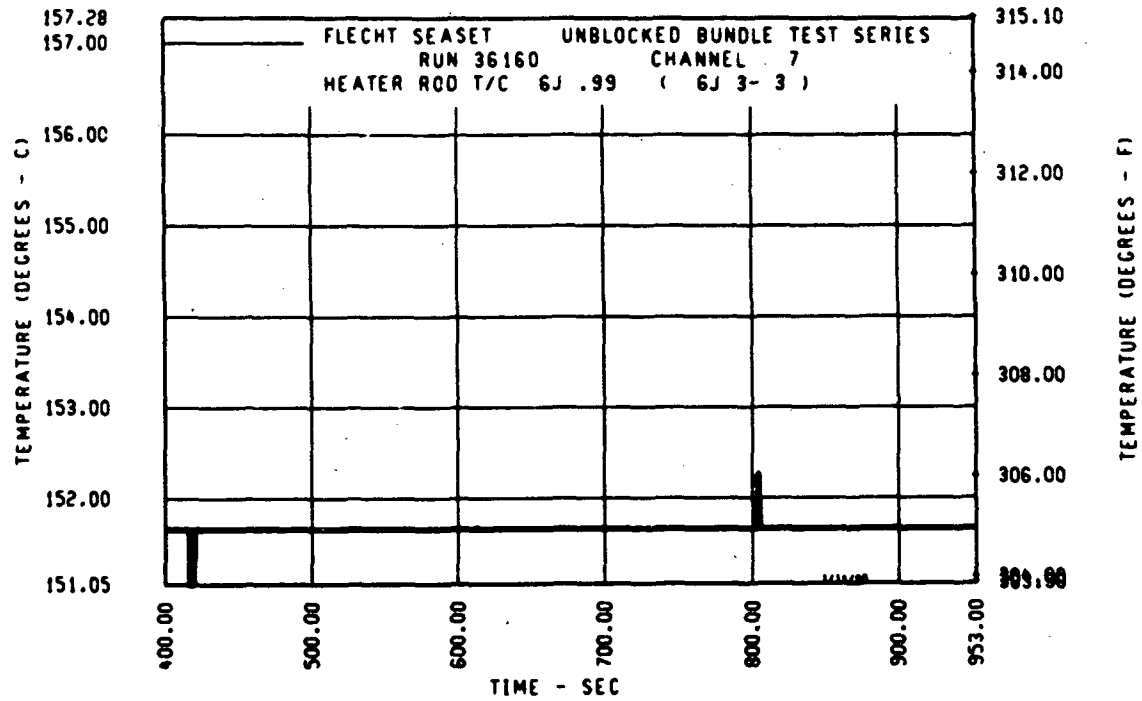


Figure 3-3. Wall Temperature at Steady State (sheet 1 of 2)

RUN 36160
 PRESSURE = 0.28 MPa (40 psia)
 PEAK POWER = 0.16 kw/m (0.049 kw/ft)
 INLET FLOW RATE = 0.37 kg/sec (0.81 lb/sec)
 INLET FLOW TEMPERATURE = 144°C (292°F)

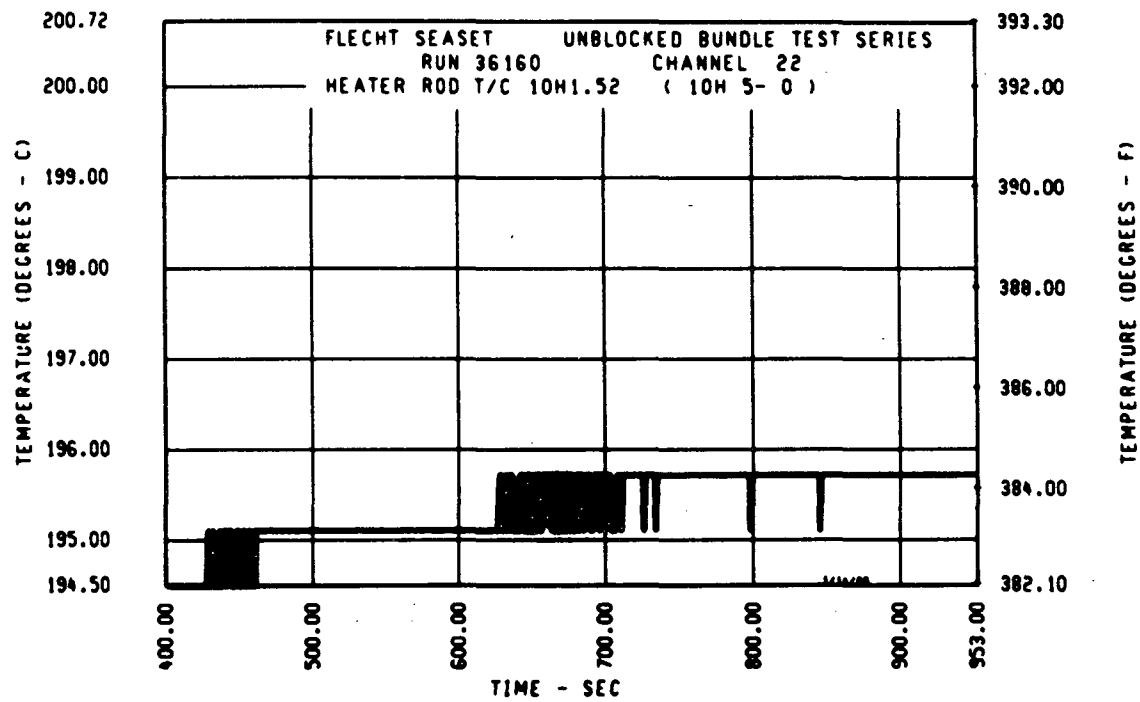


Figure 3-3. Wall Temperature at Steady State (sheet 2 of 2)

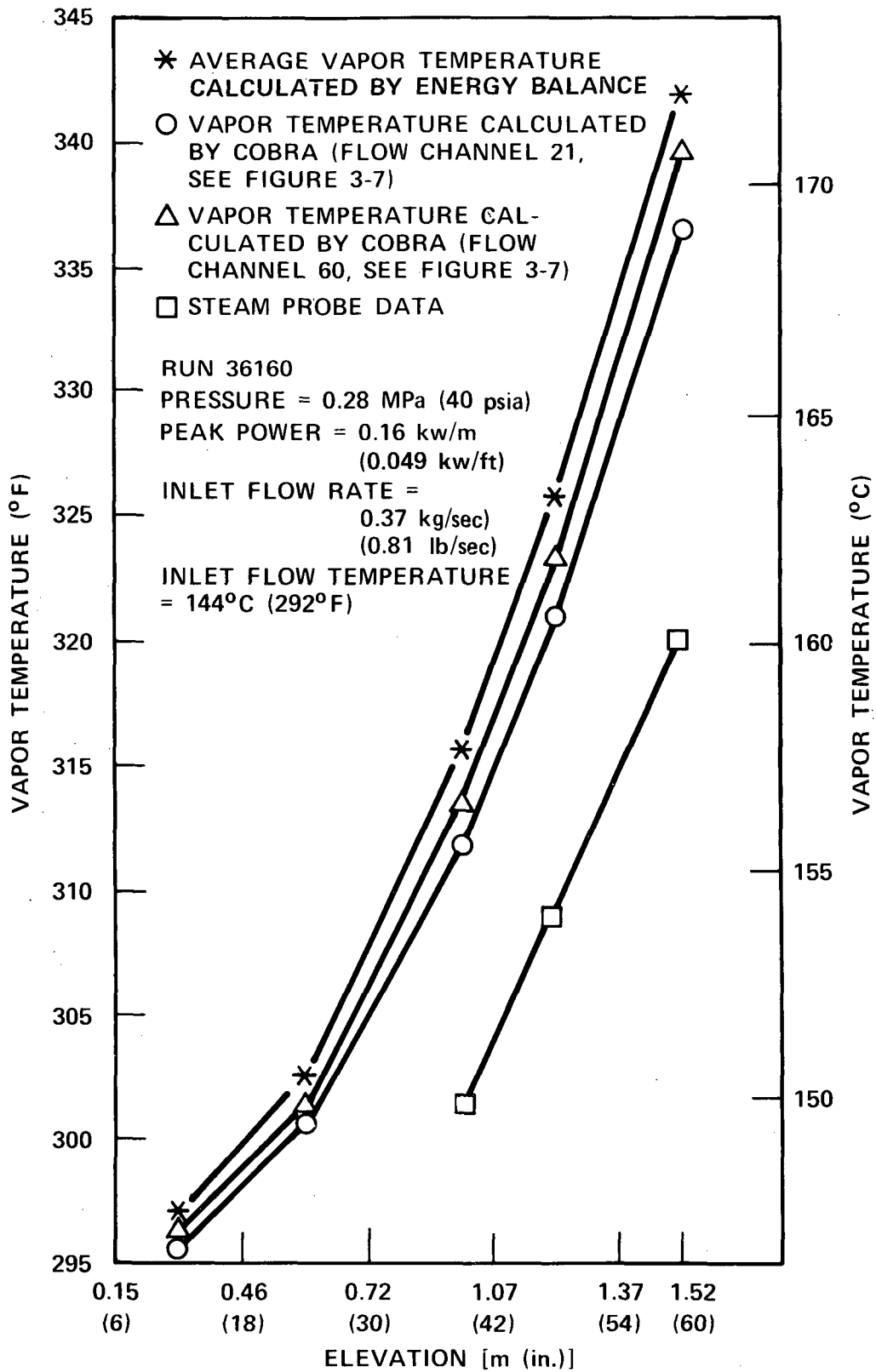


Figure 3-4. Comparison of Vapor Temperature Data With Vapor Temperature Calculated by Rod-Centered Subchannel Energy Balance and COBRA-IV-I Code

where

$T_v(z)$ = vapor temperature in the flow channel at elevation z ($^{\circ}\text{C}$)

\dot{q}' = linear heat generation rate of the heater rod (kw/ft)

G = vapor mass flux in flow channel ($\text{kg}/\text{m}^2\text{-sec}$)

A = flow area of channel (m^2)

C_p = specific heat of vapor at constant pressure of vapor ($\text{kw-sec}/\text{kg-}^{\circ}\text{K}$)

T_o = inlet vapor temperature ($^{\circ}\text{C}$)

The parameters \dot{q}' and G were calculated by methods described above, and the inlet vapor temperature T_o was measured by a fluid thermocouple (channel 221) located at the injection line. Values of T_o are listed in table 2-1 for all the steady-state steam cooling tests. The above calculation has neglected the effects of cross-flow and subchannel mixing. A more accurate local vapor temperature is provided by the COBRA-IV-I computer code, which takes into account the effects of cross-flow and subchannel mixing. The use of the COBRA-IV-I results is described in paragraph 3-12.

3-10. Geometric Distortion and Bad Instrumentation Locations

As mentioned in paragraph 3-2, the goal of the present work is to develop heat transfer correlations in rod bundle geometry. Hence it is essential to ensure that the data used for analysis have been taken from instrumentation locations where the rod bundle geometry is accurately known.

Row-by-row photographs of the rod bundle were taken after all the FLECHT SEASET unblocked tests had been completed. The pictures indicate that the heater rods near the housing were severely bowed because of the bowing of the solid fillers. The data for the heater rods in the first row from the housing have therefore not been used. Photographs of the rod bundles also show heater rod bowing in the interior of the bundle between the 1.68 and 2.13 m (66 and 84 in.) elevations. Since geometric distortion at a lower elevation affects the flow distribution and vapor temperature at a higher elevation, an accurate calculation of vapor temperature at these elevations and above is not possible. Therefore, data taken above the 1.52 m (60 in.) elevation have not been used in the present analysis and correlation development. Also, to avoid the effects of the unpowered rods, heater rods one row from the unpowered rods were not used for analysis. Figures 3-5 and 3-6 show the discarded heater rod data for runs 36160 through 37170 and for runs 32652 through 33056, respectively.

The calculated results (T_v , h , and Nu) were also examined carefully at every instrumentation location. It was found that at three instrumentation locations, the calculated heat transfer coefficients were negative because the calculated vapor temperature was higher than the measured wall temperature; this occurred on the same heater rod for only two tests. Data from these locations for these tests were also excluded from the analysis (see tables A-1 through A-8 in appendix A).

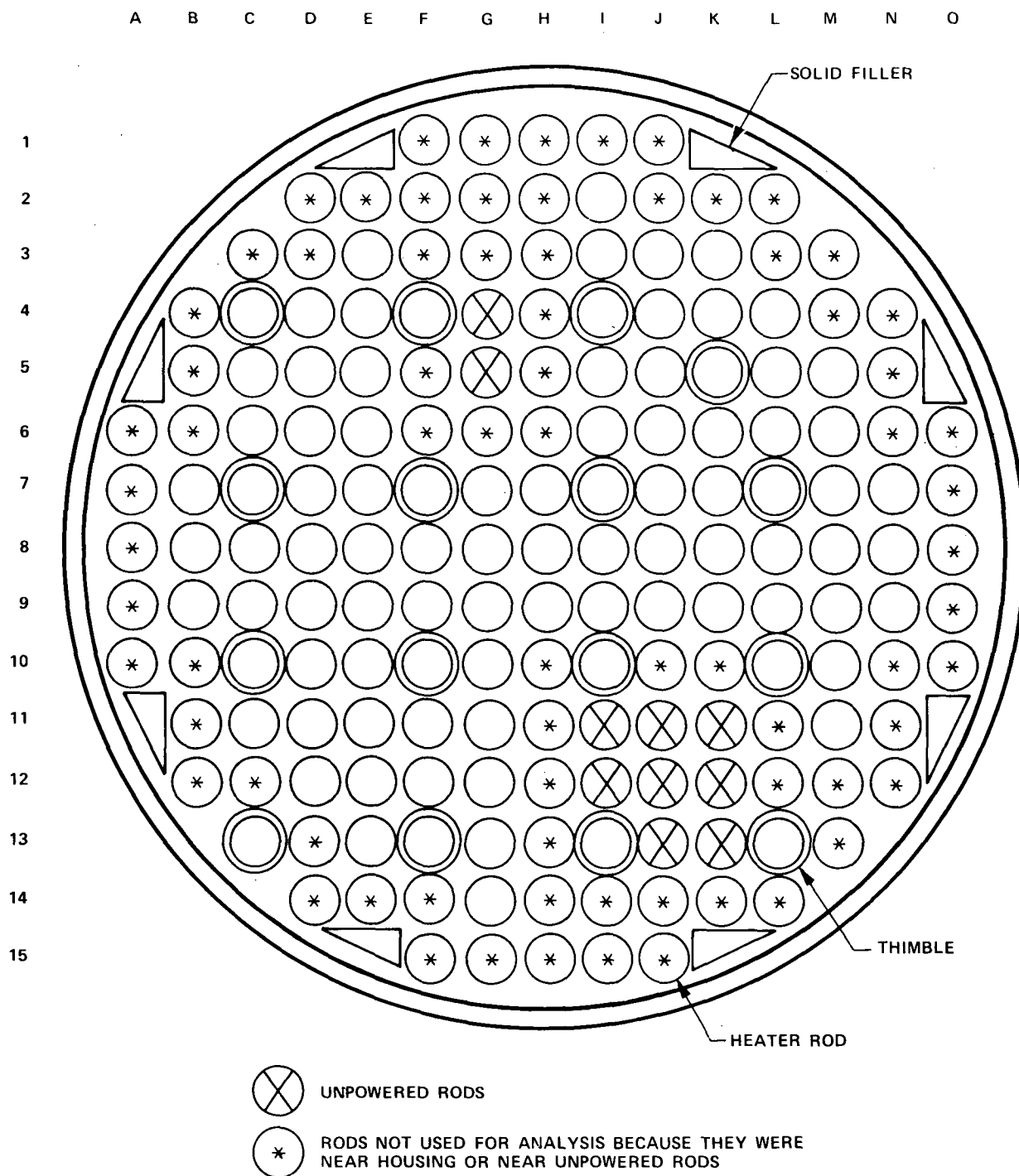


Figure 3-5. Unpowered Rods in Runs 36160 Through 37170 and Runs 35557 Through 35759

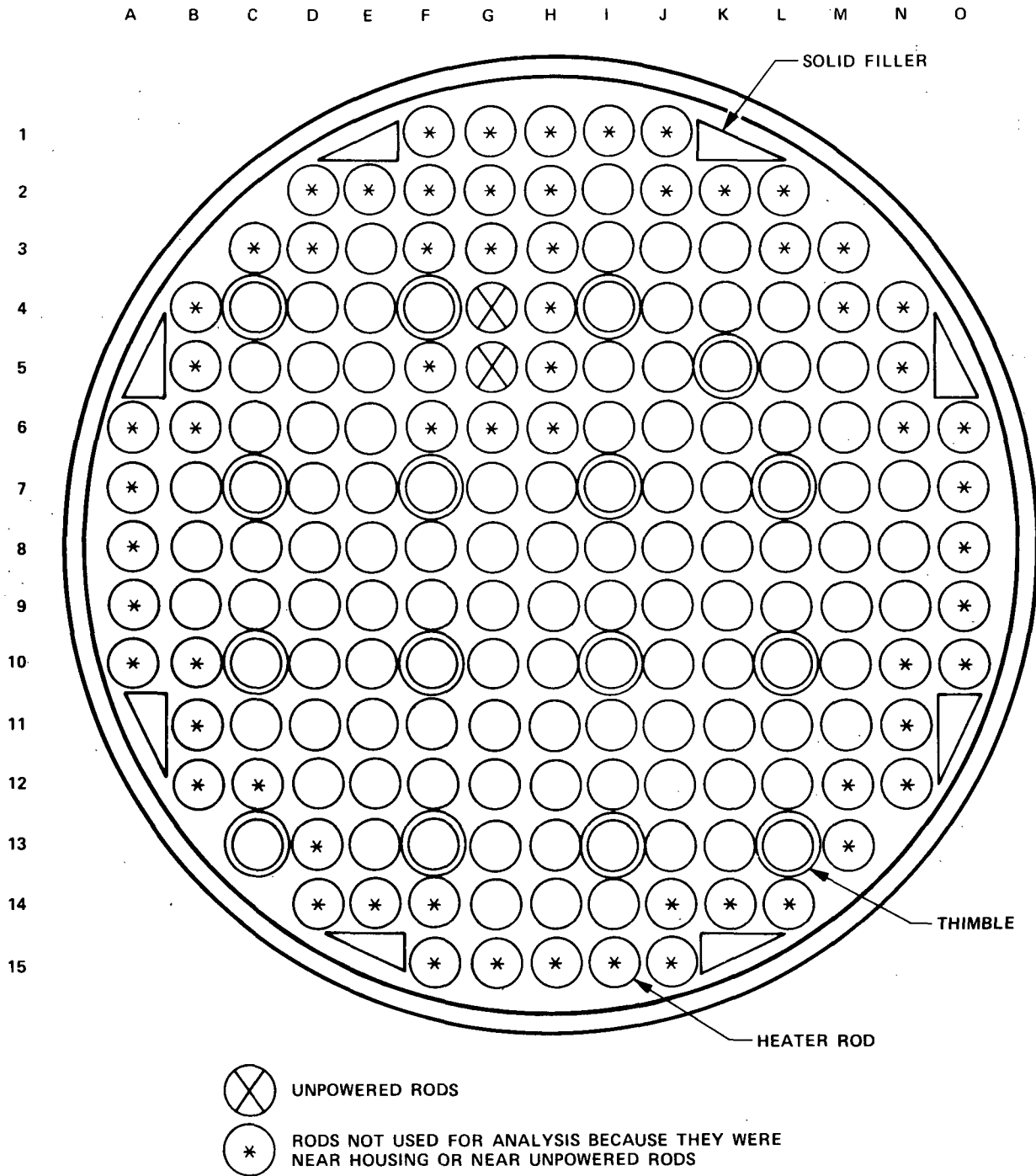


Figure 3-6. Unpowered Rods in Runs 32652 Through 33056

3-11. Summary of Data Selection Methods and Data Analyzed

The previous paragraphs indicate that a significant portion of the steam cooling data was not used in development of the heat transfer correlation. It is worthwhile to summarize the criteria for screening the data:

- Data from heater rods one row from the housing and one row from the unpowered rods were not used. This eliminated the effects of the relatively cold housing and the unpowered zones, and the effects of geometric distortion by the solid fillers.
- Data from above the 1.52 m (60 in.) elevation were not used. The severe geometric distortion of the rod bundles between the 1.68 and 2.13 m (66 and 84 in.) elevations made calculation of the vapor temperature inaccurate. Also, a majority of the heater rod temperatures at these higher elevations had not attained their steady-state values.
- The remaining data were then examined carefully to ensure that steady-state conditions were satisfied. This was done by examining the T_w versus time plots at all instrumentation locations; the wall temperatures that showed a tendency to continue rising were eliminated.
- Finally, the calculated results (T_v , h , and Nu) were examined carefully to detect any instrumentation locations that gave negative heat transfer coefficients (that is, $T_w < T_v$). Data from these locations were not used.

Of the 16 steam cooling tests conducted, seven runs were determined to be unsatisfactory for steady-state calculations (most of the wall temperatures for these runs did not attain steady-state conditions), and one (run 36968) did not have reliable flow rate measurement. Hence only data from the remaining eight runs were used for analysis and correlation development, runs 32753, 36160, 36261, 36362, 36463, 36564, 36766, and 36867. The test conditions for these runs are summarized in table 2-1. The wall temperature data from the 0 to 1.52 m (60 in.) elevations for these runs were examined carefully, and unreliable data were discarded according to the criteria summarized above. Tables A-1 through A-8 in appendix A summarize the data used for development of the heat transfer correlation, and also summarize the reasons for discarding some of the data for each run. The data used to develop the heat transfer correlation are presented in section 4 (and also in table A-9 in appendix A.)

3-12. Subchannel Mixing and Effects of Unpowered Zone

The COBRA-IV-I computer code was used to simulate the steady-state steam cooling tests so that the subchannel mixing and the effect of the unpowered rods could be more accurately accounted for. Figure 3-7 shows the subchannel simulation of the FLECHT SEASET 161-rod unblocked

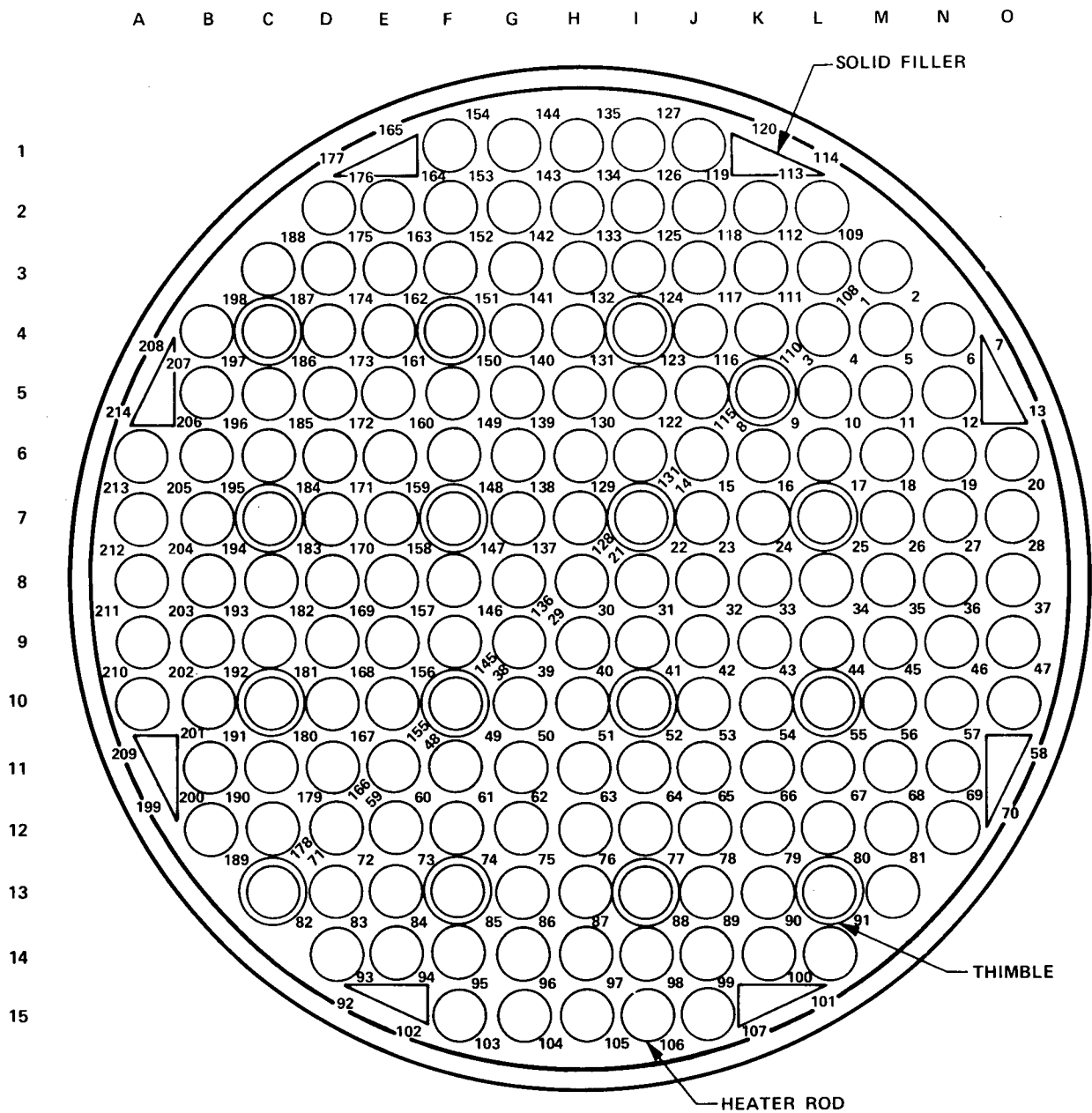


Figure 3-7. FLECHT SEASET 161-Rod Unblocked Bundle Subchannel Simulation by COBRA-IV-I Code

bundle test section by the COBRA-IV-I computer code. The eight steam cooling tests were simulated from the inlet to the 1.52 m (60 in.) elevation. Typical results of subchannel vapor temperatures and mass flow are shown in figures 3-8 and 3-9, respectively. These figures show that, away from the housing and the unpowered rods, the vapor temperatures and vapor mass flow rates are quite uniformly distributed. Thus the effects of the housing and unpowered rods can practically be neglected in subchannels more than one rod row away. Also, the vapor temperatures calculated by the COBRA-IV-I code (figure 3-4) were generally less than those calculated by a rod-centered subchannel energy balance. This is to be expected, since the ratio of the heated perimeter to the flow area for a single rod subchannel (figure 3-1) is bigger than that of the entire bundle cross section because of the presence of the thimble guide tubes, unpowered rods, fillers, and housing.

The local Reynolds and Nusselt numbers were calculated by equations (3-1) through (3-3). The vapor temperature, T_v , and vapor mass flux, G , were taken to be the mean of the vapor temperatures and mass flux in the four COBRA subchannels (figure 3-7) surrounding the particular heater rod. This rod-centered approach is consistent with the single-rod energy balance. The heat transfer results obtained by using the COBRA-IV-I code are shown in section 4 and appendix A.

3-13. BOILOFF TESTS DATA REDUCTION METHODS

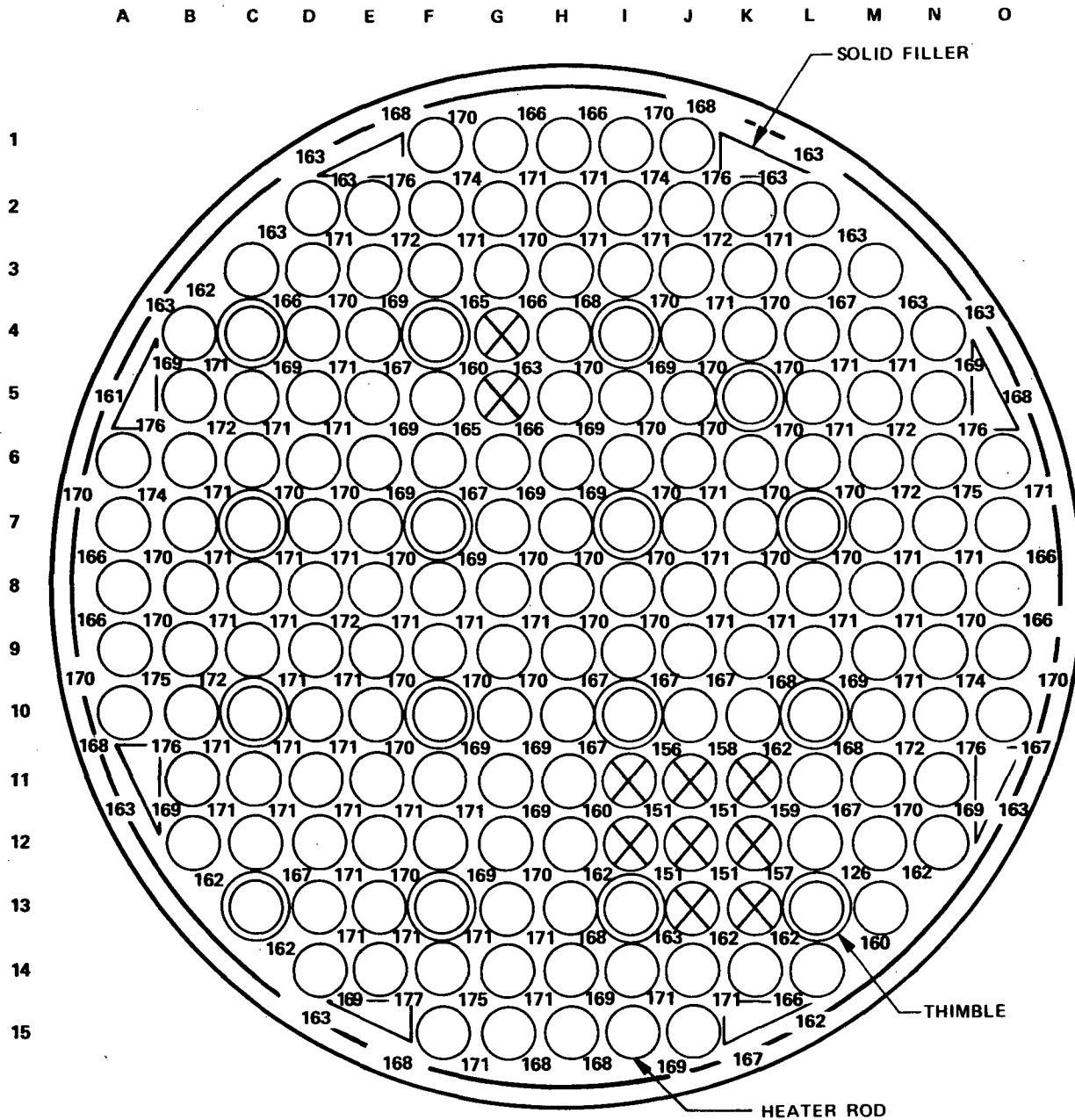
Unlike the steam cooling tests, the boiloff tests were transient experiments. The wall heat flux can no longer be obtained simply from rod power; it can only be calculated by an inverse conduction method and is available only at heater rod thermocouple locations. It is shown below that there was a wide variation in heat flux among heater rods at the same elevation, and that the heat flux on some of the rods was calculated to be negative. Because of the uncertainty in the wall heat flux, an accurate energy balance cannot be performed. Hence for the boiloff tests, neither the vapor temperature nor the heat transfer coefficient has been calculated, and the data from the boiloff tests were not used to develop heat transfer correlations. Only limited data analysis is possible for the boiloff tests; in the following paragraphs, methods to calculate the froth level, the mass flow rate above the froth level, and the void fraction are described. The test conditions for the boiloff tests are summarized in table 2-1.

3-14. Data Averaging

Unless otherwise specified, all transient boiloff data used for analysis were averaged over a 5-second interval to smooth out the random time fluctuation. To be more specific, the data at i seconds were averaged over the interval $i-2.5$ to $i+2.5$ seconds before being used in the analysis.

3-15. Rod-To-Rod Variation of Wall Heat Flux

Very large variation in the wall heat flux calculated by the DATARH inverse conduction code was observed among different heater rods at the same elevation for the boiloff tests. The wall heat flux



UNPOWERED RODS

VAPOR TEMPERATURE IN °C

RUN 36160

PRESSURE

= 0.28 MPa (40 psia)

PEAK POWER

= 0.16 kw/m (0.049 kw/ft)

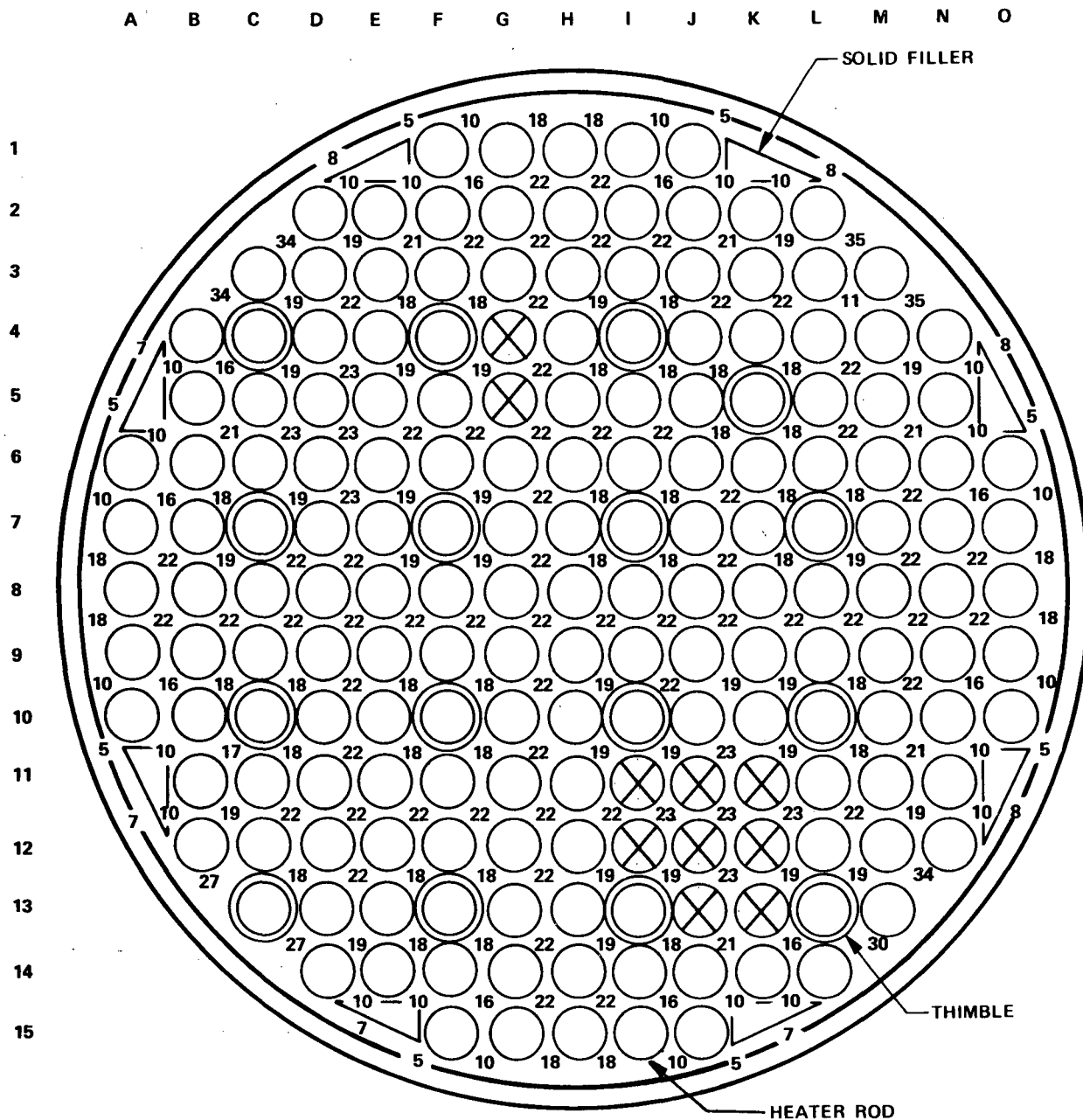
INLET FLOW RATE

= 0.37 kg/sec (0.81 lb/sec)

INLET FLOW TEMPERATURE

= 144°C (292°F)

Figure 3-8. Vapor Temperature at Various Subchannels Calculated by COBRA-IV-I Code for Run 36160, 1.52 m (60 in.) Elevation



 UNPOWERED RODS

VAPOR MASS FLOW RATE IN (kg/sec) $\times 10^4$

RUN 36160

PRESSURE = 0.28 MPa (40 psia)

PEAK POWER = 0.16 kw/m (0.049 kw/ft)

INLET FLOW RATE = 0.37 kg/sec (0.81 lb/sec)

INLET FLOW TEMPERATURE = 144°C (292°F)

Figure 3-9. Vapor Mass Flow Rate at Various Subchannels Calculated by COBRA-IV-1 Code for Run 36160, 1.52 m (60 in.) Elevation

on many of the rods was calculated to be negative, especially at higher elevations, 3.05 m (120 in.) or above. Figures 3-10 through 3-12 show typical wall heat flux values across the rod bundles at various times during the boiloff tests. The approximate froth level at these times is also given for reference. A possible explanation for the existence of such wide variation and negative heat flux is the rod bundle geometry distortion described in paragraph 3-10.

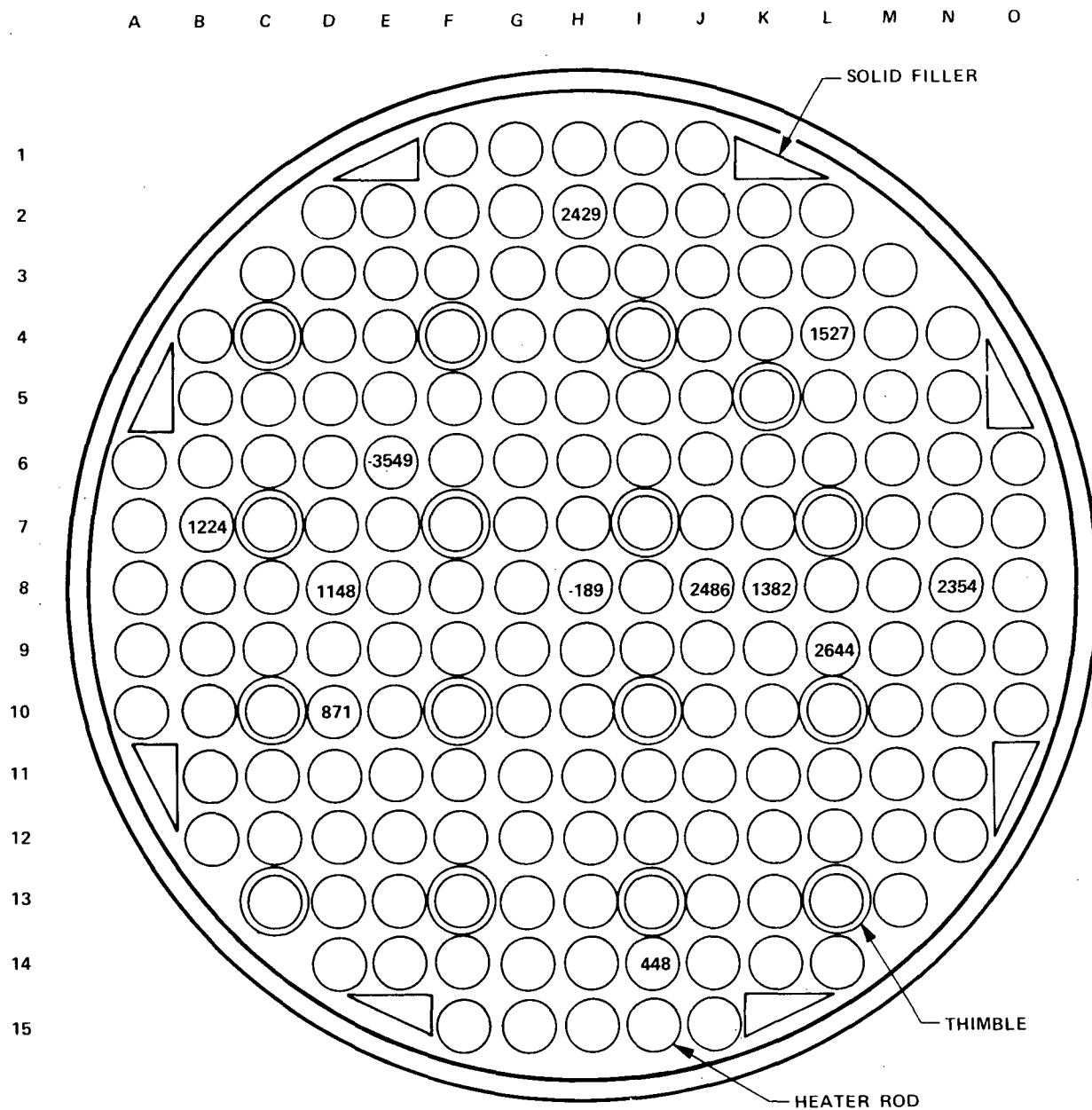
3-16. Determination of Rod Dryout Time and Froth Level

The dryout time at a particular thermocouple location can be obtained easily by observing the wall temperature time history, such as that shown in figures 3-13 and 3-14. The wall temperatures were not time-averaged for these calculations. Estimated froth level versus time curves for each of the three boiloff tests are shown in figures 3-15 through 3-17; they were obtained as follows:

- (1) The dryout time at each instrumentation location was obtained from the wall temperature time history.
- (2) The average dryout time at a certain elevation was taken to be the arithmetic mean of the dryout times obtained from available thermocouple locations at the same elevation.
- (3) The froth level during the boiloff test was then estimated by drawing a smooth curve through the dryout time results obtained above.

A computer program (BOILOFF) was developed to perform the above calculations. Only data between the 0.99 and 3.05 m (39 and 120 in.) elevations were used. Below the 0.99 m (39 in.) elevation, the wall temperatures were generally quenched throughout the entire test; above the 3.05 m (120 in.) elevation, the wall temperature data showed occasional oscillations near the dryout time. The oscillations made the calculations inaccurate. As in the steam cooling tests, data from heater rods near the housing and unpowered rods were not used (figure 3-5). The criterion used to determine the dryout time at each instrumentation location was that the wall temperature must rise at a rate of at least 1.6°C (3°F) per second for at least 10 consecutive seconds; this criterion was found to work well for all three boil-off tests. Tables of the calculated dryout times at each instrumentation locations can be found in appendix C.

As shown in figures 3-15 through 3-17, the froth level at higher elevations (or early in time) is not very well defined. In fact, early in time, wall temperature data show that the dryout time of a rod at a particular elevation could be earlier than the dryout time of the same rod at a higher elevation. An example is given in figures 3-13 and 3-14; the wall temperature data show that the 2.44 m (96 in.) elevation of rod 8E had a dryout time about 4 seconds less than the 2.59 m (102 in.) elevation of the same rod. This phenomenon is even more apparent when the dryout times for different rods are compared [for example, the dryout times at 2.59 m (102 in.) for runs 35557 and 35759 in figures 3-15 and 3-17 respectively, and at 2.13 m (84 in.) for run 35658 in figure 3-16]. An explanation for this observation is that the spacer grids in the bundle may still be wet even after uncover.



← HEAT FLUX IN w/m^2

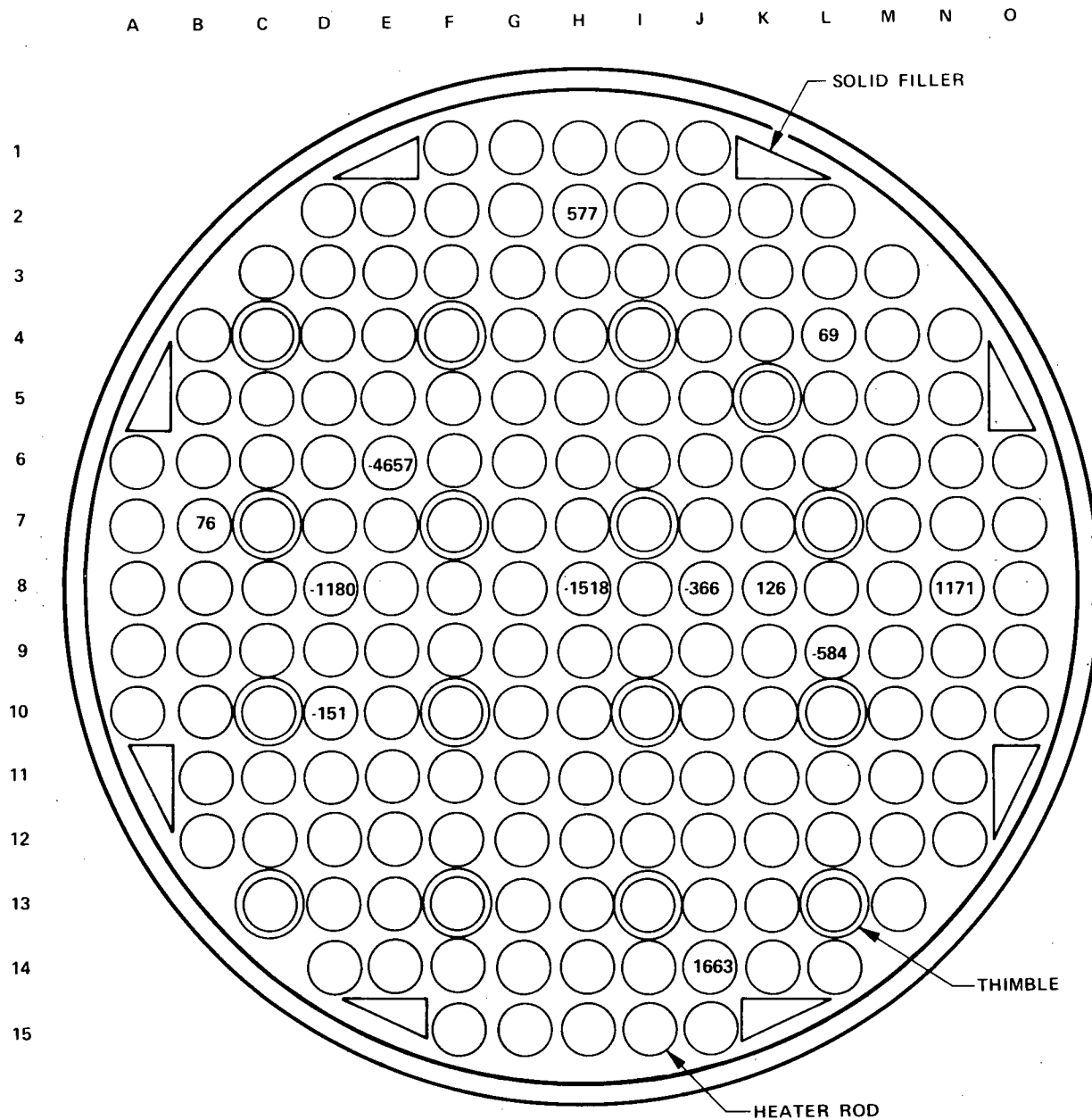
FROTH LEVEL \approx 1.68 m (66 in.)

RUN 35557

PRESSURE = 0.41 MPa (60 psia)

ROD PEAK POWER = 1.38 kw/m (0.422 kw/ft)

Figure 3-10. Wall Heat Flux, Run 35557 at 3.05 m (120 in.),
70 Seconds After Beginning of Test



← HEAT FLUX IN w/m^2

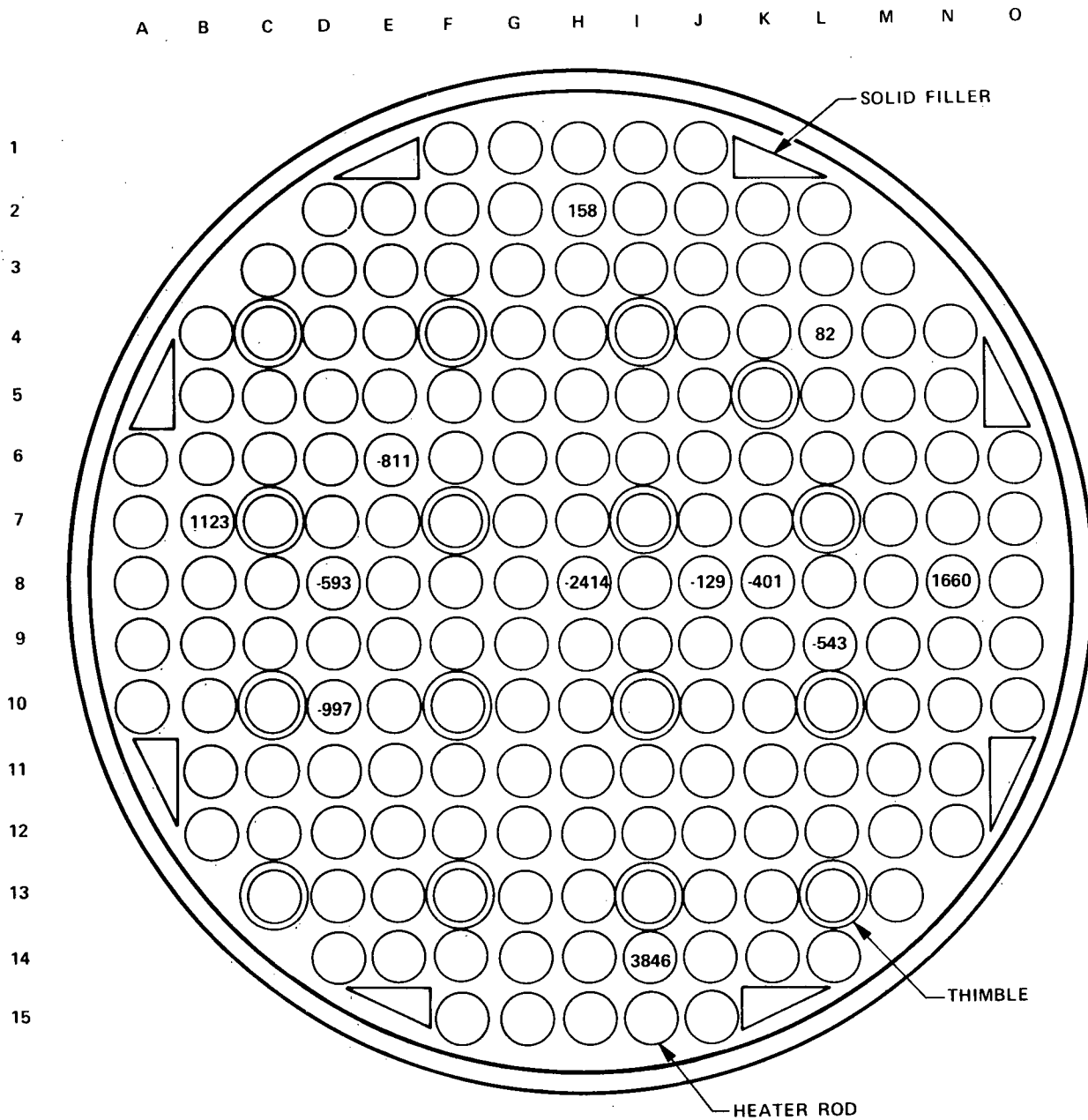
FROTH LEVEL \approx 1.01 m (40 in.)

RUN 35557

PRESSURE = 0.41 MPa (60 psia)

ROD PEAK POWER = 1.38 kw/m (0.422 kw/ft)

Figure 3-11. Wall Heat Flux, Run 35557 at 3.05 m (120 in.), 145 Seconds After Beginning of Test



← HEAT FLUX IN w/m^2

FROTH LEVEL \approx 0.762 m (30 in.)

RUN 35557

PRESSURE = 0.41 MPa (60 psia)

ROD PEAK POWER = 1.38 kw/m (0.422 kw/ft)

Figure 3-12. Wall Heat Flux, Run 35557 at 3.05 m (120 in.), 220 Seconds After Beginning of Test

RUN 35557
PRESSURE = 0.41 MPa (60 psia)
ROD PEAK POWER = 1.38 kw/m (0.422 kw/ft)

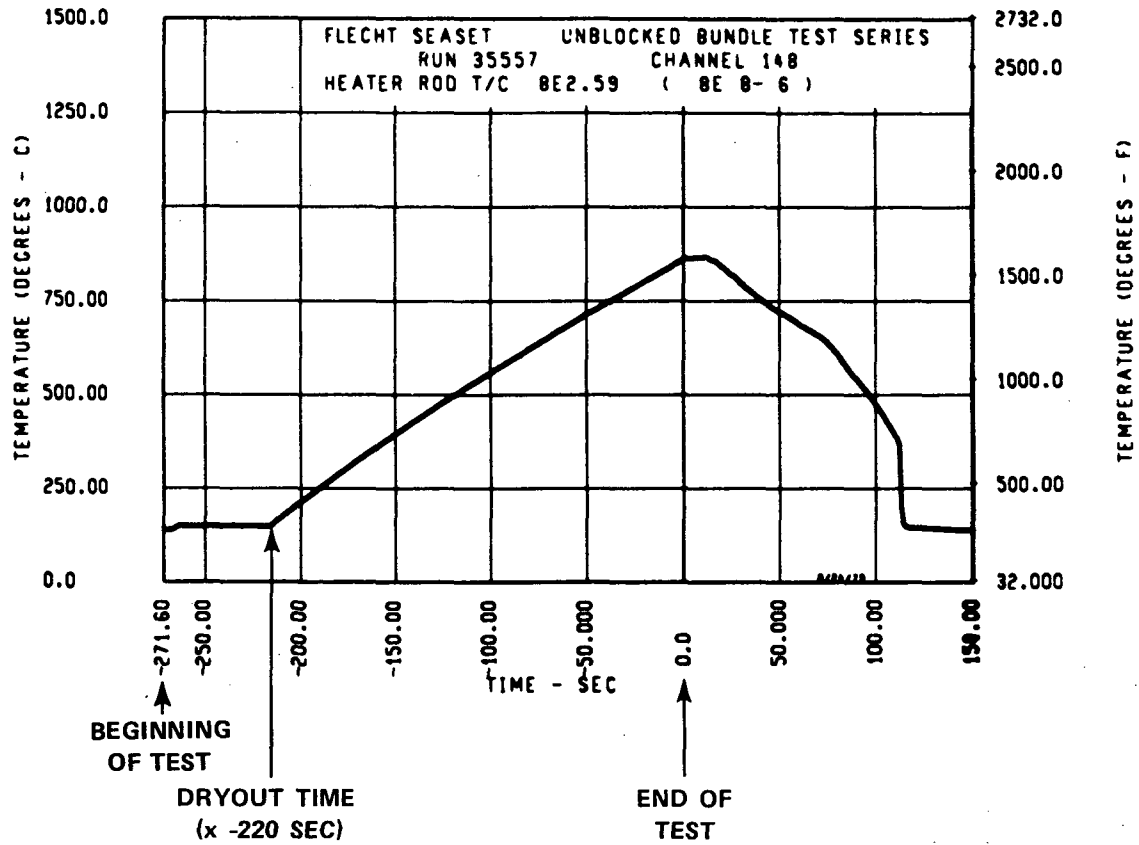


Figure 3-13. Wall Temperature History, Run 35557, Rod 8E, 2.44 m (96 in.) Elevation

RUN 35557
 PRESSURE = 0.41 MPa (60 psia)
 ROD PEAK POWER = 1.38 kw/m (0.422 kw/ft)

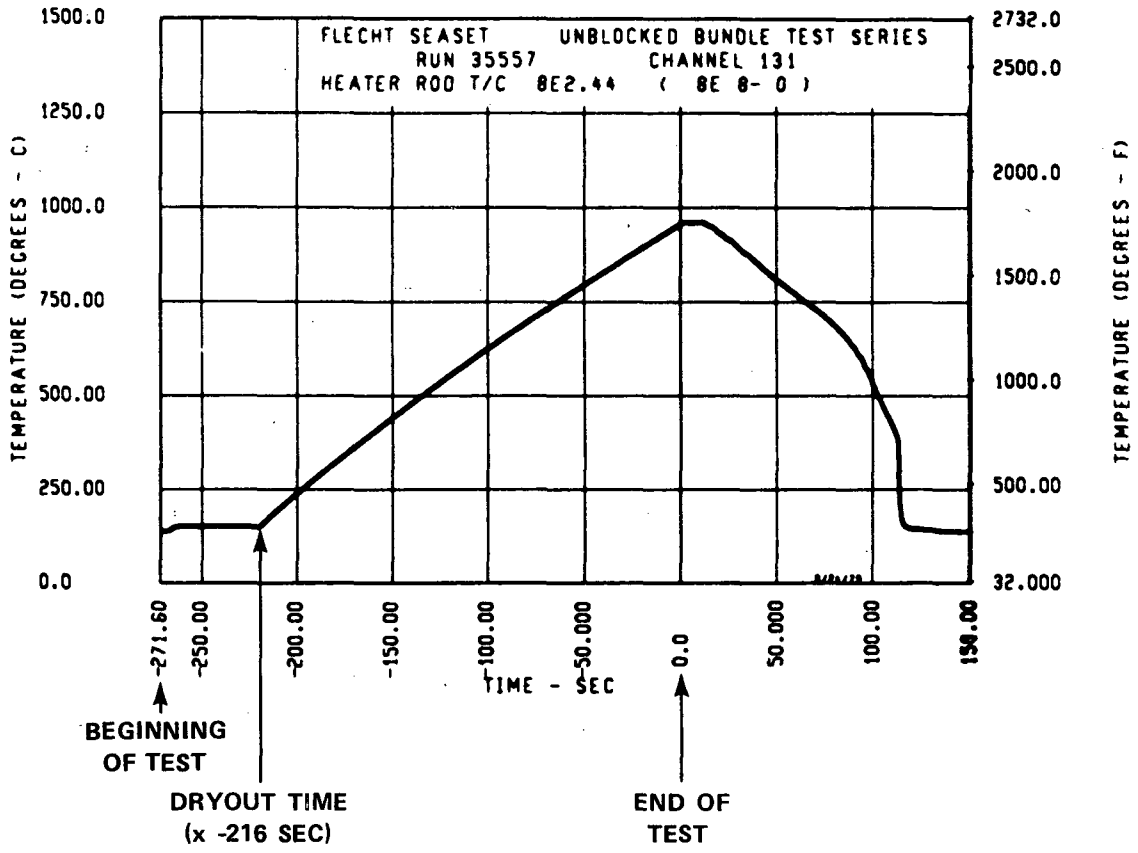


Figure 3-14. Wall Temperature History, Run 35557, Rod 8E, 2.59 m (102 in.) Elevation

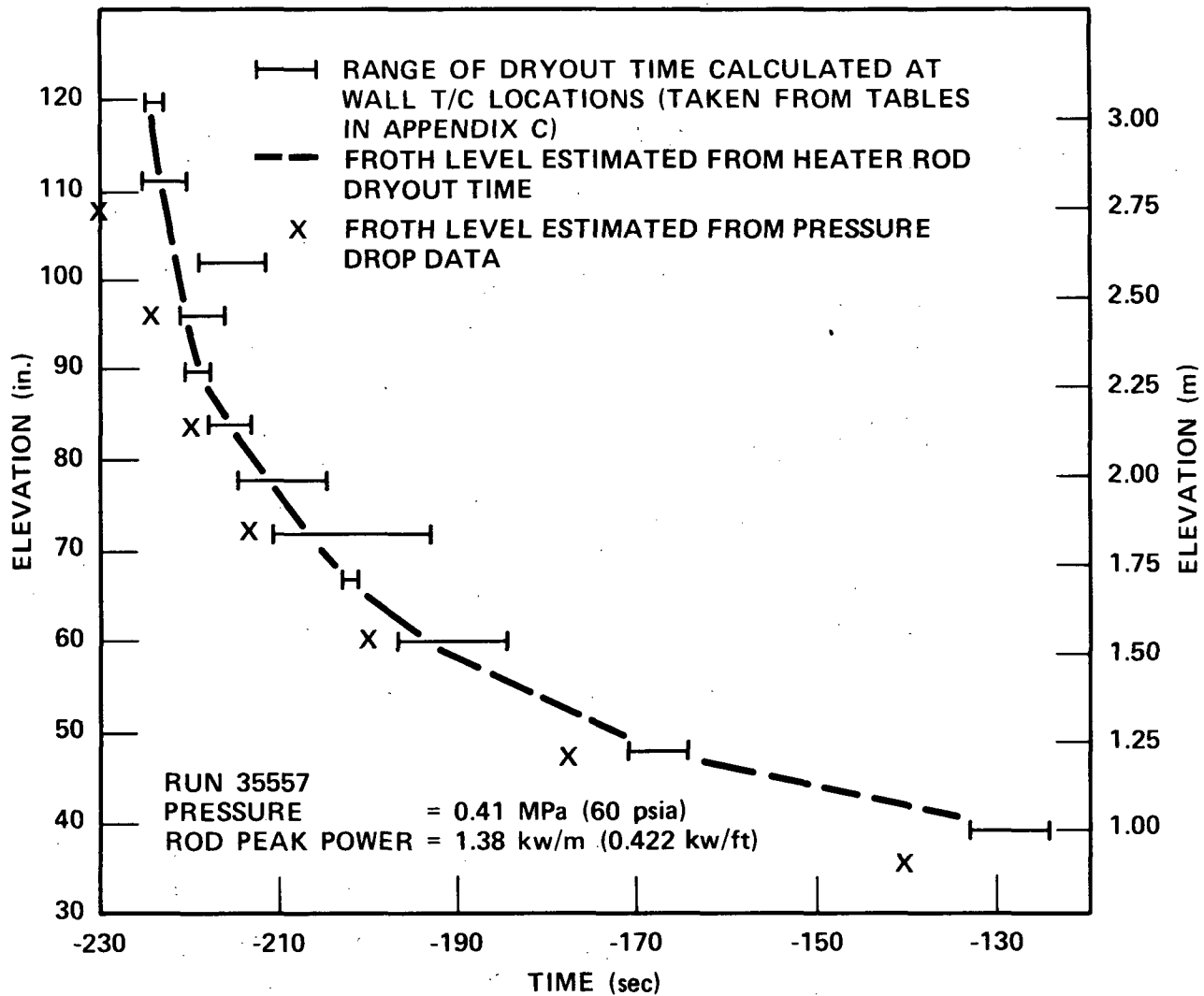


Figure 3-15. Dryout Time and Froth Level, Run 35557

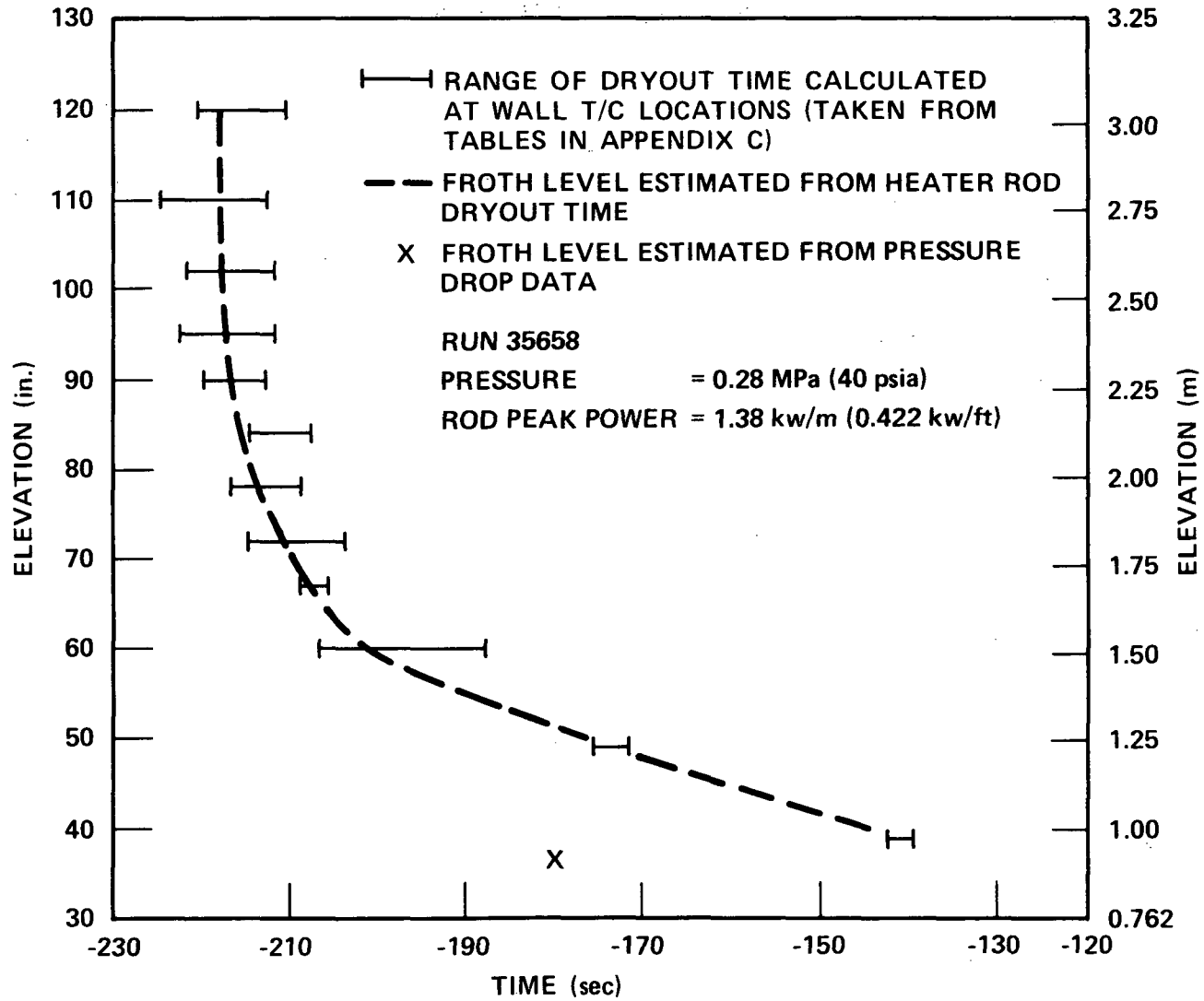


Figure 3-16. Dryout Time and Froth Level, Run 35658

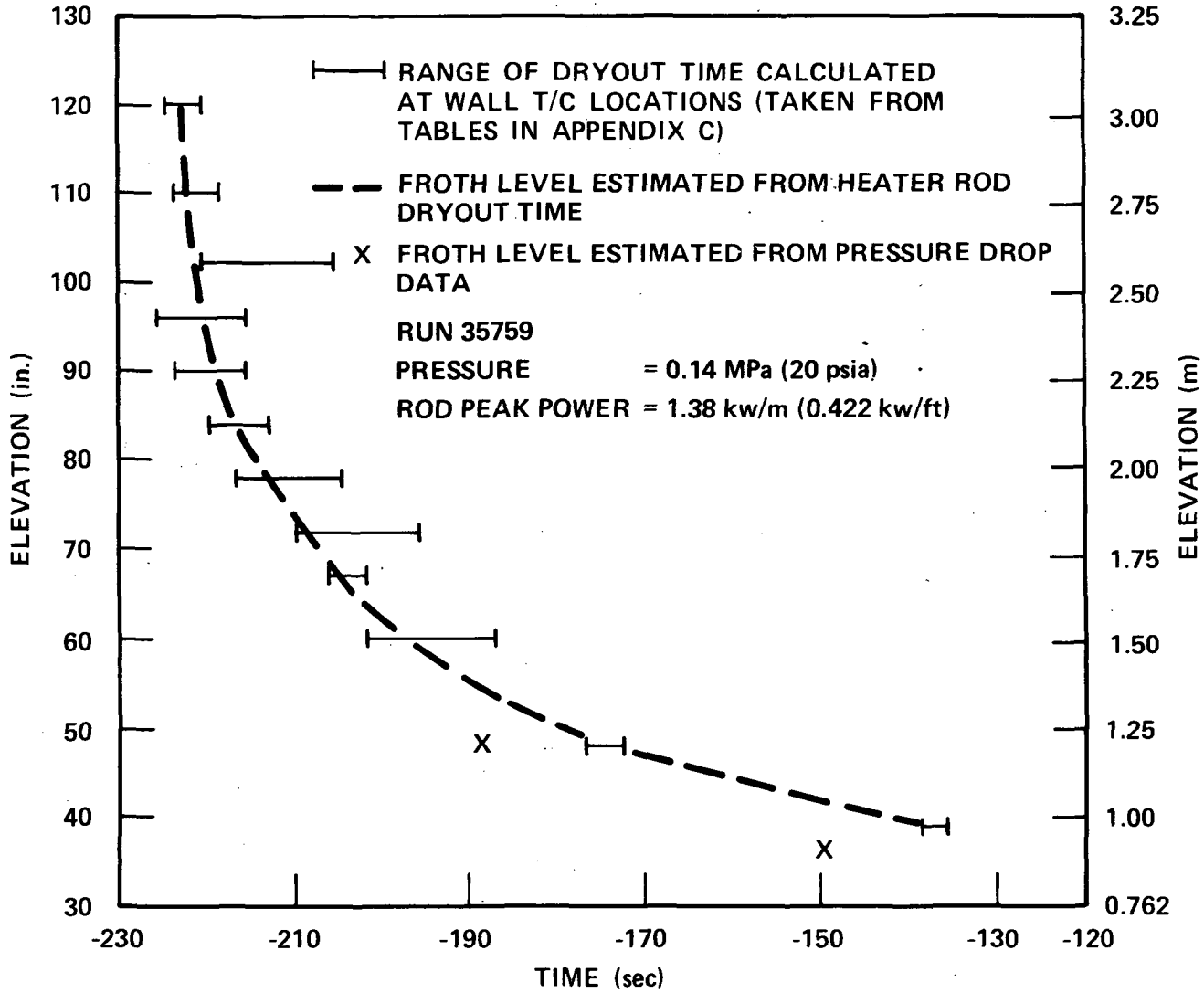


Figure 3-17. Dryout Time and Froth Level, Run 35759

There are spacer grids located at the 2.11 m (83 in.) and 2.62 m (102 in.) elevations which are only 0.02 m (1 in.) from the locations where late dryout was observed. Wall thermocouple locations close to the spacer grids may still be wet for a period of time even above the froth level; this explains the late dryout time shown at 2.59 m (102 in.) in figures 3-15 and 3-17, and at 2.13 m (84 in.) in figure 3-16. Note that the froth level was below these wet thermocouple locations; therefore the froth level curves in figures 3-15 through 3-17 were drawn neglecting them. The present observations are consistent with a recent study by Shires et al.⁽¹⁾

Right after power was turned on during the boiloff tests, because of the cosine-shaped power profile, much void was generated above the midplane, causing rapid pool swell. Much water was forced out of the bundle. This is confirmed by the rapid dryout curves shown in figures 3-15 through 3-17 and the large amount of water collected in the carryover tank at the beginning of the boiloff tests (figure 3-18).

Another method to determine the froth level from the pressure drop data is described in paragraph 3-19:

3-17. Mass Flow Rate Above Froth Level

Data from the water carryover tank indicated that there was little water carryover shortly after the beginning of the boiloff tests (figure 3-18). Although data from the steam separator drain tank for run 35557 show some liquid accumulation (figure 3-19), this could be due to steam condensation in the upper plenum. Also, calculations using the pressure drop data (for example, figures 3-18 and 3-19) show that the liquid accumulation rate was an order of magnitude smaller than the calculated mass flow rate above the froth level. Hence it can be concluded that the mass flow from the bundle into the upper plenum was mainly steam. In any case, the mass flow rate (whether pure steam or steam and liquid mixture) above the froth level can be calculated from the total pressure drop data⁽²⁾ [pressure drop between the 0 and 3.05 m (0 and 120 in.) elevations]:

$$\dot{m} = \frac{A}{g} \frac{dP_T}{dt} \quad (3-12)$$

where

$$\begin{aligned} \dot{m} &= \text{mass flow rate above froth level (kg/sec)} \\ \frac{dP_T}{dt} &= \text{rate of total pressure drop between 0 and 3.05 m (120 in.) elevations} \\ &\quad (\text{J/m}^2\text{-sec}) \end{aligned}$$

1. Shires, G. L., et al., "An Experimental Study of Level Swell in a Partially Water-Filled Fuel Cluster," *Nucl. Energy* 79, 381-388 (1980).
2. The total pressure drop is basically a measure of the "collapsed liquid level" or the total mass inventory in the bundle.

RUN 35557
PRESSURE = 0.41 MPa (60 psia)
ROD PEAK POWER = 1.38 kw/m (0.422 kw/ft)

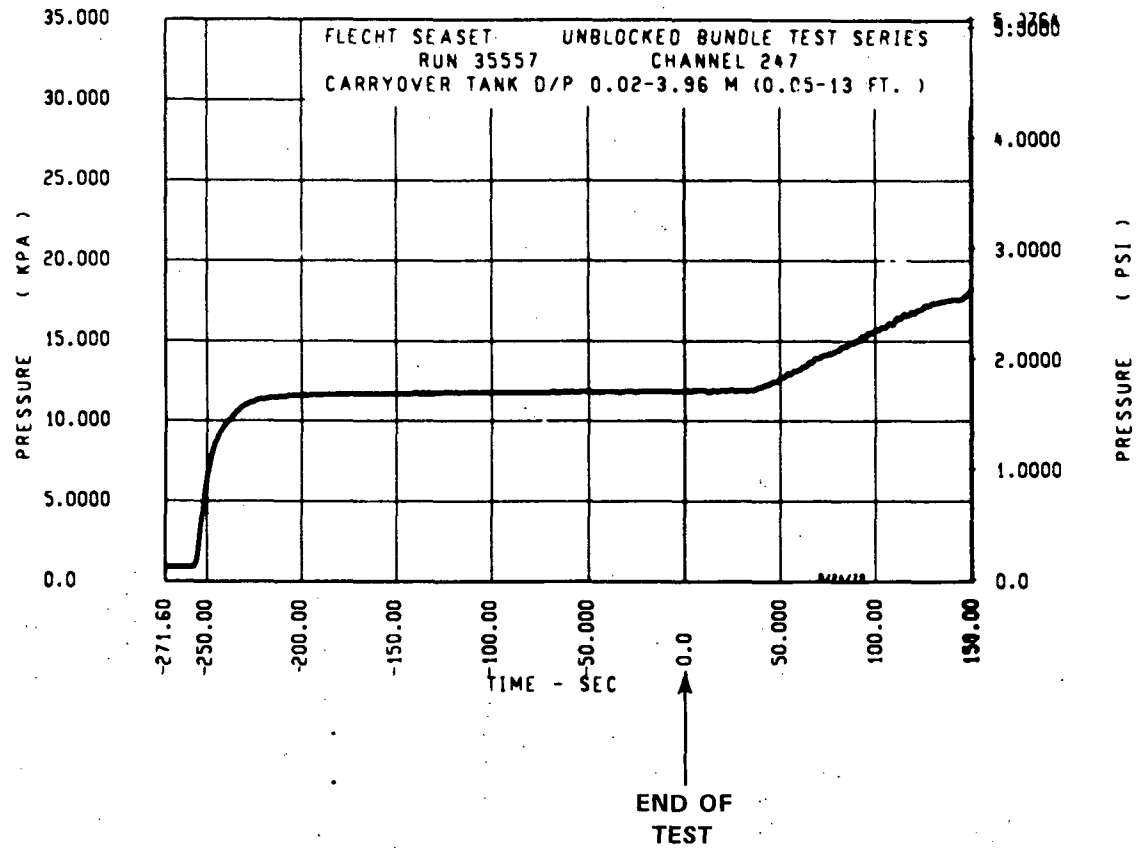


Figure 3-18. Pressure Drop Measurements at Carryover Tank, Run 35557

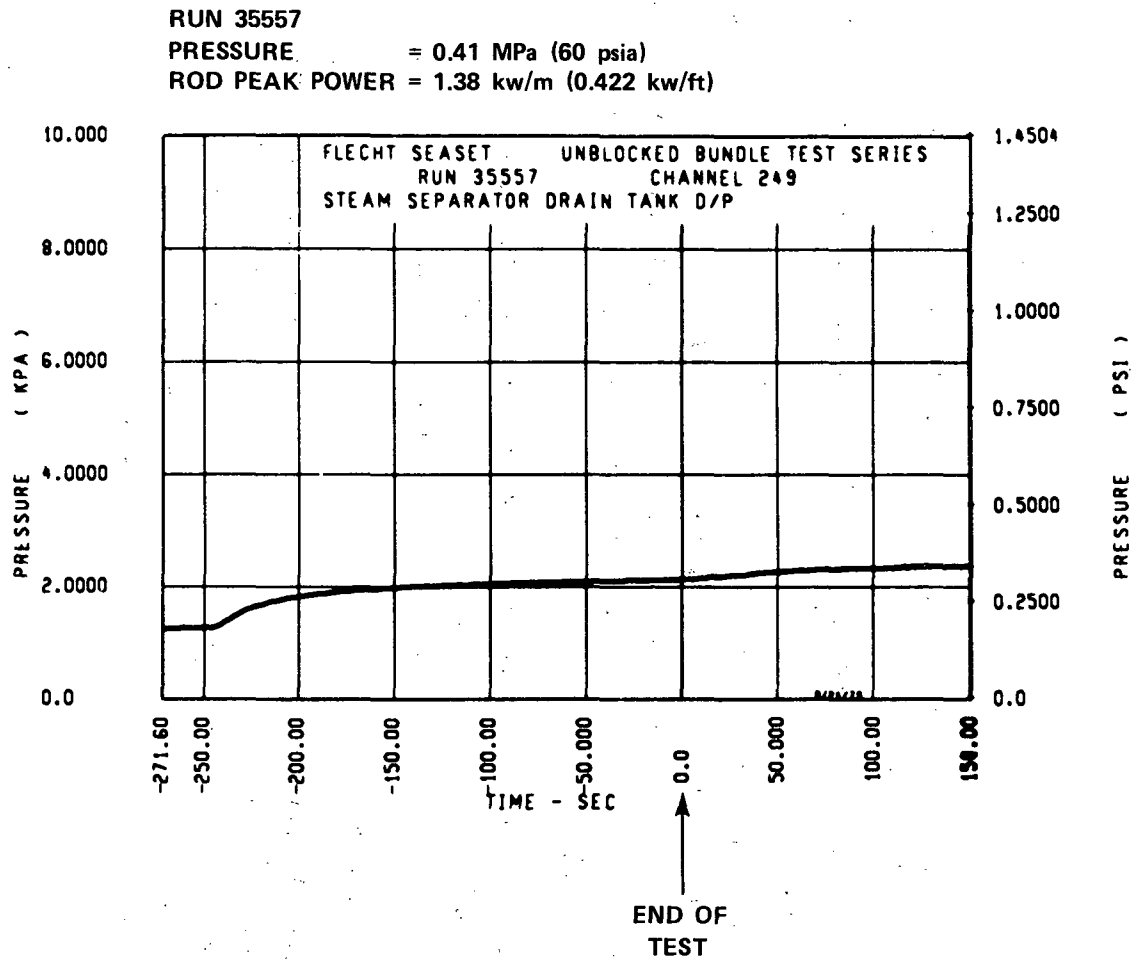


Figure 3-19. Pressure Drop Measurements at Steam Separator Drain Tank, Run 3557

A = bundle cross-sectional flow area (m²)

g = gravitational acceleration (m/sec²)

In the actual calculations, the rate of pressure drop was calculated by a forward difference:

$$\frac{dP_T}{dt_i} = \frac{P_T(i+5) - P_T(i)}{5}$$

where

$\frac{dP_T}{dt_i}$ = rate of total pressure drop between 0 and 3.05 m (120 in.) elevations at i seconds (J/m²-sec)

$P_T(i)$ = total pressure drop between 0 and 3.05 m (120 in.) elevations at i seconds (J/m²)

The frictional pressure drop⁽¹⁾ in the bundle under these conditions was found to be two orders of magnitude less than the total pressure drop; it was neglected. The mass flow rate was hence calculated at 5-second intervals. Typical total pressure drop data and the calculated mass flow rate are shown in figures 3-20 and 3-21, respectively. (Figure 3-21 plots the calculated mass flow rate only at 10-second intervals.)

The mass flow above the froth level is very small. Also, because of the slight fluctuation of the pressure drop data (figure 3-20), the calculated mass flow shows considerable oscillation. Figure 3-21, however, shows clearly that the mass flow decreased toward the end of the test.

3-18. Void Fraction

The void fraction⁽²⁾ can be deduced from the pressure drop data, which were read at intervals of 0.305 m (12 in.) along the entire bundle. The void fraction calculations were hand calculations, and the data used were not time-averaged. Typical pressure drop data are shown in figures 3-22 and 3-23. Because the power supply was constant for the boiloff tests, the flow below the froth level should have been quasi-steady after the initial developing period. This is illustrated by the period

1. Loftus, M. J., et al., "PWR FLECHT SEASET Unblocked Bundle, Forced and Gravity Reflood Task: Data Report," NRC EPRI Westinghouse Report No. 7, to be published.
2. Void fraction in this discussion means an averaged void fraction across the bundle at the 0.305 m (12 in.) intervals where pressure drop data were taken.

RUN 35557
 PRESSURE = 0.41 MPa (60 psia)
 ROD PEAK POWER = 1.38 kw/m (0.422 kw/ft)

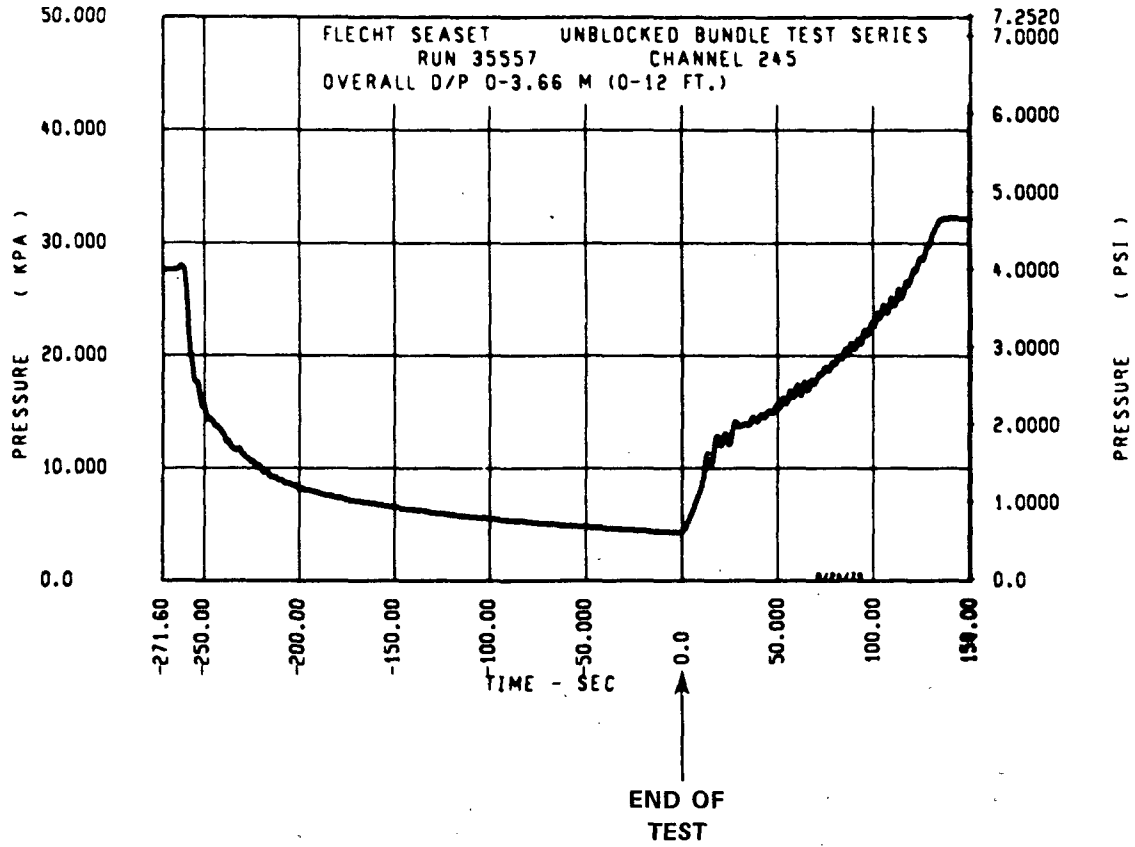


Figure 3-20. Overall Pressure Drop Data, Run 35557, 0 to 3.05 m (0 to 120 in.)

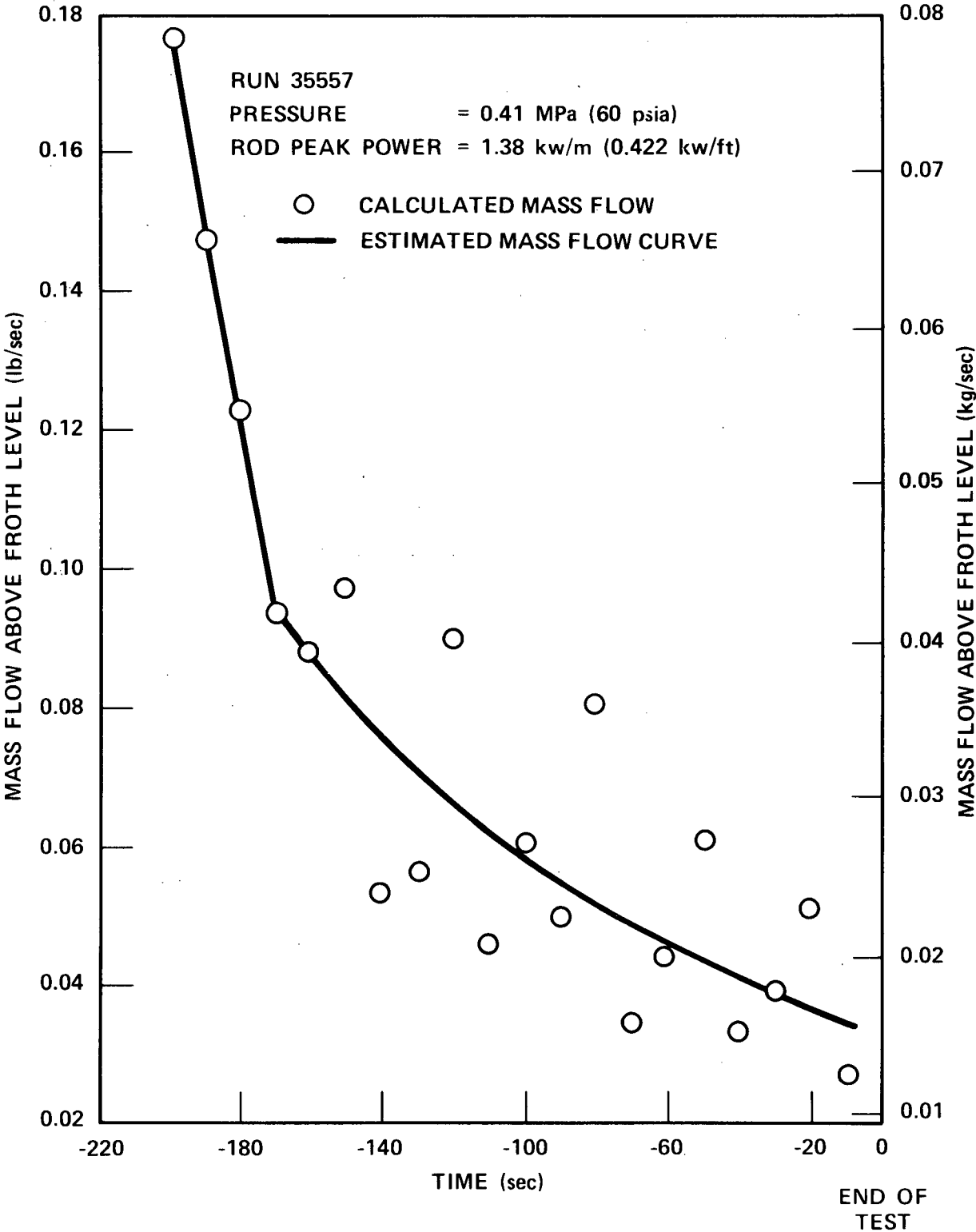


Figure 3-21. Calculated Mass Flow Rate Above Froth Level, Run 35557

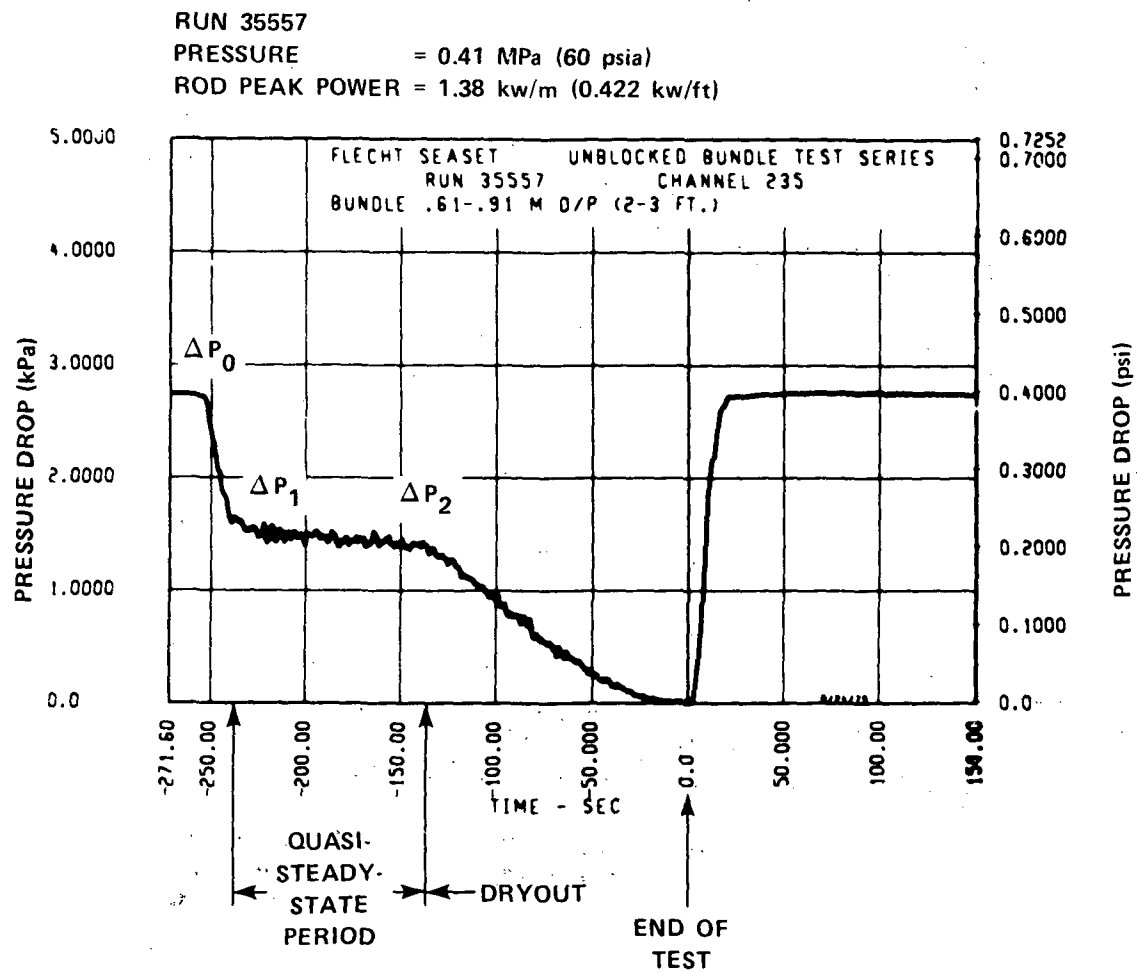


Figure 3-22. Pressure Drop Between 0.61 and 0.91 m (24 and 36 in.), Run 35557, Showing a Quasi-Steady-State Period

RUN 35557
PRESSURE = 0.41 MPa (60 psia)
ROD PEAK POWER = 1.38 kw/m (0.422 kw/ft)

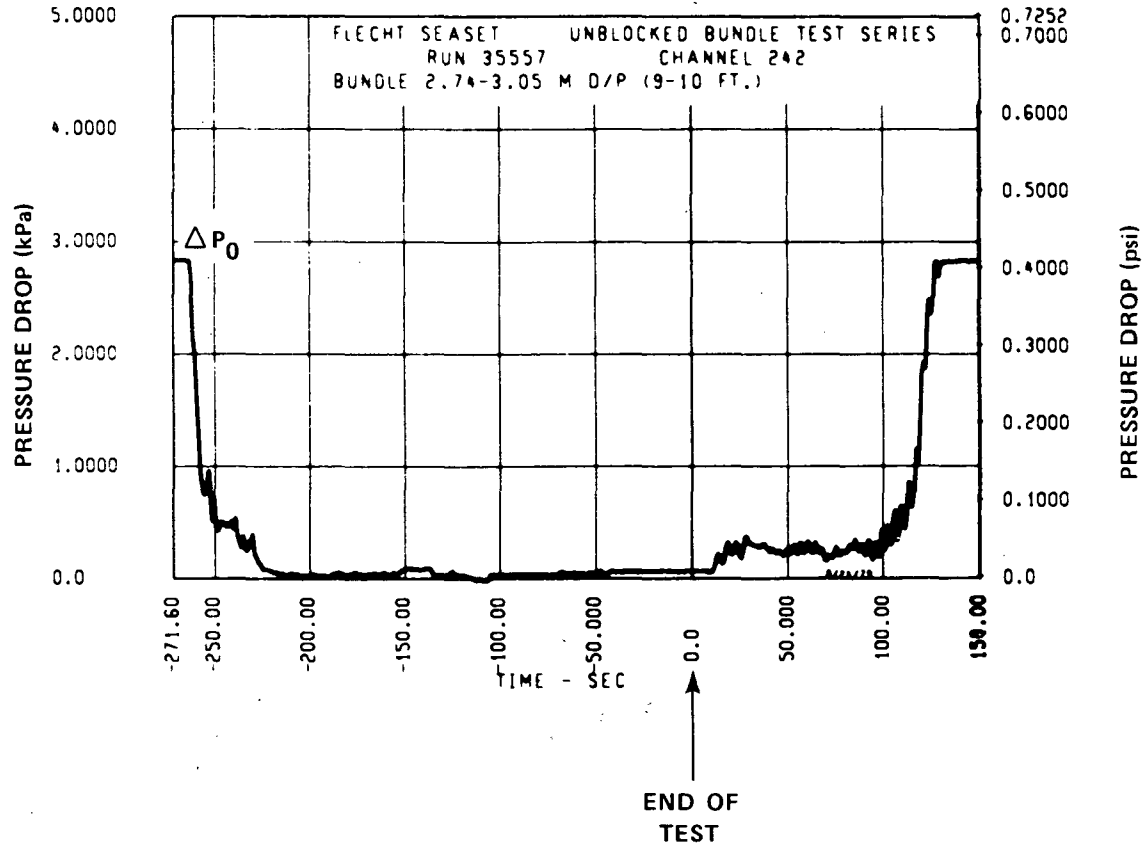


Figure 3-23. Pressure Drop Between 2.74 and 3.05 m (108 and 120 in.), Run 35557, Showing No Distinct Quasi-Steady-State Period

of quasi-steady pressure drop data shown in figure 3-22. The higher elevations were uncovered immediately after the initial developing period (see figures 3-15 through 3-17); hence the quasi-steady period was either very short or nonexistent, as manifested in the pressure drop data of figure 3-23. The average quasi-steady-state void fraction between the i and $i+0.305$ m (12 in.) elevations can be calculated from the pressure drop data:

$$\alpha_i = \frac{\Delta P_{oi} - \Delta P_{si}}{\Delta P_{oi}}$$

where

- α_i = average steady-state void fraction between the i and $i+3.05$ m (12 in.) elevations
- ΔP_{oi} = pressure drop between the i and $i+3.05$ m (12 in.) elevations at beginning of test (kPa) (that is, pressure drop when there is no void present)
- ΔP_{si} = pressure drop between the i and $i+3.05$ m (12 in.) elevations at quasi-steady-state conditions (kPa)

In performing the calculations, ΔP_{si} was taken to be the mean of the two data points (P_1 and P_2) such as that shown in figure 3-22. Because the steady-state pressure drops at many higher bundle elevations, such as that shown in figure 3-23, were not well defined, the void fractions for these locations were not calculated.

3-19. Determination of Froth Level by Pressure Drop Data

Another method to determine the froth level is to use the pressure drop data, such as those shown in figure 3-22. In figure 3-22, the sudden change in pressure drop at point ΔP_2 is an indication of the froth level. This method has an advantage, in that the froth level detected from the pressure data is not affected by the bundle geometric distortion, since the pressure taps are on the housing. Unfortunately, there are only limited pressure drop data that show a distinct quasi-steady-state period and a sudden change in pressure drop such as those shown in figure 3-22; other pressure drop data (especially at higher elevations where uncovering occurred early) exhibit monotonic decrease, and no distinct froth level exists (figure 3-23). All applicable pressure drop data were used to determine the froth level; the results are shown in figures 3-15 through 3-17 for comparison. One sees that the froth level determined by the pressure drop data was always lower (for a given

time) than that determined by the heater rod dryout time. An explanation was the presence of a liquid film on the rods, which would be replenished by drops of water entrained from the free water surface; the liquid film delayed the dryout time by keeping the rods cool for up to 0.25 to 0.38 m (10 to 15 in.) above the froth level.

SECTION 4

DATA ANALYSIS AND CORRELATION DEVELOPMENT

4-1. INTRODUCTION

The Nusselt and Reynolds numbers calculated from the steam cooling data by the rod-centered subchannel energy balance method and by the COBRA-IV-I analysis were compared. It was found that by neglecting subchannel interactions, the rod-centered subchannel energy balance method consistently calculated a higher vapor temperature and hence a higher heat transfer coefficient or Nusselt number. Taking into account the subchannel interactions by the COBRA-IV-I code, the calculated vapor temperature and heat transfer coefficient were reduced. The COBRA-IV-I analysis was a more accurate simulation of the steam cooling tests, and so the COBRA results were used to develop a heat transfer correlation for rod bundles. Unless otherwise stated, all calculated Nusselt and Reynolds numbers presented were calculated from the COBRA-IV-I results.

The calculated Nusselt numbers were generally above those predicted by the Dittus-Boelter turbulent flow heat transfer correlation.⁽¹⁾ Also, the data at different elevations showed considerable scattering, especially at low Reynolds numbers, but seemed to converge to the Dittus-Boelter correlation at high Reynolds numbers.

For the reasons already discussed in section 3, only very limited analysis was possible for the boiloff tests. The effects of free convection during the boiloff tests are estimated in paragraph 4-6; the calculated void fraction (paragraph 3-18) is compared with the Yeh void fraction correlation⁽²⁾ in paragraph 4-7.

4-2. COMPARISONS OF ROD-CENTERED SUBCHANNEL ENERGY BALANCE AND COBRA-IV-I ANALYSIS

Typical comparisons of vapor temperatures calculated by the rod-centered subchannel energy balance method (equation 3-11) and the COBRA-IV-I subchannel analysis are given in figure 3-4. Because subchannel mixing was neglected, the rod-centered subchannel energy balance method consistently calculated a higher vapor temperature. The calculated heat transfer coefficient and Nusselt number were hence also higher, according to equations (3-2) and (3-3). Comparisons of

-
1. Dittus, F. W., and Boelter, L. M. K., "Heat Transfer in Automobile Radiators of the Tubular Type," *Univ. Calif., Berkeley Publ. Eng.* 2, 13, 443-362 (1930).
 2. Yeh, H. C., and Hochreiter, L. E., "Mass Effluence During FLECHT Forced Reflood Experiments," to be published in *Nucl. Eng. and Design*.

the calculated Nusselt and Reynolds numbers by the rod-centered subchannel energy balance method and by the COBRA-IV-I code are given in figure 4-1. Rod-to-rod comparisons of the two methods are tabulated in appendix A. The COBRA-IV-I analysis, which took into account the effects of the housing, the thimble guide tubes, the disconnected rods, the rod-to-rod variation of input power (that is, the rod-to-rod variation of heater rod resistance), and subchannel interactions, was a more accurate simulation of the steam cooling experiments. In the remainder of this section, a heat transfer correlation is developed using the COBRA-IV-I results.

4-3. EFFECT OF ELEVATION AND GRID SPACERS ON HEAT TRANSFER FOR STEAM COOLING TESTS

As explained in paragraph 3-11, only selected data from the test section inlet to the 1.52 m (60 in.) elevation in eight steam cooling tests were used to develop the heat transfer correlation in rod bundles. Tables A-1 through A-8 in appendix A show all the connected heater rod thermocouple channels for these eight runs between the inlet and 1.52 m (60 in.) elevations (five instrumentation elevations), and also summarize the data used for analysis and the reasons for eliminating some of the data. The calculated vapor temperature, heat transfer coefficient, Nusselt number, and Reynolds number at each instrumentation location are also given in appendix A, table A-9. An average Nusselt number and Reynolds number were calculated at each elevation. Figures 4-2 through 4-9 are plots of $Nu/(0.023 Re^{0.8})$, obtained by COBRA-IV-I analysis, versus elevation for the eight steam cooling tests. Also shown on the graphs are the grid spacer locations, as dotted vertical lines. There is no apparent correlation of the heat transfer coefficient with elevation; also no apparent grid effects can be observed. The reason that no grid effects can be observed was probably that the instrumentation in the present FLECHT SEASET unblocked bundle test section was not designed for this purpose. Hence no attempt was made to incorporate any elevation dependence in the heat transfer correlation (paragraph 4-4), and the heat transfer correlation developed is a function of the Reynolds number only.

4-4. DATA-BASED HEAT TRANSFER CORRELATION IN ROD BUNDLES

A data-based heat transfer correlation in rod bundles was obtained by a linear regression technique from the Nusselt and Reynolds numbers calculated from the steam cooling steady-state data (at least one rod row away from the housing and disconnected rods) in the FLECHT SEASET 161-rod bundle. The calculation can be summarized as follows:

- The wall surface temperature was obtained from the measured cladding inner surface temperature by an inverse conduction method.
- Rod heat flux was obtained from measured bundle power, individual rod resistance, and axial power steps.

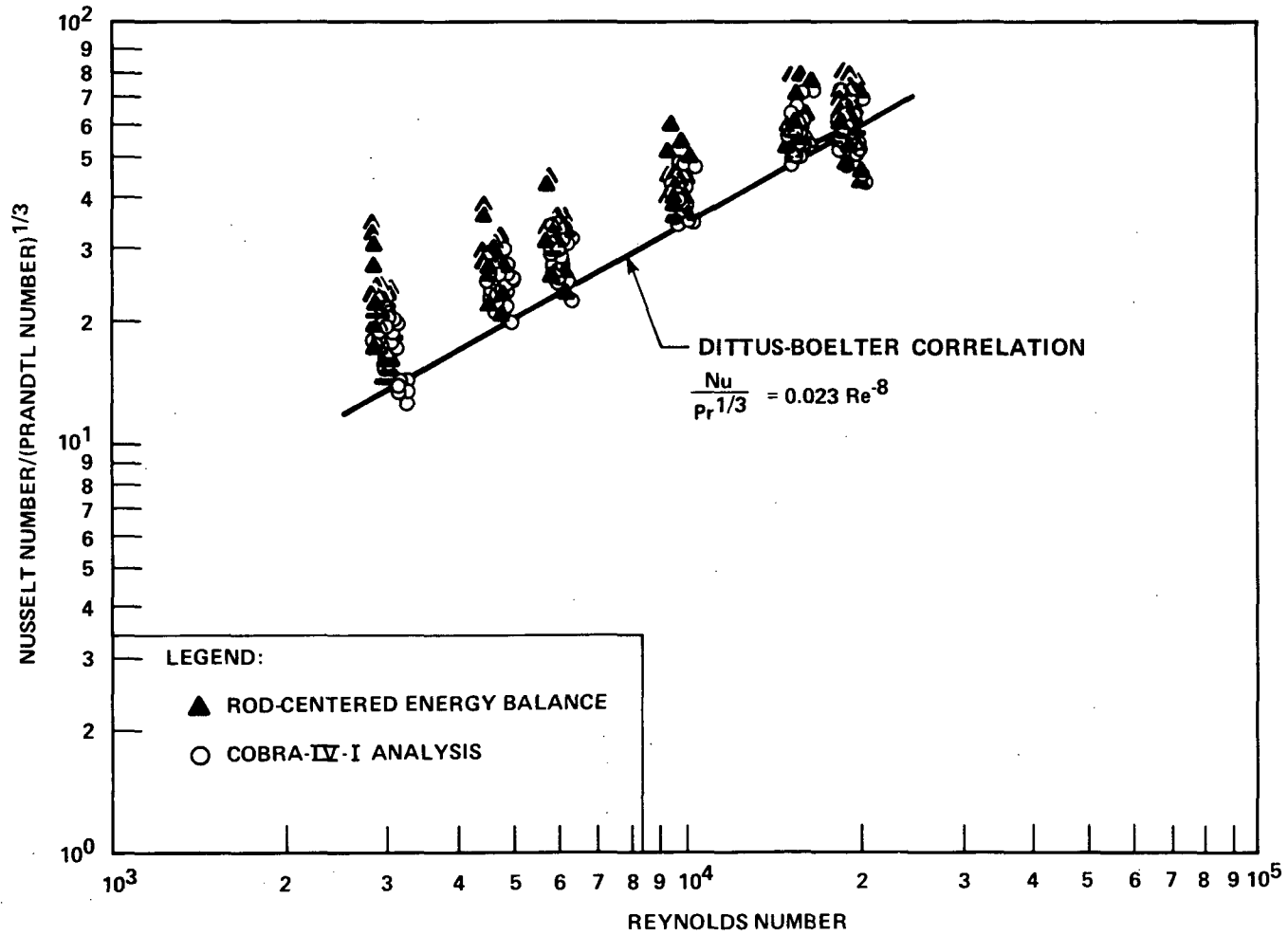


Figure 4-1. Comparisons of Calculated Nusselt and Reynolds Numbers by Rod-Centered Subchannel Energy Balance and COBRA-IV-I Analysis

PRESSURE = 0.28 MPa (40 psia)
 ROD PEAK POWER = 0.205 kw/m (0.0625 kw/ft)
 INLET FLOW RATE = 0.4 kg/sec (0.8 lb/sec)
 INLET FLOW TEMPERATURE = 132°C (269°F)

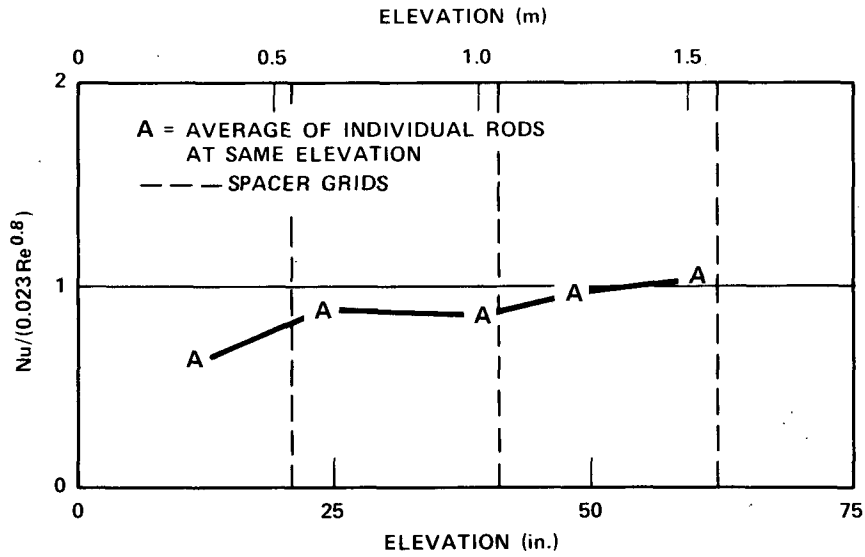


Figure 4-2. Effect of Elevation on Heat Transfer, Run 32753

PRESSURE = 0.28 MPa (40 psia)
 ROD PEAK POWER = 0.16 kw/m (0.049 kw/ft)
 INLET FLOW RATE = 0.37 kg/sec (0.81 lb/sec)
 INLET FLOW TEMPERATURE = 144°C (292°F)

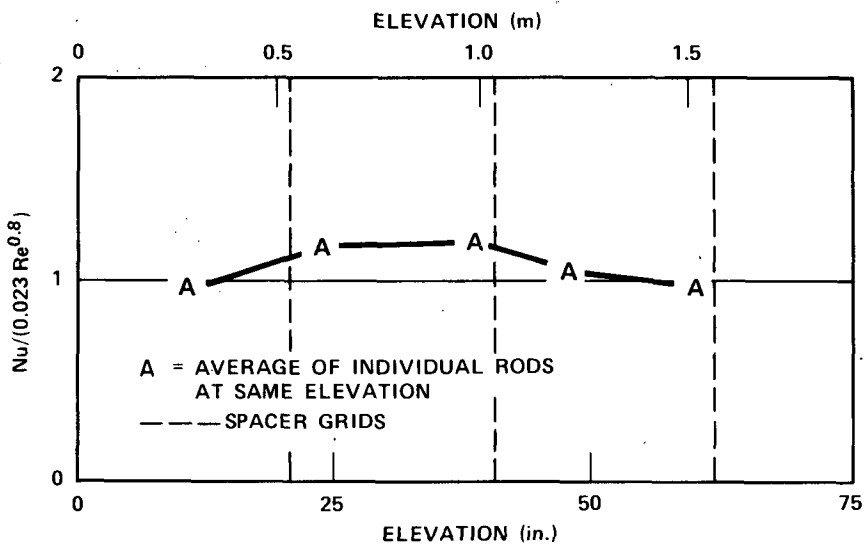


Figure 4-3. Effect of Elevation on Heat Transfer, Run 36160

PRESSURE = 0.28 MPa (40 psia)
 ROD PEAK POWER = 0.13 kw/m (0.039 kw/ft)
 INLET FLOW RATE = 0.297 kg/sec (0.655 lb/sec)
 INLET FLOW TEMPERATURE = 142°C (287°F)

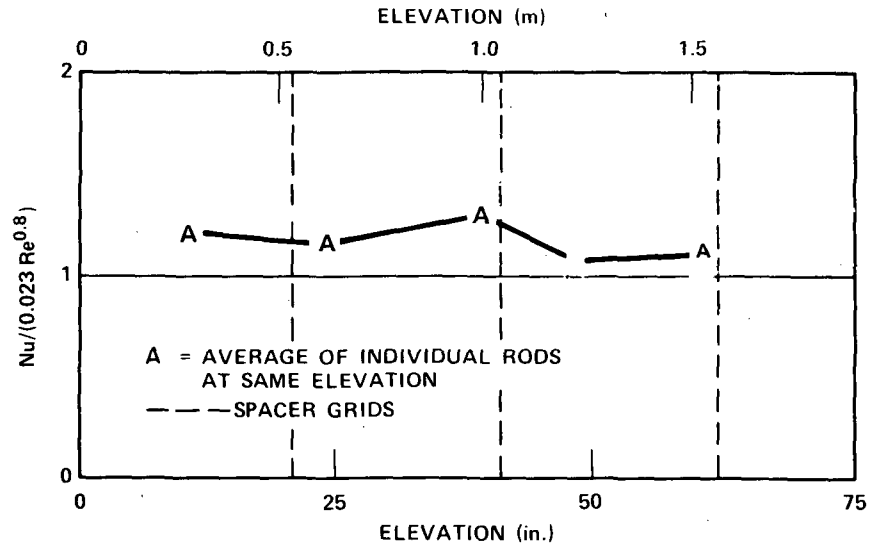


Figure 4-4. Effect of Elevation on Heat Transfer, Run 36261

PRESSURE = 0.28 MPa (40 psia)
 ROD PEAK POWER = 0.79 kw/m (0.24 kw/ft)
 INLET FLOW RATE = 0.18 kg/sec (0.40 lb/sec)
 INLET FLOW TEMPERATURE = 138°C (280°F)

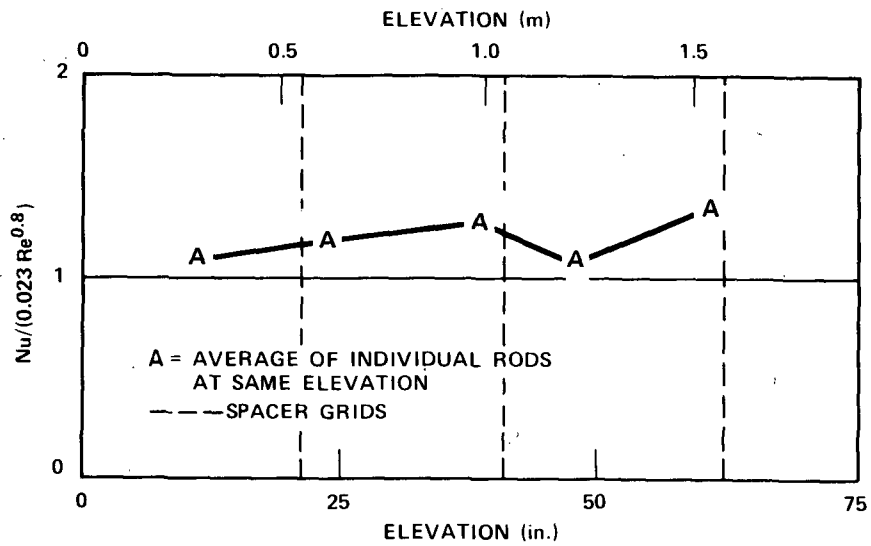


Figure 4-5. Effect of Elevation on Heat Transfer, Run 36362

PRESSURE = 0.28 MPa (40 psia)
 ROD PEAK POWER = 0.0479 kw/m (0.0146 kw/ft)
 INLET FLOW RATE = 0.110 kg/sec (0.243 lb/sec)
 INLET FLOW TEMPERATURE = 134°C (273°F)

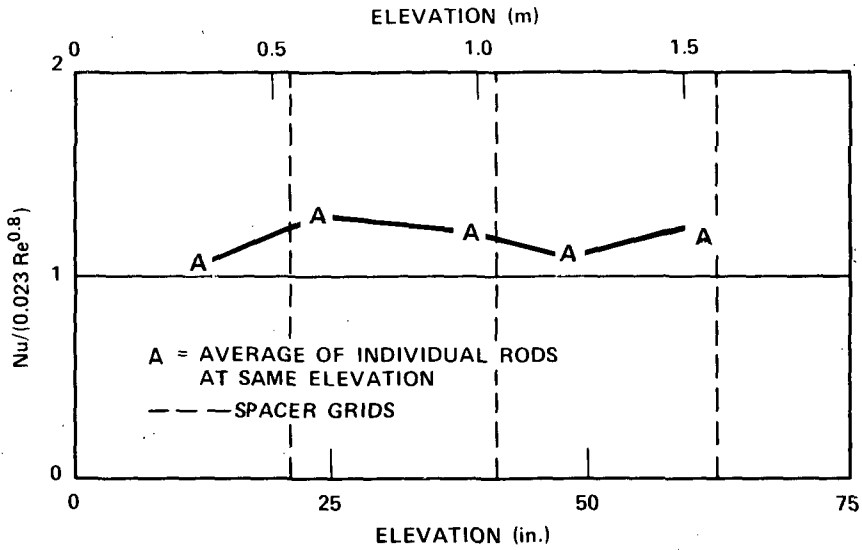


Figure 4-6. Effect of Elevation on Heat Transfer, Run 36463

PRESSURE = 0.28 MPa (40 psia)
 ROD PEAK POWER = 0.039 kw/m (0.012 kw/ft)
 INLET FLOW RATE = 0.0853 kg/sec (0.188 lb/sec)
 INLET FLOW TEMPERATURE = 133°C (271°F)

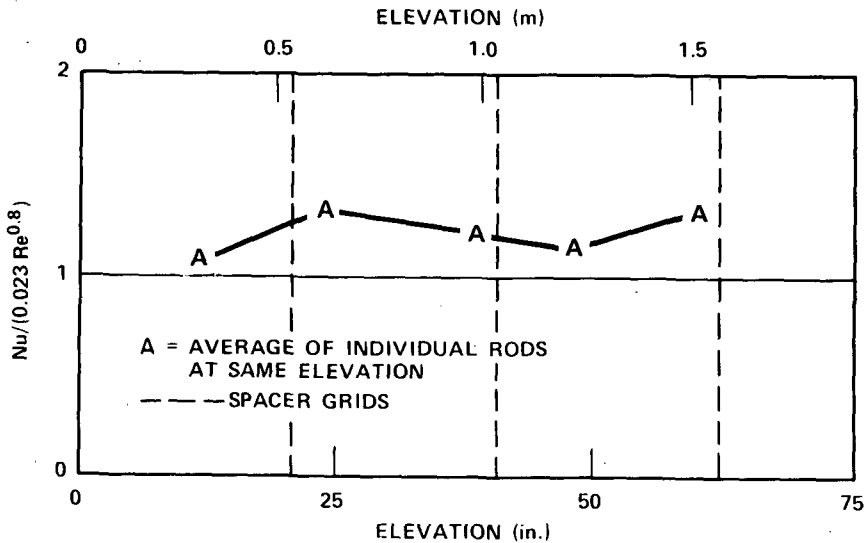


Figure 4-7. Effect of Elevation on Heat Transfer, Run 36564

PRESSURE = 0.28 MPa (40 psia)
 ROD PEAK POWER = 0.02 kw/m (0.007 kw/ft)
 INLET FLOW RATE = 0.054 kg/sec (0.12 lb/sec)
 INLET FLOW TEMPERATURE = 131°C (267°F)

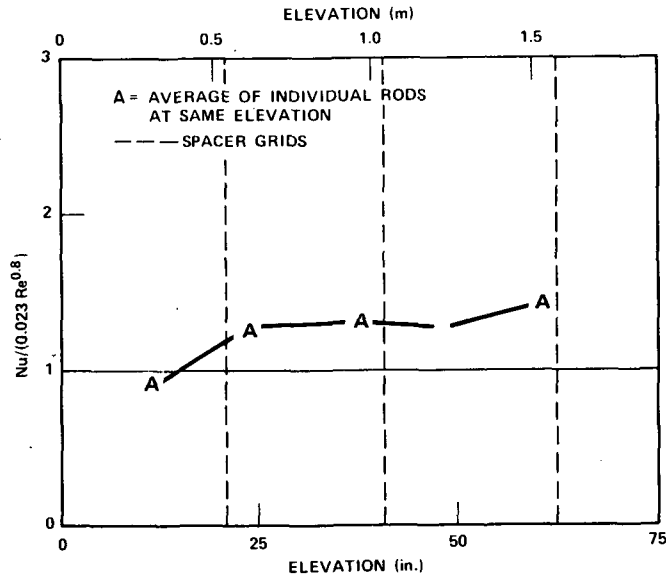


Figure 4-8. Effect of Elevation on Heat Transfer, Run 36766

PRESSURE = 0.28 MPa (40 psia)
 ROD PEAK POWER = 0.02 kw/m (0.006 kw/ft)
 INLET FLOW RATE = 0.0531 kg/sec (0.117 lb/sec)
 INLET FLOW TEMPERATURE = 131°C (267°F)

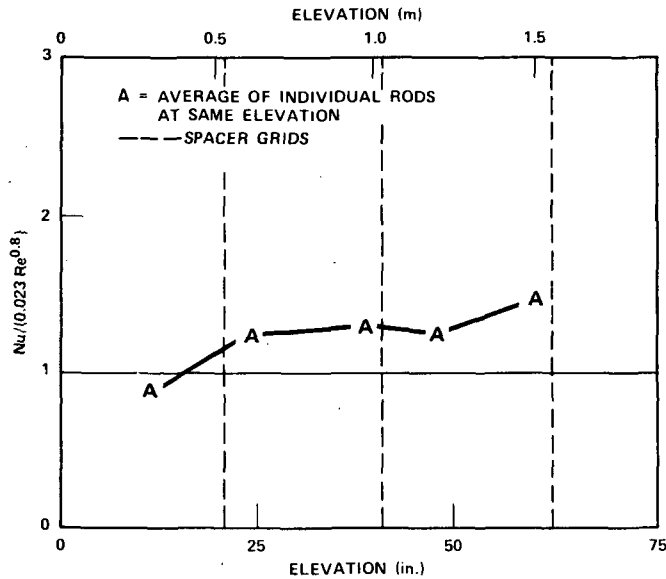


Figure 4-9. Effect of Elevation on Heat Transfer, Run 36867

- Subchannel mass flux and vapor temperature were obtained from the COBRA-IV-I computer code.

The results, using 155 data points, are tabulated in appendix A and plotted in figure 4-10. The linear regression fit of the 155 data points can be represented by

$$\frac{Nu}{Pr^{1/3}} = 0.0797 Re^{0.6774} \quad (4-1)$$

The Prandtl number of the present steam cooling tests was about 1, and a Prandtl number dependence was introduced in equation (4-1) according to the recommendation by Colburn.⁽¹⁾ An error analysis of the calculated Nusselt and Reynolds numbers is given in appendix B.

4-5. RECOMMENDED CORRELATION FOR STEAM COOLING IN ROD BUNDLES

In the correlation of fully developed single-phase heat transfer results, the two most important parameters to be considered are the Reynolds number and the geometry. The Reynolds number marks the transition between laminar and turbulent flow. Also, the heat transfer coefficient calculated for a circular tube should not be applied to rod bundle geometry without some justification, especially for low Reynolds number cases. In fact, it is known that the calculated Nusselt number for fully developed laminar flow in a circular pipe for the constant heat rate case is 4.364; a recent analysis,⁽²⁾ however, has shown that the corresponding Nusselt number for an infinite rod bundle with a square pitch of 1.33 (the same pitch-to-diameter ratio as the FLECHT SEASET 161-rod unblocked bundle) is 7.86. Hence geometric factors must be considered in the development of heat transfer correlations.

The Reynolds number (or the Reynolds number range) at which the flow in rod bundles undergoes a transition from laminar flow to turbulent flow is unknown. For circular tubes, a critical Reynolds number of 2,000 is commonly used. But since the minimum Reynolds number for the data shown in figure 4-10 is about 2,500, an assumption on the transition heat transfer region must be used. Hence it is recommended that, for Reynolds numbers between 2,500 and 2,000, the heat transfer be linearly interpolated from the data-based correlation [equation (4-1)] at a Reynolds number of 2,500 to the fully developed laminar heat transfer coefficient at a Reynolds number of 2,000.

1. Colburn, A. P., "A Method of Correlating Forced Convection Heat Transfer Data and a Comparison With Fluid Friction," *Trans. A.I.Ch.E.* 29, 174 (1933).
2. Kim, J. H., "Heat Transfer in Longitudinal Laminar Flow Along Cylinders in Square Array," in *Fluid Flow and Heat Transfer Over Rod or Tube Bundles*, American Society of Mechanical Engineers, New York, 1979, pp 155-161.

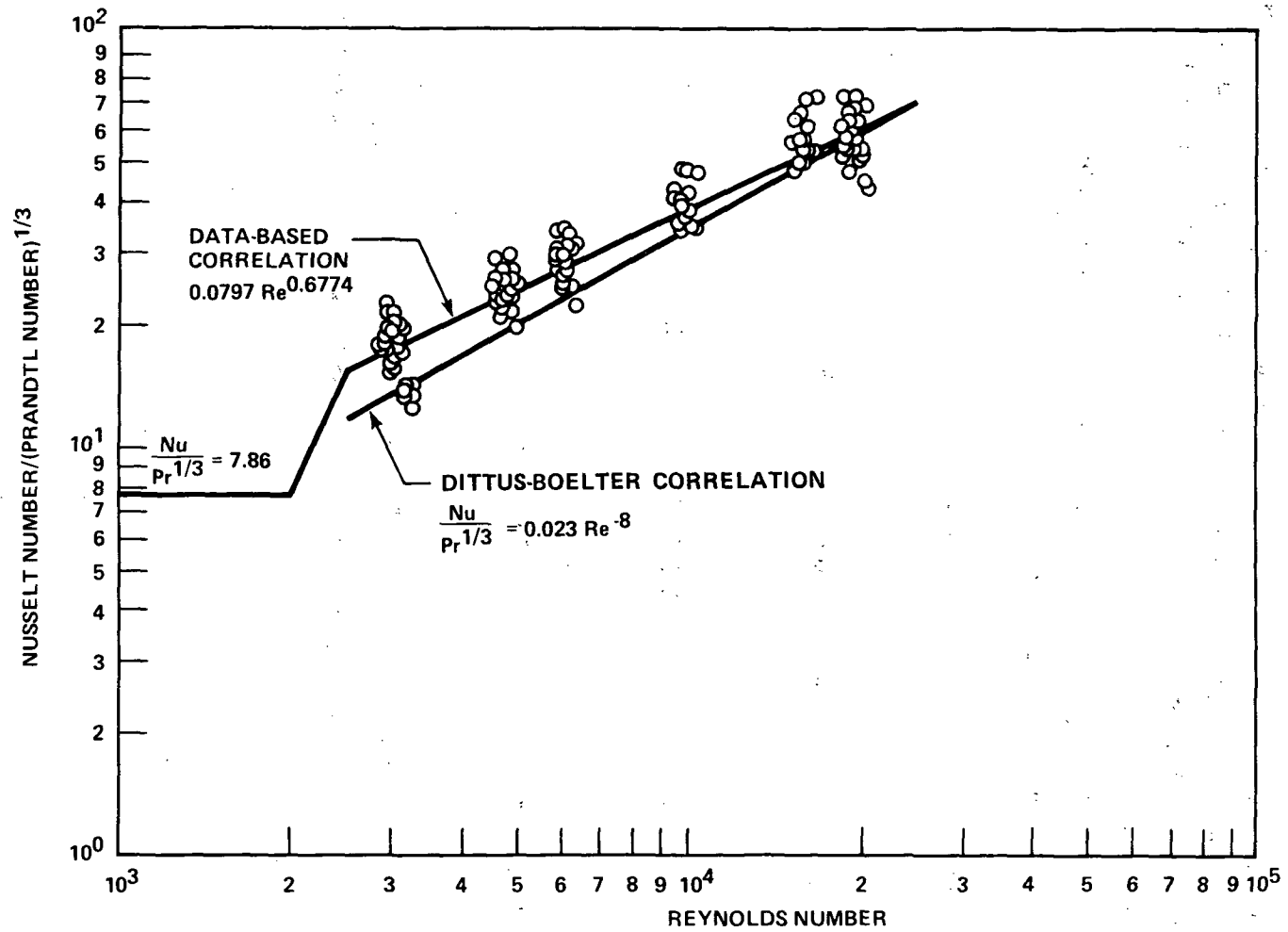


Figure 4-10. Data-Based* Nusselt Number Versus Reynolds Number for Eight Steam Cooling Tests

* Data at least 1 row from housing and disconnected rods, a total of 155 data points used to develop the correlation

Equation (4-1) and the Dittus-Boelter correlation intersect at a Reynolds number equal to 25,200. Hence for Reynolds numbers between 2,500 and 25,200, the data-based correlation [equation (4-1)] is recommended.

At high Reynolds numbers ($Re > 25,200$), the flow is fully turbulent and geometric effects apparently become less important. As the Reynolds number increases, the Nusselt number approaches that predicted by the Dittus-Boelter correlation. Hence for Reynolds numbers above 25,200, the Dittus-Boelter correlation is recommended.

The recommended heat transfer correlations for square rod bundle geometry with a pitch-to-diameter ratio of 1.33 are summarized below:

$$\frac{Nu}{Pr^{1/3}} = 7.86 \quad Re \leq 2,000$$

$$\frac{Nu}{Pr^{1/3}} = -24.55 + 0.0162 Re \quad 2,000 < Re < 2,500$$

$$\frac{Nu}{Pr^{1/3}} = 0.0797 Re^{0.6774} \quad 2,500 \leq Re \leq 25,200$$

(4-2)

$$\frac{Nu}{Pr^{1/3}} = 0.023 Re^{0.8} \quad 25,200 < Re$$

4-6. EFFECTS OF FREE CONVECTION IN BOILOFF TESTS

The effects of free convection can be estimated by comparing the relative magnitudes of Re and $Gr \times Pr \times (D_h/L)$:

$$Gr = \frac{g \beta \Delta T D_h^3}{\nu^2} \quad (4-3)$$

where

- Gr = Grashof number
G = gravitational acceleration (m/sec²)
 β = coefficient of thermal expansion (1/°C)
D_h = hydraulic diameter (m)
L = elevation above froth level (m)
 ν = kinematic viscosity (m²/sec)
 ΔT = temperature difference between wall and fluid (°C)

Figures 4-11 through 4-13 compare the relative effects of forced and free convection for the three boiloff tests at various times and elevations. The Reynolds number is calculated by the mass flow rate (paragraph 3-17), L is calculated from the froth level (paragraph 3-16), the vapor temperature is taken to be the average of all available steam probe data at the same elevation, the wall temperature is taken to be the average of all available heater rod thermocouple data [except those near the housing and the unpowered rods (paragraph 3-10 and figure 3-5)] at the same elevation, and the physical properties are evaluated at the film temperature. Flow regimes in these figures are taken from Metais and Eckert.⁽¹⁾

Figures 4-11 through 4-13 show that effects of forced convection generally dominated those of free convection during the boiloff tests. Hence free convection is not a likely explanation for the large variation in wall heat flux observed among heater rods at the same elevation.

4-7. COMPARISON OF VOID FRACTION AND PRESSURE DROP DATA WITH YEH VOID FRACTION CORRELATION

The measured steady-state void fraction as reduced from pressure drop data in 0.305 m (12 in.) intervals (see paragraph 3-18) was compared with the void fraction predicted by the Yeh void fraction correlation,⁽²⁾ as shown in figures 4-14 through 4-16. These calculations were hand calculations and the data used were not time-averaged. The Yeh void correlation is given below for reference:

$$\alpha = 0.925 \left(\frac{\rho_g}{\rho_f} \right)^{0.239} \left(\frac{V_g}{V_{bcr}} \right)^a \left(\frac{V_g}{V_g + V_f} \right)^{0.6} \quad (4-4)$$

1. Metais, B., and Eckert, E. R. G., "Forced, Mixed, and Free Convection Regimes," *Trans. Am. Soc. Mech. Engrs.* 86, Series C, 295-296 (1964).

2. Yeh, H. C., and Hochreiter, L. E., "Mass Effluence During FLECHT Forced Reflood Experiments," to be published in *Nucl. Eng. and Design*.

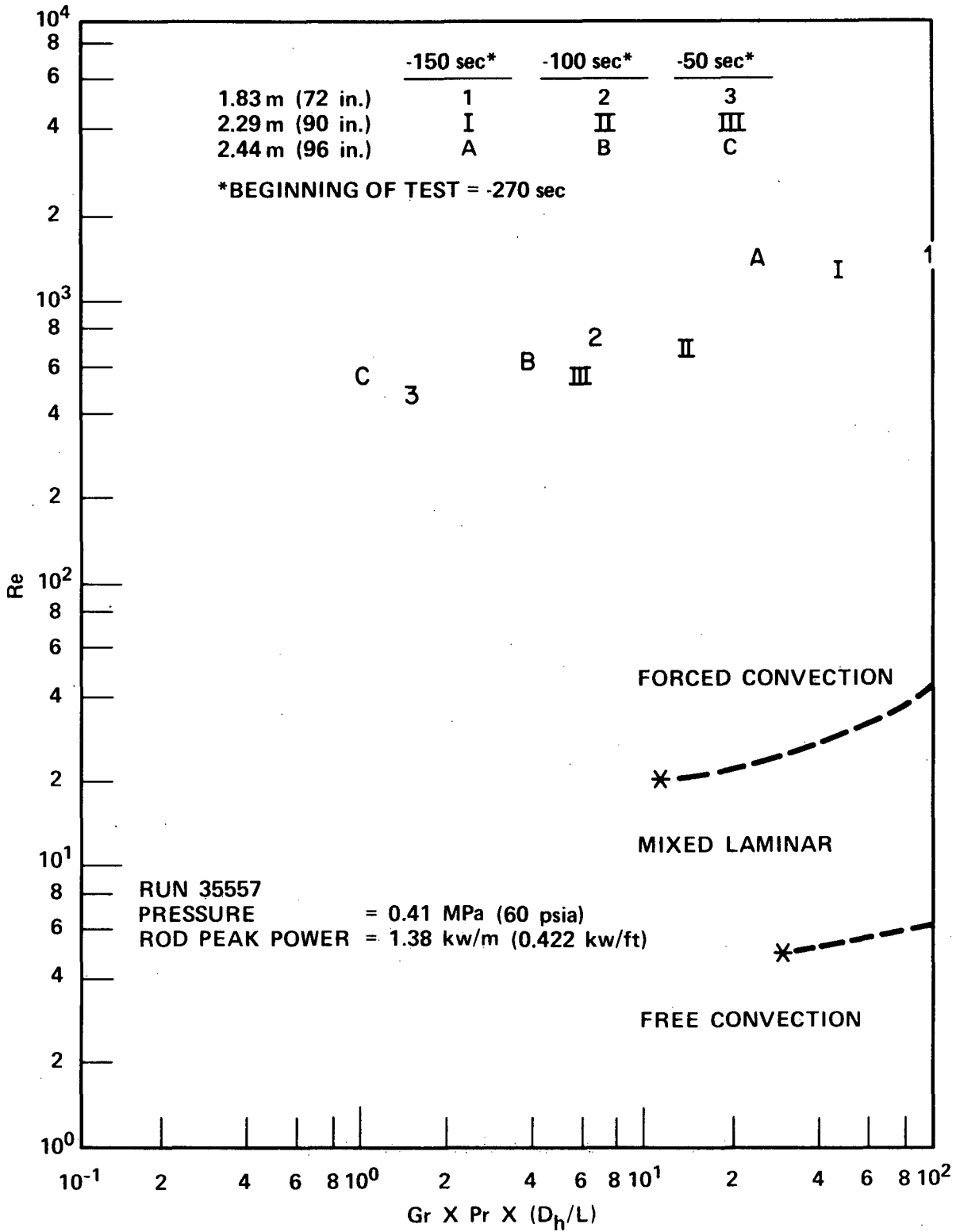


Figure 4-11. Effects of Free Convection in Boiloff Tests, Run 35557

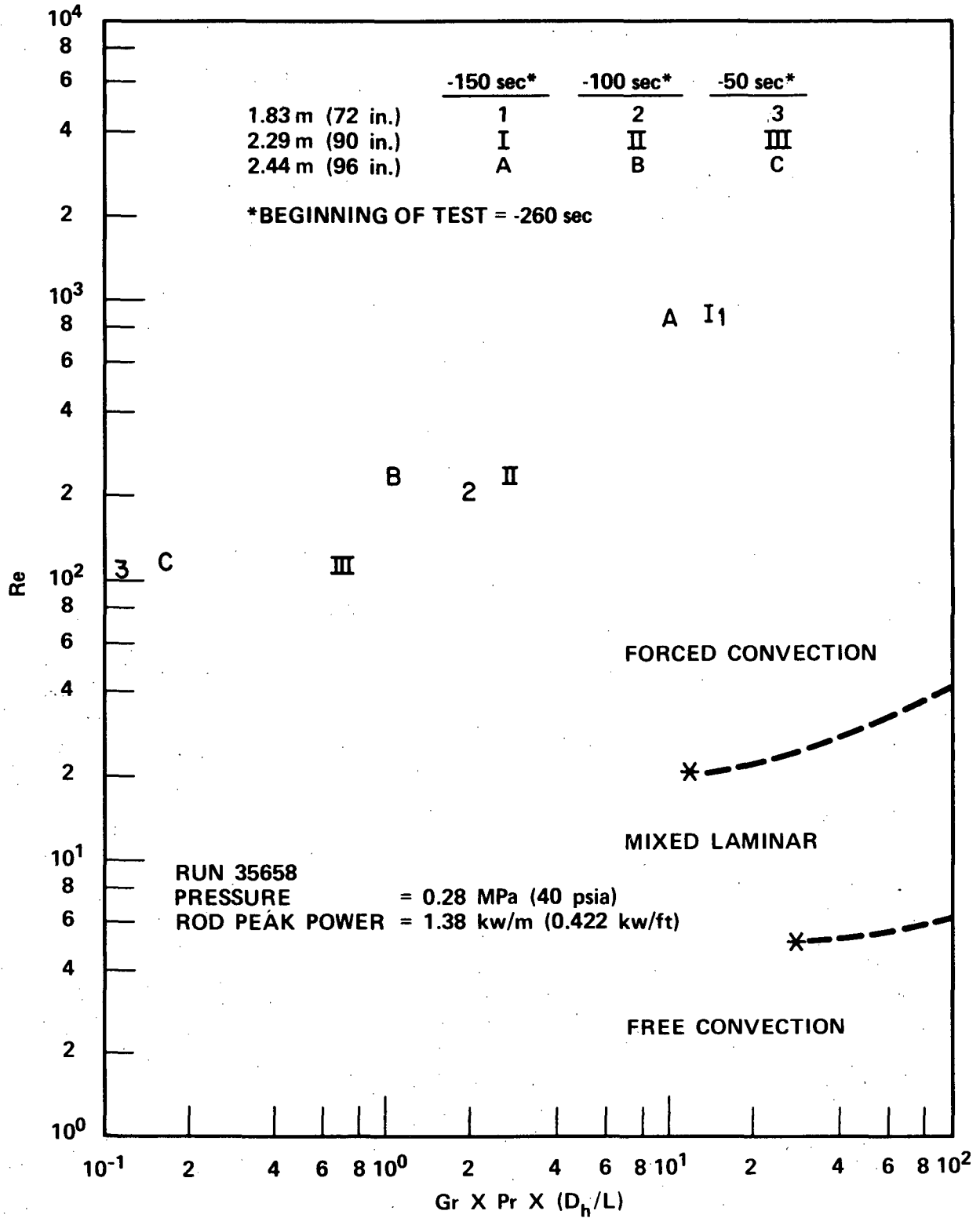


Figure 4-12. Effects of Free Convection in Boiloff Tests, Run 35658

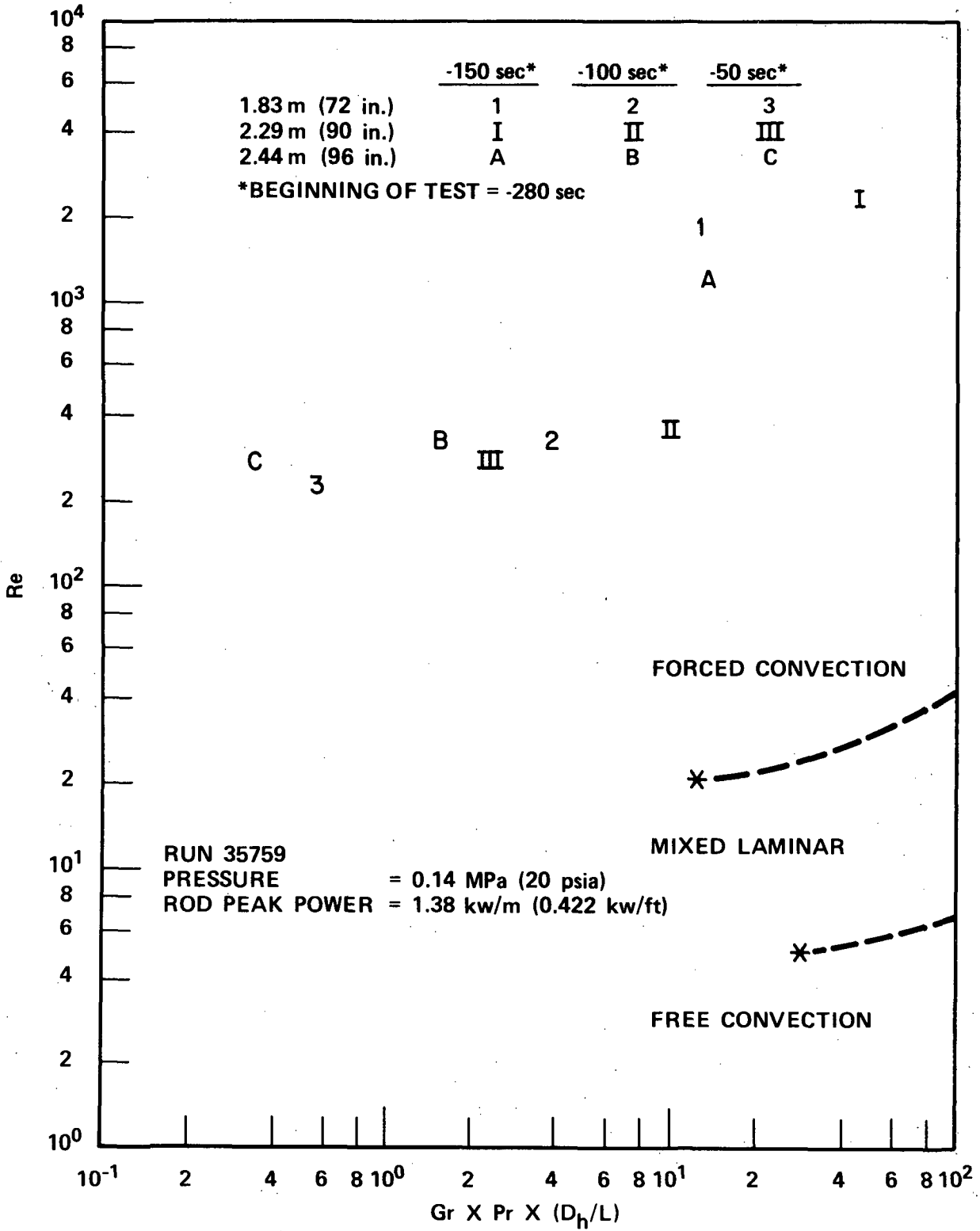


Figure 4-13. Effects of Free Convection in Boiloff Tests, Run 35759

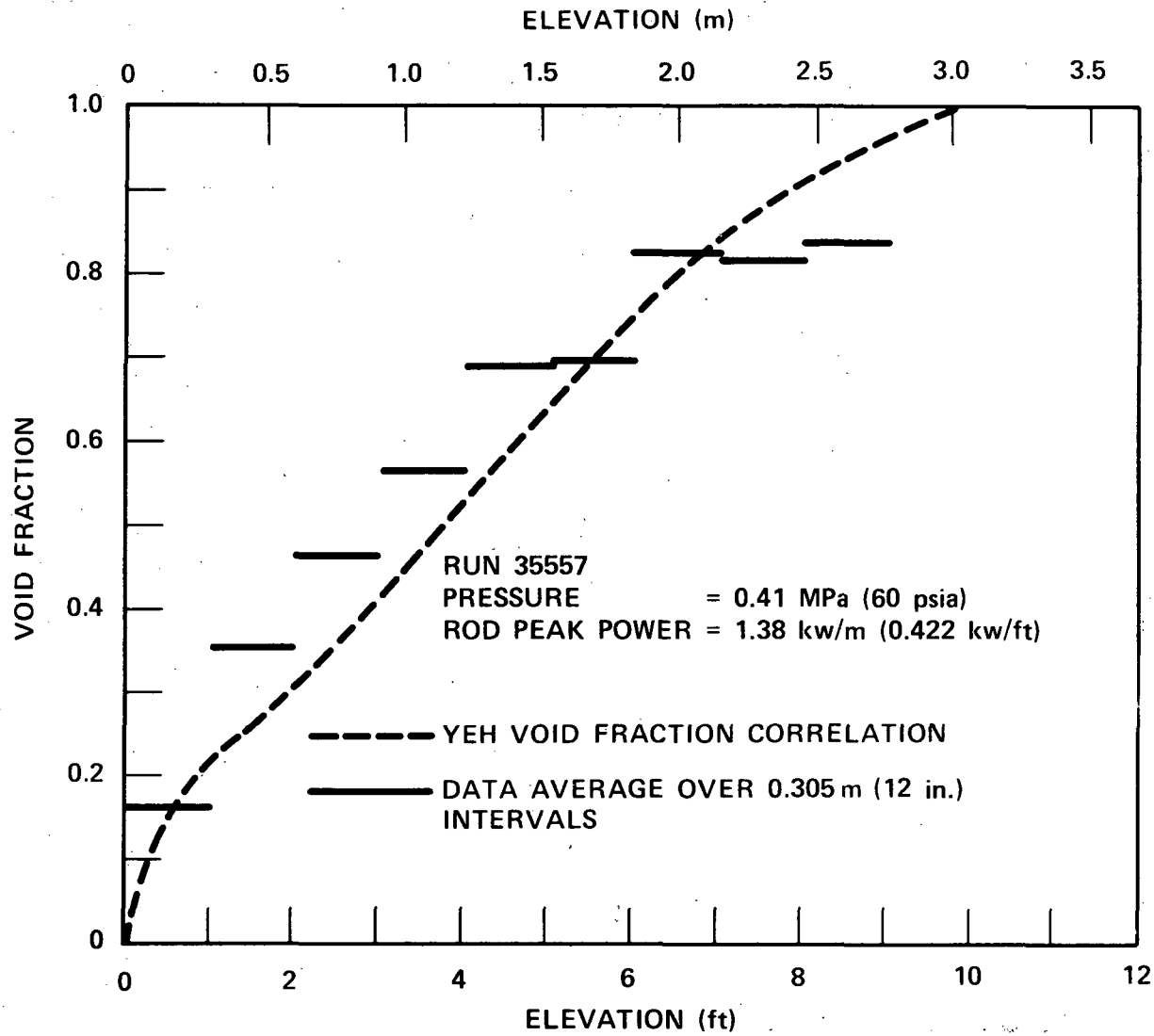


Figure 4-14. Comparison of Steady-State Void Fraction Data With Yeh Correlation, Run 35557

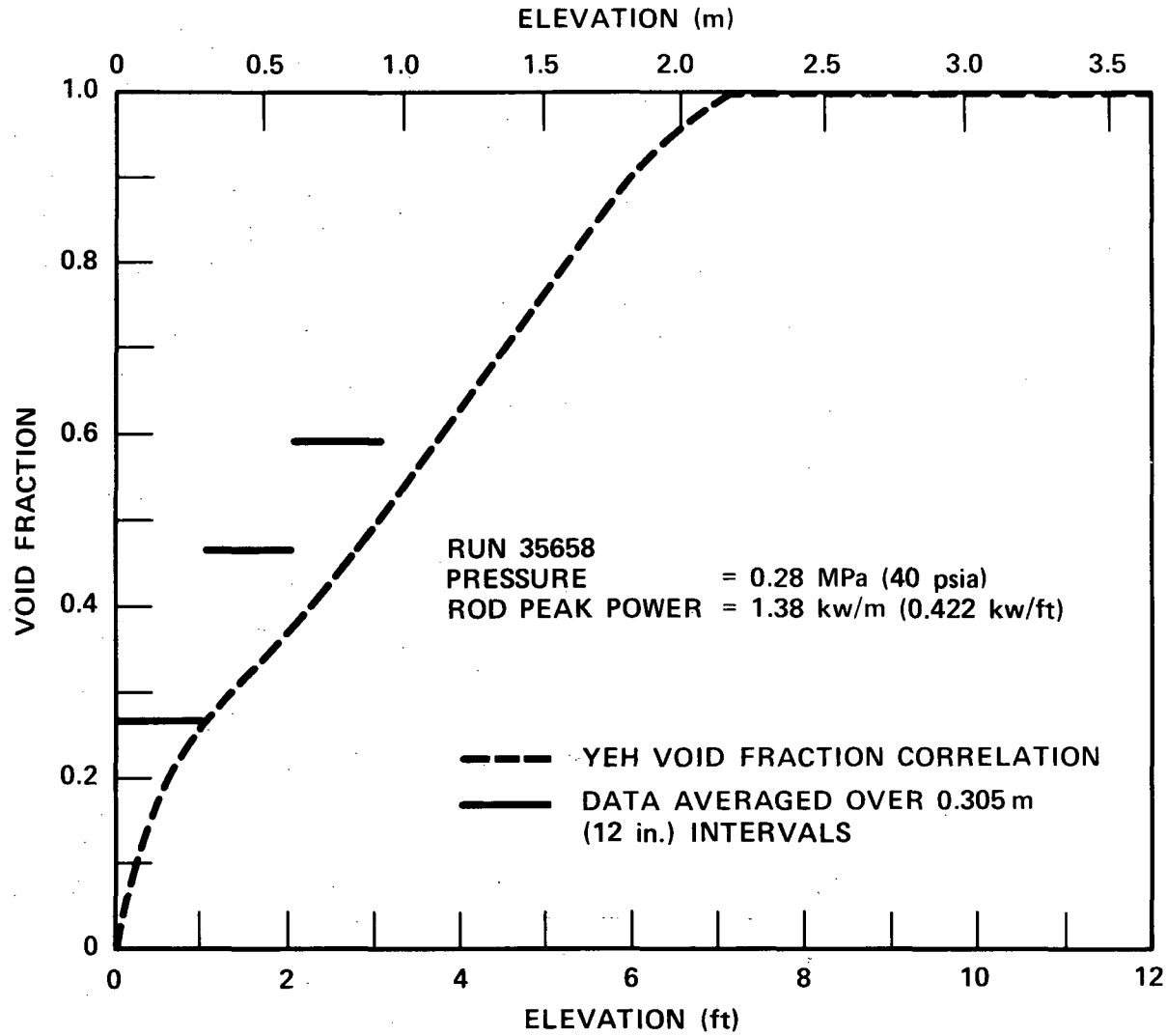


Figure 4-15. Comparison of Steady-State Void Fraction Data With Yeh Correlation, Run 35658

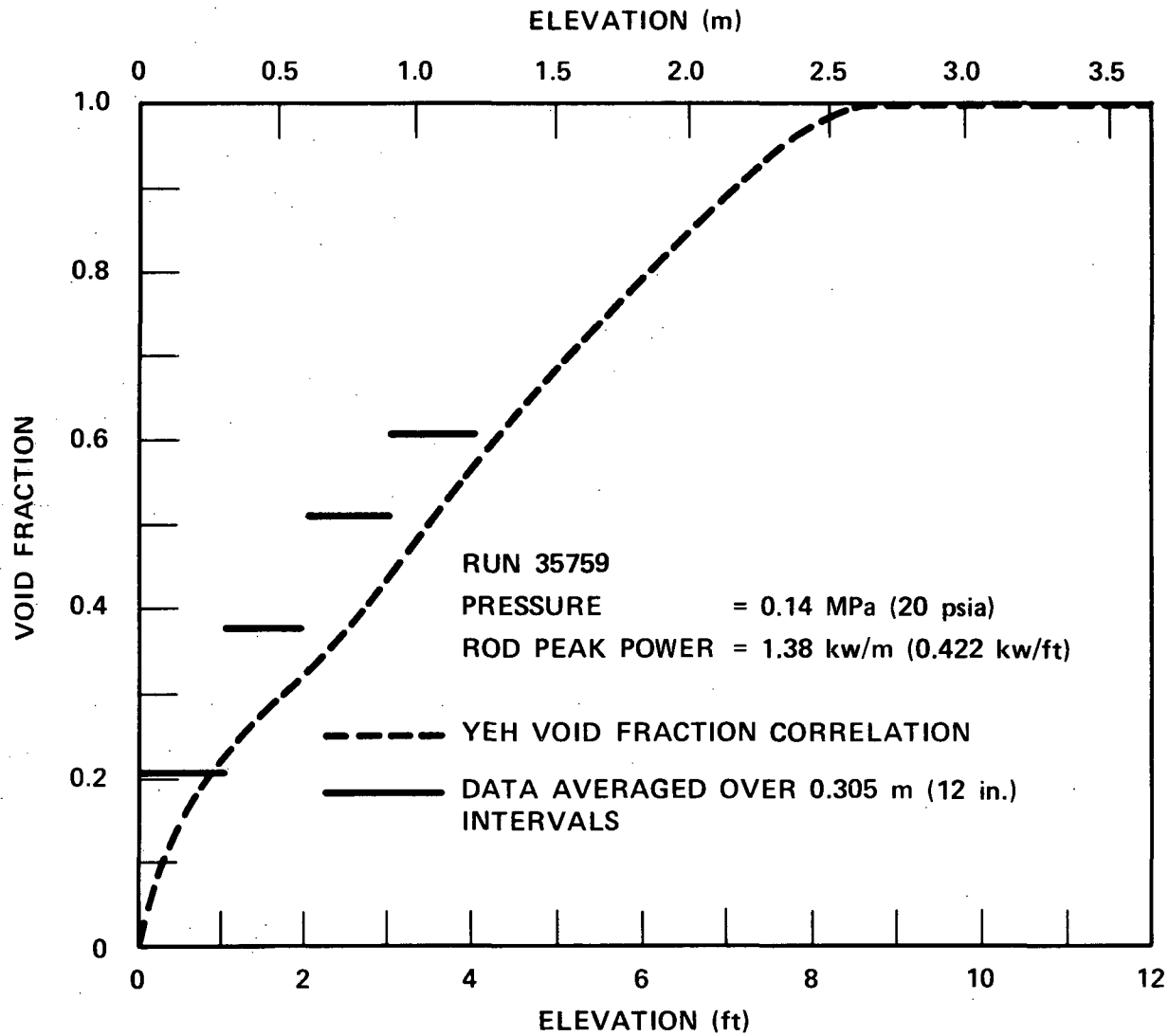


Figure 4-16. Comparison of Steady-State Void Fraction Data With Yeh Correlation, Run 35759

where

$$a = 0.67, \frac{V_g}{V_{bcr}} < 1$$

$$a = 0.47, \frac{V_g}{V_{bcr}} \geq 1$$

$$V_{bcr} = \frac{2}{3} \sqrt{gR_{bcr}}$$

$$R_{bcr} = \left(\frac{1.53}{2/3} \right)^2 \sqrt{\frac{\sigma}{g\rho_f}}$$

α = void fraction

V_g, V_f = superficial velocities of vapor and liquid respectively (m/sec)

σ = surface tension (kg/sec²)

ρ_g, ρ_f = mass densities of vapor and liquid, respectively (kg/m³)

g = gravitational acceleration (m/sec²)

R_{bcr} = critical radius of bubble at the forward stagnation point as defined above (m)

V_{bcr} = critical bubble rise velocity as defined above (m/sec)

When α computed by equation (4-4) is larger than 1, α is defined to be equal to 1.

A better comparison of the Yeh correlation with test data is the comparison of the bundle total pressure drop [the pressure drop between the 0 and 3.05 m (0 and 120 in.) elevations] or the collapsed liquid level. Since the steam flow rate above the froth level is low, both the frictional pressure drop and the pressure drop due to droplets can be neglected. Therefore the bundle total pressure drop is approximately equal to the gravitational pressure drop due to the liquid below the froth level. Thus the total pressure drop can be computed by integrating the net liquid below the froth level with the void fraction predicted by the Yeh correlation, and can be plotted as a function of the froth level. The total pressure drop data are available as a function of time. To convert the time dependence to a function of the froth level, two different methods can be used. In the first method, the froth level as a function of time can be obtained from the wall temperature time history, as described in paragraph 3-16. The second method uses the pressure drop data, as described in paragraph 3-19.

Comparisons of the bundle pressure drop (or collapsed liquid level) calculated by the first and second methods are shown in figures 4-17 through 4-19. For the first method, it is seen that the agreement is good at both the high and the low elevations, but is poor at the middle; this is

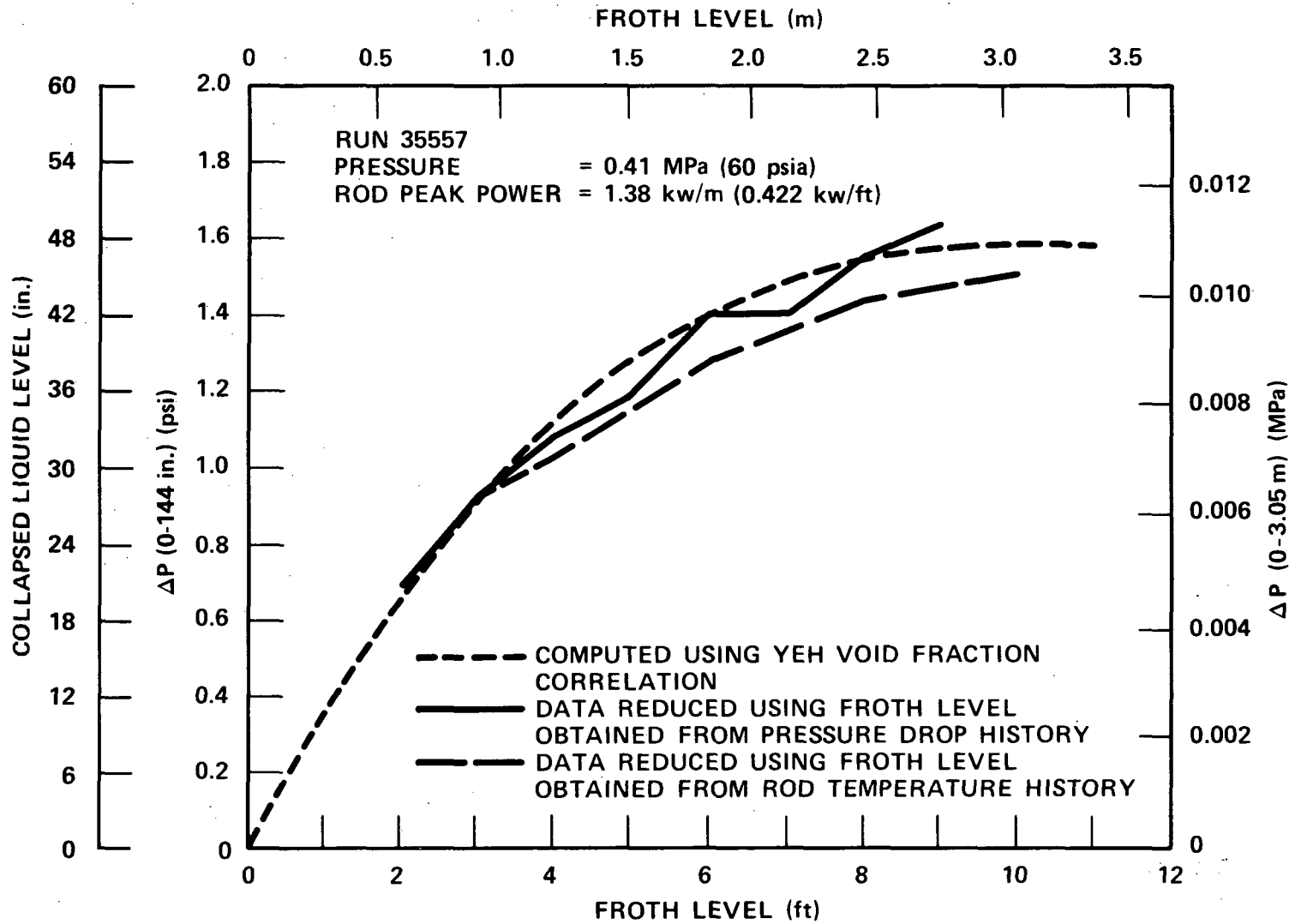


Figure 4-17. Comparison of Pressure Drop Data With Yeh Correlation, Run 35557

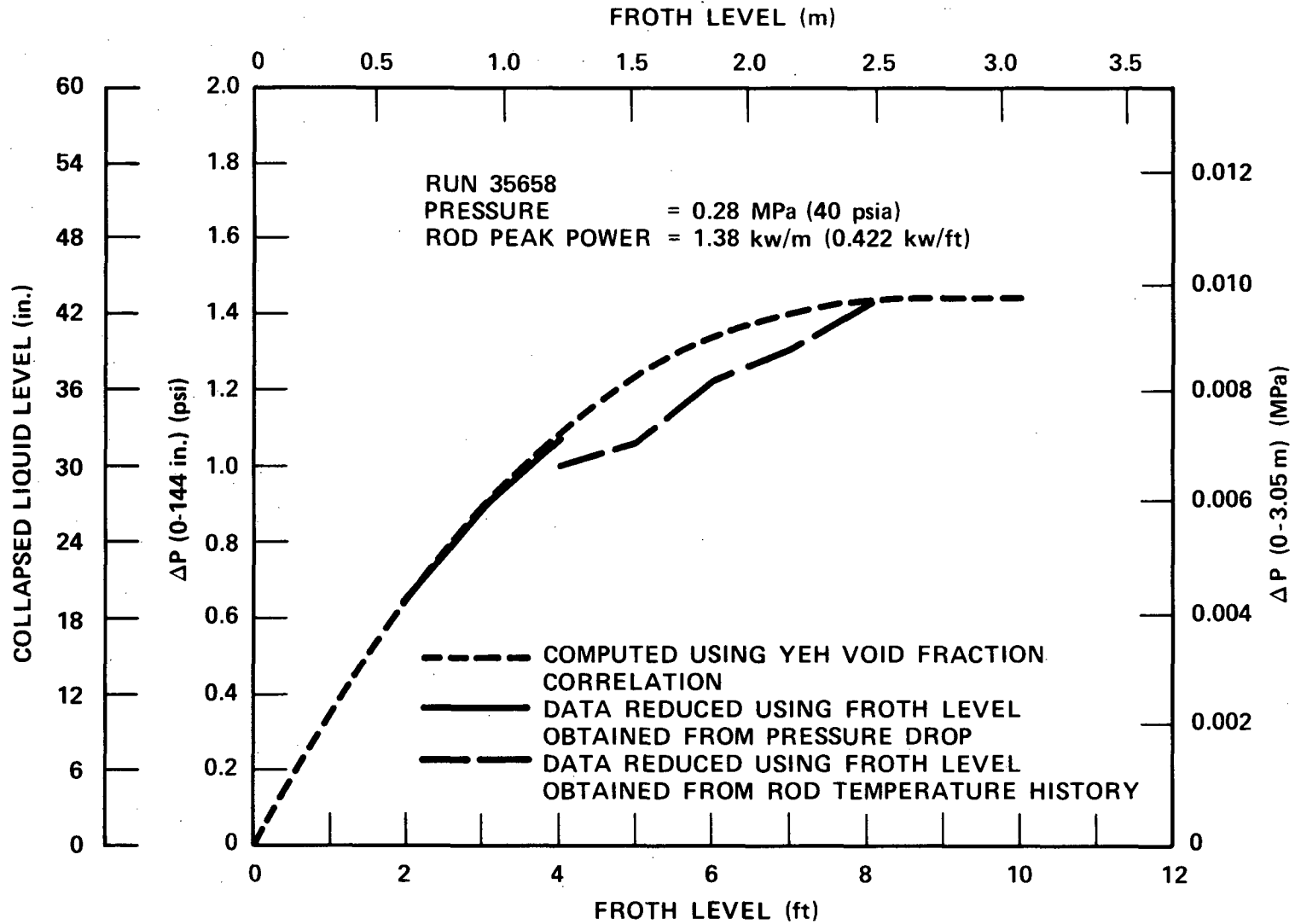


Figure 4-18. Comparison of Pressure Drop Data With Yeh Correlation, Run 35658

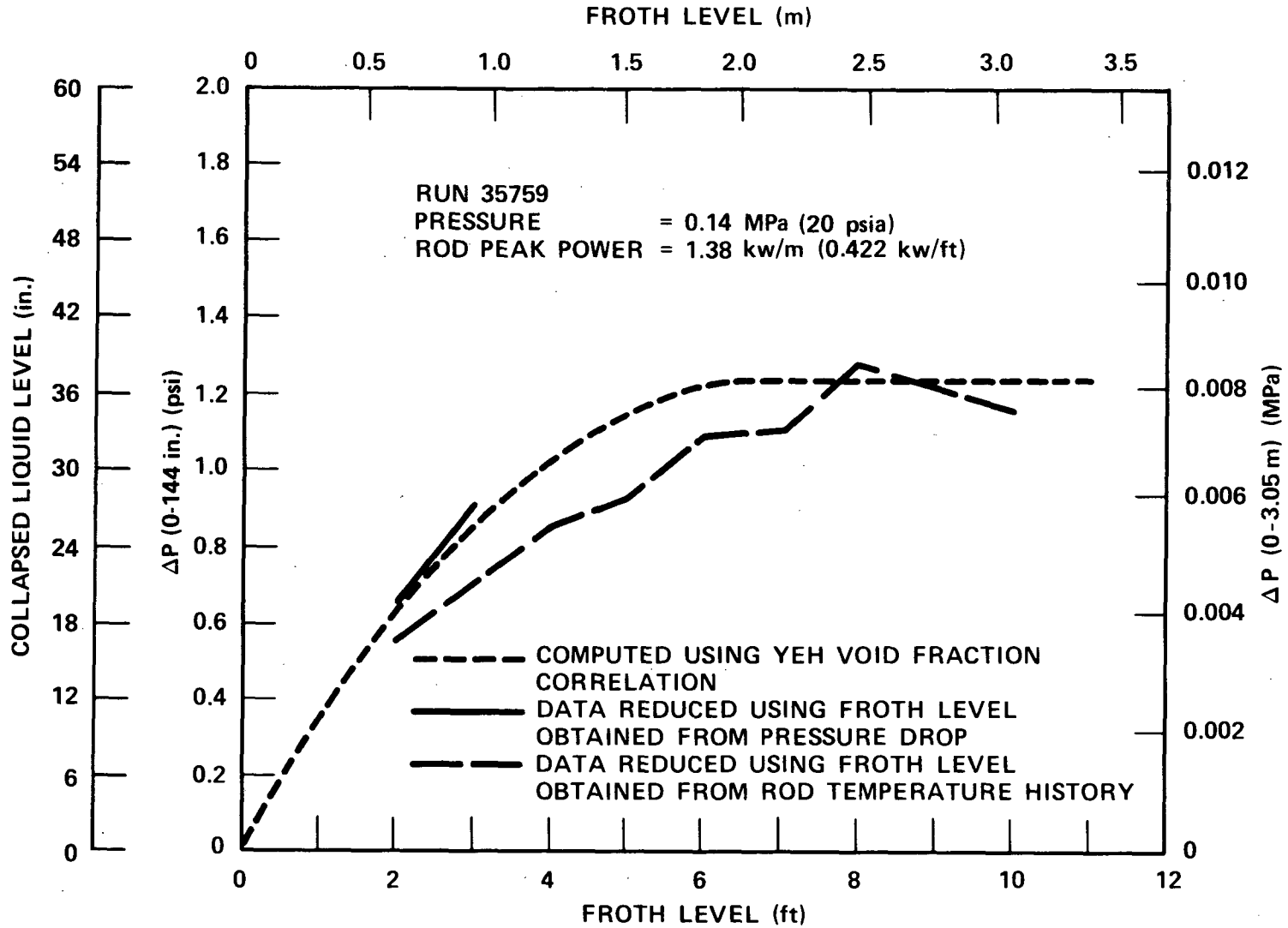


Figure 4-19. Comparison of Pressure Drop Data With Yeh Correlation, Run 35759

probably due to the bundle distortion. For the second method, the agreement is good even at the middle elevations; this is because the determination of the froth level by pressure drop data is not affected by the rod distortion, as explained above. From these comparisons, it can be concluded that the Yeh correlation which was derived from the 15 x 15 rod bundle array data is also valid for 17 x 17 rod bundle array data.

SECTION 5 CONCLUSIONS

5-1. STEAM COOLING TESTS

Heat transfer results calculated from the steam cooling test data show considerable scattering. This is thought to be due to three reasons. First, the rod bundle geometry was distorted, near the housing and between the 1.52 and 2.13 m (60 and 84 in.) elevations. Second, steady-state conditions were not achieved at many of the instrumentation locations. Last, the typical wall-to-vapor temperature difference for the steam cooling tests was small; hence a small error in the calculated vapor temperatures or measured wall temperatures could cause a large error in the calculated heat transfer coefficient (or Nusselt number).

The COBRA-IV-I code was used to simulate the steam cooling experiments, and the most reliable data (that is, data which represent steady-state conditions and good geometry) were used to develop a data-based heat transfer correlation. The data-based Nusselt numbers are generally above those predicted by the Dittus-Boelter correlation, but seem to converge to the Dittus-Boelter correlation at high Reynolds numbers.

The data-based correlation (strictly applicable in the Reynolds number range of data) and the recommended heat transfer correlations for an extended range of Reynolds numbers are given in equation (4-2).

5-2. BOILOFF TESTS

Because of the rod bundle geometry distortion and the large variation of wall heat flux among different rods at the same elevation, no reliable energy balance could be performed for the boiloff tests. The boiloff data were not used to develop heat transfer correlations.

The important information obtained from the boiloff test data is the froth level, the collapsed liquid level (or the total pressure drop), and the void fraction below the froth level. In the event of a core uncover, the froth level marks the interface between two distinct heat transfer regimes. Below the froth level, the walls are wet and the heat removal (usually by nucleate boiling) from the heated rods is extremely efficient. Above the froth level, there is a marked increase in void fraction and wall temperatures; the walls are dry and are cooled by forced convection to pure steam flow or dispersed droplet flow. The froth level must be predicted correctly for accurate calculation of the wall temperature transients.

The mass flow above the froth level was calculated from the total pressure drop data. The effects of free convection were also estimated by comparing the calculated Reynolds number and the Grashof number. It was found that forced convection dominated for all three boiloff tests.

The pressure drop and void fraction data were compared with predictions by the Yeh void fraction correlation. The satisfactory agreement shown by the comparisons verifies the Yeh correlation and the validity of the boiloff test pressure drop data.

APPENDIX A

SUMMARY OF DATA SCREENING AND CALCULATED HEAT TRANSFER RESULTS FOR EIGHT STEAM COOLING TESTS

Tables A-1 through A-8 summarize all the connected heater rod thermocouple data between the inlet and 1.52 m (60 in.) elevations for runs 32753, 36160, 36261, 36362, 36463, 36564, 36766, and 36867. The tables also show which thermocouple data were used for analysis and include the reasons for discarding the others.

Table A-9 presents the calculated wall heat flux, wall surface temperature, vapor temperature, Nusselt number, and Reynolds number at each instrumentation location for the eight steam cooling tests. The vapor temperature and the Nusselt and Reynolds numbers calculated by the rod-centered subchannel energy balance and the COBRA-IV-I analysis are presented for comparison. (Table A-9a presents the results in metric units and table A-9b in English units.)

TABLE A-1
SUMMARY OF DATA SELECTION BETWEEN 0 AND 1.52 m (0 AND 60 in.)
ELEVATIONS, RUN 32753

Connected Thermocouple Location	Elevation [m(in.)]	Used for Analysis?	Reason	
6J	0.305 (12)	Yes	Non-steady-state Near unpowered rods	
9G	0.305 (12)	Yes		
11I	0.305 (12)	No		
5H	0.610 (24)	No		
8N	0.610 (24)	Yes		
12F	0.610 (24)	Yes		
6J	0.991 (39)	Yes		
9G	0.991 (39)	Yes		
5E	0.991 (39)	Yes		
2H	1.22 (48)	Yes		Near unpowered rods
5H	1.22 (48)	No		
5J	1.22 (48)	Yes		
8H	1.22 (48)	Yes		
8K	1.22 (48)	Yes		
8N	1.22 (48)	Yes		
12D	1.22 (48)	Yes		
3C	1.52 (60)	No	Near housing Near housing	
3M	1.52 (60)	No		
4J	1.52 (60)	Yes		
11G	1.52 (60)	Yes		
6J	1.52 (60)	Yes		
10H	1.52 (60)	Yes		
7G	1.52 (60)	Yes		
9I	1.52 (60)	Yes		
11I	1.52 (60)	Yes		
11E	1.52 (60)	Yes		
13M	1.52 (60)	No		Near housing
10G	1.52 (60)	Yes		Non-steady-state
7J	1.52 (60)	Yes		
13J	1.52 (60)	No		

TABLE A-2
SUMMARY OF DATA SELECTION BETWEEN 0 AND 1.52 m (0 AND 60 in.)
ELEVATIONS, RUN 36160

Connected Thermocouple Location	Elevation [m(in.)]	Used for Analysis?	Reason
6J	0.305 (12)	No	Negative heat transfer coefficient ($T_w < T_v$)
9G	0.305 (12)	Yes	
11E	0.305 (12)	Yes	
5H	0.610 (24)	No	Near unpowered rods
8N	0.610 (24)	Yes	
8K	0.610 (24)	Yes	
6J	0.991 (39)	No	Negative heat transfer coefficient ($T_w < T_v$)
9G	0.991 (39)	Yes	
11G	0.991 (39)	Yes	
2H	1.22 (48)	Yes	
5H	1.22 (48)	No	Near unpowered rods
5J	1.22 (48)	Yes	
8H	1.22 (48)	Yes	
8K	1.22 (48)	Yes	
8N	1.22 (48)	Yes	
8E	1.22 (48)	Yes	
12D	1.22 (48)	Yes	
3C	1.52 (60)	No	Near housing
10M	1.52 (60)	Yes	
3M	1.52 (60)	No	Near housing
11G	1.52 (60)	No	Non-steady-state
6J	1.52 (60)	No	Negative heat transfer coefficient ($T_w < T_v$)
10H	1.52 (60)	No	Near unpowered rods
7G	1.52 (60)	Yes	
9I	1.52 (60)	Yes	
6G	1.52 (60)	No	Near unpowered rods
13M	1.52 (60)	No	Near housing

TABLE A-3
SUMMARY OF DATA SELECTION BETWEEN 0 AND 1.52 m (0 AND 60 in.)
ELEVATIONS, RUN 36261

Connected Thermocouple Location	Elevation [m(in.)]	Used for Analysis?	Reason
6J	0.305 (12)	No	Negative heat transfer coefficient ($T_w < T_v$)
9G	0.305 (12)	Yes	
11E	0.305 (12)	Yes	
5H	0.610 (24)	No	Near unpowered rods
8N	0.610 (24)	Yes	
8K	0.610 (24)	Yes	
6J	0.991 (39)	No	Negative heat transfer coefficient ($T_w < T_v$)
9G	0.991 (39)	Yes	
11G	0.991 (39)	Yes	
2H	1.22 (48)	Yes	
5H	1.22 (48)		Near unpowered rods
5J	1.22 (48)	Yes	
8H	1.22 (48)	Yes	
8K	1.22 (48)	Yes	
8N	1.22 (48)	Yes	
8E	1.22 (48)	Yes	
12D	1.22 (48)	Yes	
3C	1.52 (60)	No	Near housing
10M	1.52 (60)	Yes	
3M	1.52 (60)	No	Near housing
11G	1.52 (60)	Yes	
6J	1.52 (60)	No	Negative heat transfer coefficient ($T_w < T_v$)
10H	1.52 (60)	No	Near unpowered rods
7G	1.52 (60)	Yes	
9I	1.52 (60)	Yes	
6G	1.52 (60)	No	Near unpowered rods
13M	1.52 (60)	No	Near housing

TABLE A-4
SUMMARY OF DATA SELECTION BETWEEN 0 AND 1.52 m (0 AND 60 in.)
ELEVATIONS, RUN 36362

Connected Thermocouple Location	Elevation [m(in.)]	Used for Analysis?	Reason
6J	0.305 (12)	Yes	Near unpowered rods
9G	0.305 (12)	Yes	
11E	0.305 (12)	Yes	
5H	0.610 (24)	No	
8N	0.610 (24)	Yes	
8K	0.610 (24)	Yes	
6J	0.991 (39)	Yes	
9G	0.991 (39)	Yes	
11G	0.991 (39)	Yes	
2H	1.22 (48)	Yes	
5H	1.22 (48)	No	
5J	1.22 (48)	Yes	
8H	1.22 (48)	Yes	
8K	1.22 (48)	Yes	
8N	1.22 (48)	Yes	
12D	1.22 (48)	Yes	
8E	1.22 (48)	Yes	
3C	1.52 (60)	No	Near housing
10M	1.52 (60)	Yes	Near housing
3M	1.52 (60)	No	
11G	1.52 (60)	Yes	Near unpowered rods
6J	1.52 (60)	Yes	
10H	1.52 (60)	No	
7G	1.52 (60)	No	Non-steady-state
9I	1.52 (60)	Yes	Near unpowered rods
6G	1.52 (60)	No	
13M	1.52 (60)	No	

TABLE A-5
SUMMARY OF DATA SELECTION BETWEEN 0 AND 1.52 m (0 AND 60 in.)
ELEVATIONS, RUN 36463

Connected Thermocouple Location	Elevation [m(in.)]	Used for Analysis?	Reason
6J	0.305 (12)	Yes	
9G	0.305 (12)	Yes	
11E	0.305 (12)	Yes	
5H	0.610 (24)	No	Near unpowered rods
8N	0.610 (24)	Yes	
8K	0.610 (24)	Yes	
8E	0.610 (24)	No	Non-steady-state
6J	0.991 (39)	Yes	
9G	0.991 (39)	Yes	
11G	0.991 (39)	Yes	
2H	1.22 (48)	Yes	
5H	1.22 (48)	No	Near unpowered rods
5J	1.22 (48)	Yes	
8H	1.22 (48)	Yes	
8K	1.22 (48)	Yes	
8N	1.22 (48)	Yes	
12D	1.22 (48)	Yes	
8E	1.22 (48)	Yes	
3C	1.52 (60)	No	Near housing
10M	1.52 (60)	Yes	
3M	1.52 (60)	No	Near housing
11G	1.52 (60)	Yes	
6J	1.52 (60)	Yes	
10H	1.52 (60)	No	Near unpowered rods
7G	1.52 (60)	Yes	
9I	1.52 (60)	Yes	
6G	1.52 (60)	No	Near unpowered rods
13M	1.52 (60)	No	Near housing

TABLE A-6
SUMMARY OF DATA SELECTION BETWEEN 0 AND 1.52 m (0 AND 60 in.)
ELEVATIONS, RUN 36564

Connected Thermocouple Location	Elevation [m(in.)]	Used for Analysis?	Reason
6J	0.305 (12)	Yes	
9G	0.305 (12)	Yes	
11E	0.305 (12)	Yes	
5H	0.610 (24)	No	Near unpowered rods
8N	0.610 (24)	Yes	
8K	0.610 (24)	Yes	
8E	0.610 (24)	No	Non-steady-state
6J	0.991 (39)	Yes	
9G	0.991 (39)	Yes	
11G	0.991 (39)	Yes	
2H	1.22 (48)	Yes	
5H	1.22 (48)	No	Near unpowered rods
5J	1.22 (48)	Yes	
8H	1.22 (48)	Yes	
8K	1.22 (48)	Yes	
8N	1.22 (48)	Yes	
12D	1.22 (48)	Yes	
8E	1.22 (48)	Yes	
3C	1.52 (60)	No	Near housing
10M	1.52 (60)	Yes	
3M	1.52 (60)	No	Near housing
11G	1.52 (60)	Yes	
6J	1.52 (60)	Yes	
10H	1.52 (60)	No	Near unpowered rods
7G	1.52 (60)	Yes	
9I	1.52 (60)	Yes	
6G	1.52 (60)	No	Near unpowered rods
13M	1.52 (60)	No	Near housing

TABLE A-7
SUMMARY OF DATA SELECTION BETWEEN 0 AND 1.52 m (0 AND 60 in.)
ELEVATIONS, RUN 36766

Connected Thermocouple Location	Elevation [m(in.)]	Used for Analysis?	Reason
6J	0.305 (12)	Yes	Near unpowered rods
9G	0.305 (12)	Yes	
11E	0.305 (12)	Yes	
5H	0.610 (24)	No	
8N	0.610 (24)	Yes	
8K	0.610 (24)	Yes	
8E	0.610 (24)	Yes	
6J	0.991 (39)	Yes	
9G	0.991 (39)	Yes	
11G	0.991 (39)	Yes	
2H	1.22 (48)	Yes	Near unpowered rods
5H	1.22 (48)	No	
5J	1.22 (48)	Yes	
8H	1.22 (48)	Yes	
8K	1.22 (48)	Yes	
8N	1.22 (48)	Yes	
12D	1.22 (48)	Yes	
8E	1.22 (48)	Yes	
3C	1.52 (60)	No	Near housing
10M	1.52 (60)	Yes	Near housing
3M	1.52 (60)	No	
11G	1.52 (60)	Yes	Near unpowered rods
6J	1.52 (60)	Yes	
10H	1.52 (60)	No	
9I	1.52 (60)	Yes	Near unpowered rods
6G	1.52 (60)	No	
13M	1.52 (60)	No	

TABLE A-8
SUMMARY OF DATA SELECTION BETWEEN 0 AND 1.52 m (0 AND 60 in.)
ELEVATIONS, RUN 36867

Connected Thermocouple Location	Elevation [m(in.)]	Used for Analysis?	Reason	
6J	0.305 (12)	Yes	Near unpowered rods	
9G	0.305 (12)	Yes		
11E	0.305 (12)	Yes		
5H	0.610 (24)	No		
8N	0.610 (24)	Yes		
8K	0.610 (24)	Yes		
8E	0.610 (24)	Yes		
6J	0.991 (39)	Yes		
9G	0.991 (39)	Yes		
11G	0.991 (39)	Yes		
2H	1.22 (48)	Yes	Near unpowered rods	
5H	1.22 (48)	No		
5J	1.22 (48)	Yes		
8H	1.22 (48)	Yes		
8K	1.22 (48)	Yes		
8N	1.22 (48)	Yes		
12D	1.22 (48)	Yes		
8E	1.22 (48)	Yes		
3C	1.52 (60)	No		Near housing
10M	1.52 (60)	Yes		Near housing
3M	1.52 (60)	No		
11G	1.52 (60)	Yes	Near unpowered rods	
6J	1.52 (60)	Yes		
10H	1.52 (60)	No		
9I	1.52 (60)	Yes	Near unpowered rods	
6G	1.52 (60)	No		
13M	1.52 (60)	No		Near housing

TABLE A-9a

CALCULATED RESULTS AT VARIOUS THERMOCOUPLE
LOCATIONS FOR EIGHT STEAM COOLING TESTS

RUN 32753

MASS FLOW = .36KG/SEC

INLET VAPOR TEMP = 131.7 DEG C

TOTAL POWER = 58.26 KW

Z (M)	ROD LOCATION	HEAT FLUX (WATT/SQM)	WALL SURFACE TEMP DEG C	VAPOR TEMP ROD*	(DEG C) COBRA+	NU /PR**+.33 ROD* COBRA+	REYNOLDS NO. ROD* COBRA+
.30	6J	1447.05	146.73	134.69	134.27	49.17 47.53	20041.8 20266.5
.30	9G	1385.04	146.75	134.59	134.27	46.62 45.39	20043.7 20665.7
	AVE	1416.05	146.74	134.64	134.27	47.89 46.46	20042.8 20466.1
.61	8N	2380.76	154.86	137.97	137.41	56.88 55.08	19743.6 20110.9
.61	12F	2135.37	151.54	137.72	137.26	62.65 60.61	19836.3 19579.9
	AVE	2258.06	153.20	137.85	137.34	59.76 57.84	19790.0 19995.4
.99	6J	3833.48	168.73	145.73	143.94	65.52 60.89	19191.3 19524.6
.99	9G	3777.09	171.38	145.29	143.93	56.73 53.98	19135.9 19896.8
.99	5E	3741.47	169.44	145.12	143.55	60.47 56.88	19188.7 20064.5
	AVE	3764.01	169.85	145.38	143.81	60.91 57.25	19172.0 19828.6
1.22	2H	4469.77	179.48	151.38	149.67	61.27 57.84	18784.9 19467.7
1.22	5J	4510.86	179.09	151.66	149.34	63.32 58.53	18787.5 18523.0
1.22	8H	3982.79	179.87	149.78	149.35	51.05 50.33	18814.3 19095.8
1.22	8K	4323.75	176.45	151.81	149.88	66.76 62.99	18858.4 19166.7
1.22	8N	4469.45	178.90	151.90	150.09	63.75 59.85	18786.6 19454.9
1.22	12D	4346.95	172.79	151.90	149.28	90.72 71.94	18936.5 19348.8
	AVE	4350.59	177.76	151.34	149.60	64.48 60.25	18828.0 19176.1
1.52	4J	5468.90	190.10	161.53	158.62	71.84 65.39	18286.8 18334.9
1.52	11G	5383.49	191.55	162.06	159.18	68.33 62.44	18239.5 19099.8
1.52	6J	5629.34	191.40	162.90	158.85	73.88 64.97	18223.5 19670.1
1.52	10H	5305.16	191.25	161.05	158.69	65.88 61.25	18270.4 18700.2
1.52	7G	5055.61	191.14	160.58	157.60	62.55 57.18	18284.1 19764.5
1.52	9I	5082.53	191.07	160.37	158.59	62.14 58.81	18290.5 18704.6
1.52	11I	5514.63	189.34	162.66	158.53	77.25 67.44	18279.8 19976.9
1.52	11E	5335.26	192.72	162.17	159.29	65.28 59.82	18209.5 19079.1
1.52	10G	5137.09	192.47	160.82	158.80	59.78 56.37	18235.4 18642.7
1.52	7J	5207.25	188.37	160.76	158.92	70.98 66.68	18345.3 18753.4
	AVE	5315.93	190.99	161.48	158.71	67.79 62.04	18266.4 18762.6

* ROD-CENTERED SUBCHANNEL ENERGY BALANCE
+ COBRA-IV-I ANALYSIS

A-10

TABLE A-9a (cont)

CALCULATED RESULTS AT VARIOUS THERMOCOUPLE
LOCATIONS FOR EIGHT STEAM COOLING TESTS

RUN 36160

MASS FLOW = .36KG/SEC

INLET VAPOR TEMP = 144.4 DEG C

TOTAL POWER = 52.89 KW

Z (M)	ROD LOCATION	HEAT FLUX (WATT/SQM)	WALL SURFACE TEMP DEG C	VAPOR TEMP (DEG C)		NU / PR** .33		REYNOLDS NO.†	
				ROD*	COBRA+	ROD*	COBRA+	ROD*	COBRA+
.30	9G	1320.15	154.03	147.24	146.93	77.67	74.18	19769.8	20237.0
.30	11E	1376.66	157.09	147.27	146.99	55.79	54.23	19690.2	20136.4
	AVE	1348.40	155.56	147.26	146.96	66.73	64.21	19730.0	20186.7
.61	8N	2264.11	163.14	150.46	149.94	70.20	67.45	19453.0	19529.0
.61	8K	2142.75	160.78	150.83	149.83	80.91	77.25	19516.8	19520.7
	AVE	2203.43	161.96	150.39	149.88	75.55	72.35	19484.9	19574.8
.99	9G	3600.11	177.13	157.45	156.24	70.15	66.15	18927.8	19204.3
.99	11G	3547.95	173.46	157.52	155.95	85.70	78.13	19016.6	19329.7
	AVE	3574.03	175.29	157.49	156.10	77.93	72.14	18972.2	19267.0
1.22	2H	4250.76	186.24	163.22	161.73	69.47	65.35	18566.7	19238.3
1.22	5J	4259.50	182.49	163.52	161.41	95.65	77.24	18649.6	18498.5
1.22	8H	3796.17	185.06	161.73	161.36	61.44	60.47	18630.6	18911.2
1.22	8K	4121.15	183.82	163.29	161.83	75.74	70.80	18623.2	18917.6
1.22	8N	4250.46	188.15	163.70	162.14	65.24	61.40	18509.5	19153.5
1.22	12D	4158.82	188.76	163.82	161.43	62.49	57.17	18492.1	18881.0
1.22	8E	4206.39	189.34	163.46	162.05	60.91	57.83	18487.0	18777.8
	AVE	4154.75	186.27	163.25	161.71	68.71	64.32	18565.5	18912.5
1.52	10M	5076.43	198.99	172.40	170.62	69.87	65.60	18052.1	18300.3
1.52	7G	4856.84	201.59	172.00	169.34	59.91	55.12	18001.4	18515.2
1.52	9I	4844.38	200.39	171.81	168.94	61.98	56.49	18033.4	18568.3
	AVE	4925.89	200.32	172.07	169.63	63.92	59.07	18029.0	18461.6

* ROD-CENTERED SUBCHANNEL ENERGY BALANCE
+ COBRA-IV-I ANALYSIS

TABLE A-9a (cont)

CALCULATED RESULTS AT VARIOUS THERMOCOUPLE
LOCATIONS FOR EIGHT STEAM COOLING TESTS

RUN 36261

MASS FLOW = .29KG/SEC

INLET VAPOR TEMP = 141.7 DEG C

TOTAL POWER = 42.81 KW

Z (M)	ROD LOCATION	HEAT FLUX (WATT/SQM)	WALL SURFACE TEMP DEG C	VAPOR TEMP (DEG C)		NU /PR** .33		REYNOLDS NO.†	
				ROD*	COBRA+	ROD*	COBRA+	ROD*	COBRA+
.30	9G	1070.98	149.77	144.47	144.15	81.33	76.72	16135.2	16533.6
.30	11E	1116.83	152.12	144.49	144.21	58.77	56.67	16084.9	16468.3
	AVE	1093.91	150.95	144.48	144.18	70.05	66.70	16110.0	16500.9
.61	8N	1836.79	160.10	147.68	147.16	58.60	56.23	15851.0	16318.7
.61	8K	1738.33	157.73	147.55	147.05	67.88	64.71	15903.1	15727.1
	AVE	1787.56	158.91	147.61	147.10	63.24	60.47	15877.0	15772.9
.99	9G	2920.63	172.26	154.63	153.46	64.30	60.17	15458.8	15710.1
.99	11G	2878.32	168.00	154.75	153.16	84.49	75.58	15543.6	15924.8
	AVE	2899.47	170.13	154.71	153.31	74.39	67.88	15501.2	15767.5
1.22	2H	3448.48	182.02	160.45	158.95	60.66	56.79	15150.0	15726.3
1.22	5J	3488.02	178.36	160.75	158.63	75.52	67.53	15216.2	15106.2
1.22	6H	3079.69	180.79	158.96	158.57	53.76	52.81	15203.6	15461.3
1.22	8K	3343.33	180.21	160.52	159.03	64.57	60.12	15184.2	15452.9
1.22	8N	3448.23	184.29	160.93	159.36	55.84	52.38	15096.0	15657.7
1.22	12D	3373.89	182.61	161.05	158.64	59.31	53.49	15126.7	15466.8
1.22	8E	3412.49	183.88	160.69	159.26	55.72	52.55	15109.0	15375.1
	AVE	3370.59	181.74	160.48	158.92	60.77	56.52	15155.1	15463.7
1.52	10M	4118.32	193.69	169.63	167.84	63.31	59.01	14748.7	14967.6
1.52	11G	4162.77	189.04	170.65	166.81	84.10	69.84	14817.4	15514.1
1.52	7G	3940.17	195.58	169.24	166.55	55.21	50.23	14720.4	15159.4
1.52	9I	3920.06	194.95	169.35	166.14	56.07	50.57	14736.0	15190.1
	AVE	4037.83	193.31	169.65	166.84	64.67	57.41	14755.6	15207.6

* ROD-CENTERED SUBCHANNEL ENERGY BALANCE
+ COBRA-IV-I ANALYSIS

TABLE A-9a (cont)

CALCULATED RESULTS AT VARIOUS THERMOCOUPLE
LOCATIONS FOR EIGHT STEAM COOLING TESTS

RUN 36362

MASS FLOW = .18KG/SEC

INLET VAPOR TEMP = 137.8 DEG C

TOTAL POWER = 26.43 KW

Z (M)	ROD LOCATION	HEAT FLUX (WATT/SQM)	WALL SURFACE TEMP DEG C	VAPOR TEMP ROD*	(DEG C) COBRA+	NU /PR** .33 ROD* COBRA+	REYNOLDS NO. ROD* COBRA+
.30	6J	689.14	148.01	140.68	140.28	38.09 36.13	9925.5 10312.9
.30	9G	659.61	145.70	140.59	140.27	52.43 49.34	9956.9 10229.5
.30	11E	687.85	148.08	140.61	140.33	37.37 35.99	9925.6 10191.3
	AVE	678.87	147.26	140.63	140.29	42.63 40.49	9936.0 10144.6
.61	8N	1131.27	154.65	143.81	143.28	41.81 39.85	9798.9 9939.1
.61	8K	1070.63	152.95	143.69	143.17	46.38 43.96	9822.5 9868.5
	AVE	1100.95	153.80	143.75	143.22	44.09 41.90	9810.7 9903.8
.99	6J	1825.65	166.78	151.27	149.67	46.07 41.81	9550.7 9585.7
.99	9G	1798.80	166.23	150.84	149.59	45.81 42.39	9562.9 9755.2
.99	11G	1772.74	163.17	150.91	149.29	56.84 50.28	9600.3 9910.2
	AVE	1759.06	165.39	151.01	149.51	49.57 44.83	9571.3 9717.0
1.22	2H	2123.90	176.60	156.64	155.09	40.86 37.97	9363.4 9761.4
1.22	5J	2148.25	174.45	156.94	154.78	47.23 42.13	9385.9 9336.5
1.22	8H	1896.76	174.78	155.15	154.71	37.25 36.43	9403.8 9504.7
1.22	8K	2059.14	174.75	156.71	155.17	43.92 40.52	9385.1 9592.6
1.22	8N	2123.74	177.62	157.13	155.50	39.33 36.52	9342.6 9732.2
1.22	12D	2077.96	177.21	157.25	154.79	39.90 35.62	9348.5 9590.8
1.22	8E	2101.73	177.21	156.88	155.40	39.66 37.01	9353.0 9559.0
	AVE	2075.93	176.12	156.57	155.06	41.16 38.03	9368.9 9596.7
1.52	10M	2536.44	186.35	165.87	164.03	46.44 42.67	9136.1 9294.6
1.52	11G	2563.82	182.26	166.90	162.96	62.84 50.21	9172.2 9538.4
1.52	6J	2660.91	186.38	167.70	163.94	53.69 44.86	9114.2 9332.4
1.52	9I	2420.50	167.06	165.29	162.30	41.68 36.77	9134.7 9439.9
	AVE	2550.42	185.51	166.44	163.31	51.16 43.63	9139.3 9426.1

* ROD-CENTERED SUBCHANNEL ENERGY BALANCE
+ COBRA-IV-I ANALYSIS

A-13

TABLE A-9a (cont)

CALCULATED RESULTS AT VARIOUS THERMOCOUPLE LOCATIONS FOR EIGHT STEAM COOLING TESTS

RUN 36463

MASS FLOW = .11KG/SEC

INLET VAPOR TEMP = 133.9 DEG C

TOTAL POWER = 15.89 KW

Z (M)	ROD LOCATION	HEAT FLUX (WATT/SQM)	WALL SURFACE TEMP (DEG C)	VAPOR TEMP (DEG C)	ROD*	COBRA*	NU /PR**	ROD*	COBRA*	REYNOLDS NO.	ROD*	COBRA*
.30	6J	414.34	143.04	136.75	136.35		26.99	25.40		6100.8		6166.1
.30	9G	396.58	141.42	136.66	136.34		34.19	32.05		6114.4		6298.9
.30	11E	413.56	143.81	136.68	136.40		23.76	22.85		6095.1		6276.5
	AVE	408.16	142.75	136.59	136.36		28.31	26.77		6103.4		6247.2
.61	8N	660.15	148.01	139.83	139.29		33.74	31.65		6036.5		6146.1
.61	8K	643.70	146.79	139.70	139.19		36.42	34.42		6047.2		6095.1
	AVE	661.93	147.40	139.77	139.24		35.33	33.04		6041.8		6120.6
.99	6J	1097.64	159.84	147.18	145.58		34.39	30.57		5886.5		5923.4
.99	9G	1081.50	160.16	146.76	145.49		32.02	29.27		5887.2		6027.9
.99	11G	1065.83	158.32	146.83	145.20		36.84	32.32		5900.9		6051.3
	AVE	1081.66	159.44	146.92	145.42		34.42	30.72		5891.5		6000.9
1.22	2H	1276.96	168.68	152.47	150.91		30.70	28.04		5778.6		6050.7
1.22	5J	1291.60	167.41	152.77	150.61		34.43	30.07		5785.8		5766.3
1.22	8H	1140.40	168.08	151.00	150.52		26.09	25.37		5794.2		5943.4
1.22	8K	1238.02	166.87	152.54	150.97		33.74	30.45		5791.7		5945.3
1.22	8N	1276.87	169.31	152.95	151.31		30.38	27.64		5770.2		6037.8
1.22	12D	1249.34	169.33	153.07	150.62		29.90	26.04		5769.2		5938.6
1.22	8E	1263.63	169.31	152.71	151.20		29.63	27.19		5772.0		5924.6
	AVE	1248.12	168.43	152.50	150.88		30.69	27.83		5780.2		5943.8
1.52	10M	1525.00	178.47	161.57	159.71		34.37	31.01		5638.3		5751.2
1.52	11G	1541.46	175.41	162.59	158.62		45.89	35.19		5653.2		5960.9
1.52	6J	1611.85	177.24	163.88	159.60		44.24	34.92		5634.0		5783.2
1.52	7G	1459.03	178.47	161.19	158.39		32.16	27.76		5641.1		5836.3
1.52	9I	1455.29	178.42	160.99	157.99		31.82	27.23		5642.8		5843.5
	AVE	1518.52	177.60	161.94	158.86		37.70	31.22		5641.9		5835.0

* ROD-CENTERED SUBCHANNEL ENERGY BALANCE

+ COBRA-IV-I ANALYSIS

A-14

TABLE A-9a (cont)

CALCULATED RESULTS AT VARIOUS THERMOCOUPLE
LOCATIONS FOR EIGHT STEAM COOLING TESTS

RUN 36564

MASS FLOW = .08KG/SEC

INLET VAPOR TEMP = 132.8 DEG C

TOTAL POWER = 12.58 KW

Z (M)	ROD LOCATION	HEAT FLUX (WATT/SQM)	WALL SURFACE TEMP DEG C	VAPOR TEMP ROD*	(DEG C) COBRA+	NU /PR** ROD* COBRA+	REYNOLDS NO. ROD* COBRA+
.30	6J	328.04	141.42	135.70	135.30	23.55 22.03	4736.4 4829.3
.30	9G	313.98	140.26	135.61	135.29	27.78 26.01	4744.3 4945.9
.30	11E	327.42	142.04	135.53	135.35	21.00 20.11	4733.1 4939.4
	AVE	323.15	141.24	135.64	135.31	24.11 22.71	4737.9 4904.9
.61	8N	538.49	146.19	138.85	138.28	29.89 27.73	4687.4 4846.3
.61	8K	509.63	145.04	138.72	138.22	32.89 30.47	4695.3 4770.5
	AVE	524.06	145.61	138.79	138.25	31.39 29.10	4691.4 4908.4
.99	6J	849.03	157.73	146.36	144.63	30.44 26.46	4571.7 4682.0
.99	9G	856.25	158.35	145.93	144.52	27.43 24.65	4570.5 4902.2
.99	11G	843.84	156.85	146.00	144.24	31.00 26.71	4579.1 4927.2
	AVE	856.37	157.64	146.10	144.46	29.62 25.94	4573.7 4770.5
1.22	2H	1011.00	166.29	151.77	150.00	27.24 24.32	4488.7 4729.7
1.22	5J	1022.59	165.66	152.08	149.90	29.47 25.45	4490.6 4452.1
1.22	8H	902.88	166.25	150.27	149.71	22.15 21.40	4497.8 4526.6
1.22	8K	980.17	164.56	151.84	150.17	30.22 26.75	4498.5 4534.0
1.22	8N	1010.93	167.01	152.27	150.41	26.80 23.84	4481.7 4719.4
1.22	12D	969.13	166.92	152.38	149.72	26.58 22.53	4481.5 4636.2
1.22	8E	1000.45	167.01	152.02	150.39	26.08 23.56	4483.1 4518.4
	AVE	988.16	166.24	151.80	150.04	26.93 23.98	4488.8 4630.9
1.52	10M	1207.38	176.37	161.08	159.07	30.16 26.71	4376.7 4510.4
1.52	11G	1220.41	174.82	162.12	157.97	36.74 27.81	4379.7 4652.8
1.52	6J	1276.14	175.43	162.93	159.01	33.96 29.79	4371.7 4508.8
1.52	7G	1155.15	176.70	160.59	157.79	27.56 23.41	4377.1 4521.7
1.52	9I	1152.18	175.94	160.49	157.41	28.51 23.65	4382.6 4531.9
	AVE	1202.25	175.65	161.46	158.25	32.39 26.31	4377.6 4545.1

A-15

* ROD-CENTERED SUBCHANNEL ENERGY BALANCE
+ COBRA-IV-I ANALYSIS

TABLE A-9a (cont)

CALCULATED RESULTS AT VARIOUS THERMOCOUPLE LOCATIONS FOR EIGHT STEAM COOLING TESTS

RUN 36766

MASS FLOW = .05KG/SEC

INLET VAPOR TEMP = 130.6 DEG C

TOTAL POWER = 8.03 KW

Z (M)	ROD LOCATION	HEAT FLUX (WATT/SQM)	WALL SURFACE TEMP DEG C	VAPOR TEMP (DEG C)		NU / PR**		REYNOLDS NO.†	
				ROD*	COBRA+	ROD*	COBRA+	ROD*	COBRA+
.30	6J	209.48	138.86	133.47	132.82	16.07	14.35	3042.3	3144.5
.30	9G	200.51	138.49	133.39	132.70	16.23	14.33	3044.2	3270.1
.30	11E	209.09	139.06	133.40	132.77	15.28	13.74	3041.8	3265.5
	AVE	206.36	138.80	133.41	132.76	15.86	14.14	3042.8	3226.7
.61	8N	343.88	142.64	136.51	135.58	23.39	19.98	3014.8	3137.7
.61	8K	325.45	142.05	136.48	135.55	23.98	20.55	3017.7	3091.4
.61	8E	353.10	143.26	136.54	135.59	21.54	18.89	3012.7	3086.0
	AVE	340.81	142.65	136.54	135.57	22.97	19.81	3015.0	3105.0
.99	6J	554.96	153.47	144.11	142.14	23.79	19.70	2943.1	2991.1
.99	9G	546.79	154.08	143.69	141.90	21.09	18.04	2942.4	3054.5
.99	11G	538.87	153.35	143.75	141.66	22.53	18.55	2945.0	3062.1
	AVE	546.87	153.63	143.84	141.90	22.47	18.76	2943.5	3035.9
1.22	2H	645.61	160.74	149.51	147.39	22.71	19.14	2894.6	3085.7
1.22	5J	653.02	161.40	149.81	147.34	22.23	18.36	2890.9	2991.5
1.22	8H	576.57	161.19	148.01	147.00	17.30	16.08	2898.6	3020.2
1.22	8K	625.93	159.57	149.59	147.49	24.77	20.52	2898.8	3023.5
1.22	8N	645.57	161.53	150.00	147.78	22.08	18.55	2889.8	3073.2
1.22	12D	631.65	161.73	150.12	147.22	21.44	17.21	2888.5	3016.6
1.22	8E	638.88	162.63	149.75	147.67	19.55	16.86	2886.5	3011.1
	AVE	631.03	161.26	149.54	147.41	21.44	18.10	2892.5	3019.3
1.52	10M	771.02	171.44	158.80	156.48	23.51	19.91	2820.0	2927.2
1.52	11G	770.34	170.70	159.84	155.26	27.64	19.54	2818.9	3019.3
1.52	6J	814.93	170.77	160.64	156.33	30.98	21.83	2815.7	2925.9
1.52	9I	735.78	170.68	158.21	154.73	22.79	17.80	2825.0	2942.8
	AVE	775.27	170.90	159.37	155.70	26.23	19.79	2819.9	2954.1

* ROD-CENTERED SUBCHANNEL ENERGY BALANCE
 † COBRA-IV-I ANALYSIS

A-16

TABLE A-9a (cont)

CALCULATED RESULTS AT VARIOUS THERMOCOUPLE LOCATIONS FOR EIGHT STEAM COOLING TESTS

RUN 36867

MASS FLOW = .05KG/SEC

INLET VAPOR TEMP = 130.6 DEG C

TOTAL POWER = 6.170 KW

Z (M)	ROD LOCATION	HEAT FLUX (WATT/SQM)	WALL SURFACE TEMP DEG C	VAPOR TEMP (DEG C)		NU /PR**		REYNOLDS NO.	
				PDD*	COBRA+	ROD*	COBRA+	ROD*	COBRA+
.30	6J	174.81	137.52	133.05	132.27	16.18	13.80	2973.1	3135.7
.30	9G	167.32	137.25	132.97	132.19	16.20	13.72	2974.5	3250.0
.30	11E	174.48	137.92	132.99	132.25	14.66	12.75	2971.8	3251.8
	AVE	172.20	137.56	133.00	132.24	15.68	13.42	2973.1	3212.5
.61	8N	286.96	141.43	135.74	134.69	20.74	17.54	2947.5	3110.4
.61	8K	271.58	140.85	135.53	134.65	21.37	18.02	2950.2	3045.3
.61	8E	294.66	141.41	135.67	134.69	21.11	18.04	2947.8	3044.1
	AVE	284.40	141.23	135.68	134.68	21.07	17.87	2948.5	3065.6
.99	6J	463.10	150.20	142.14	140.15	23.21	18.64	2889.4	2979.6
.99	9G	456.29	150.43	141.77	139.98	21.28	17.65	2889.9	3064.4
.99	11G	449.68	149.80	141.93	139.83	22.79	18.26	2892.0	3078.1
	AVE	456.36	150.14	141.91	139.99	22.43	18.18	2890.4	3040.7
1.22	2H	538.76	156.45	146.75	144.69	22.12	18.28	2848.4	3038.8
1.22	5J	544.93	156.67	147.01	144.64	22.45	18.07	2846.6	2344.9
1.22	8H	481.14	156.58	145.47	144.37	17.28	15.74	2852.8	2966.9
1.22	8K	522.33	155.32	146.81	144.79	24.44	19.83	2852.5	2971.4
1.22	8N	538.72	157.19	147.17	144.99	21.39	17.61	2844.1	3033.4
1.22	12D	527.10	157.27	147.27	144.49	20.96	16.45	2843.4	2972.8
1.22	8E	533.13	157.75	146.96	144.93	19.66	16.58	2842.8	2962.1
	AVE	526.59	156.75	146.78	144.70	21.19	17.51	2847.2	2970.0
1.52	10M	643.40	165.55	154.67	152.46	23.10	19.23	2785.7	2996.4
1.52	11G	650.35	163.24	155.56	151.48	33.10	21.72	2790.9	2992.3
1.52	6J	680.05	163.90	156.74	152.29	34.67	22.97	2785.9	2998.6
1.52	9I	613.99	164.45	154.17	151.01	23.36	17.93	2791.5	2909.1
	AVE	646.95	164.28	155.16	151.81	28.56	20.46	2788.5	2924.1

* PDD-CENTERED SUBCHANNEL ENERGY BALANCE
+ COBRA-IV-I ANALYSIS

A-17

TABLE A-9b

CALCULATED RESULTS AT VARIOUS THERMOCOUPLE
LOCATIONS FOR EIGHT STEAM COOLING TESTS

RUN 32753

MASS FLOW = .80LBM/SEC

INLET VAPOR TEMP = 269.0 DEG F

TOTAL POWER = 55.22 BTU/SEC

Z (IN)	ROD LOCATION	HEAT FLUX (BTU/HR-SQFT)	WALL SURFACE TEMP DEG F	VAPOR TEMP ROD*	(DEG F) COBRA+	NU /PR** .33 ROD* COBRA+	REYNOLDS NO.1 ROD* COBRA+		
12	6J	458.65	296.11	274.44	273.69	47.17	47.53	20041.8	20266.5
12	9G	429.00	296.14	274.27	273.68	46.62	45.39	20043.7	20565.7
	AVE	448.83	296.13	274.85	273.69	47.89	46.46	20042.8	20466.1
24	8N	754.60	310.74	280.84	279.35	56.88	55.08	19743.6	20110.9
24	12F	676.82	304.76	279.90	279.07	62.65	60.61	19836.3	19579.9
	AVE	715.71	307.75	280.12	279.21	59.76	57.84	19790.0	19895.4
39	6J	1215.05	335.71	294.32	291.09	65.52	60.89	19191.3	19524.6
39	9G	1197.18	340.49	293.52	291.07	56.73	53.98	19135.9	19976.8
39	5E	1165.89	336.99	293.22	290.40	60.47	56.88	19188.7	20064.5
	AVE	1199.37	337.73	293.69	290.85	60.91	57.25	19172.0	19828.6
48	2H	1416.72	355.06	304.49	301.40	61.27	57.84	18784.9	19467.7
48	5J	1429.75	354.37	304.98	300.81	63.32	58.53	18787.5	19523.0
48	8H	1262.38	355.77	301.61	300.84	51.05	50.33	18814.3	19095.8
48	8K	1370.44	349.60	304.64	301.78	66.76	62.99	18858.4	19166.7
48	8N	1416.62	354.02	305.41	302.16	63.75	59.85	18786.4	19454.9
48	12D	1377.80	343.03	305.41	300.71	80.72	71.94	18936.5	19348.8
	AVE	1378.95	351.97	304.41	301.28	64.48	60.25	18828.0	19176.1
60	4J	1733.41	374.18	322.75	317.51	71.84	65.39	18286.3	18834.9
60	11G	1706.33	376.80	323.77	318.53	68.33	62.44	18239.5	19099.8
60	6J	1784.26	376.51	325.22	317.93	73.88	64.97	18223.5	18570.1
60	10H	1661.51	376.24	321.90	317.65	65.88	61.25	18270.4	18700.2
60	7G	1615.09	376.05	321.04	315.68	62.55	57.18	18284.1	18764.5
60	9I	1610.95	375.93	320.57	317.45	62.14	58.81	18290.5	18704.6
60	11I	1747.90	372.81	324.61	317.35	77.25	67.44	18279.8	18976.5
60	11E	1651.05	378.89	323.91	318.72	65.28	59.82	18209.5	19079.1
60	10G	1628.24	379.35	321.47	317.85	59.78	56.37	18235.4	19542.7
60	7J	1650.47	371.07	321.86	318.06	70.98	66.68	18345.3	19753.4
	AVE	1664.92	375.78	322.67	317.67	67.79	62.04	18266.4	18762.6

* ROD-CENTERED SUBCHANNEL ENERGY BALANCE
+ COBRA-IV-I ANALYSIS

A-18

TABLE A-9b (cont)

CALCULATED RESULTS AT VARIOUS THERMOCOUPLE LOCATIONS FOR EIGHT STEAM COOLING TESTS

RUN 36160

MASS FLOW = .81LBM/SEC

INLET VAPOR TEMP = 292.0 DEG F

TOTAL POWER = 50.13 BTU/SEC

Z (IN)	ROD LOCATION	HEAT FLUX (BTU/HR-SQFT)	WALL SURFACE TEMP DEG F	VAPOR TEMP DEG F	(DEG F) COBRA+	NU /PR** .33 ROU* COBRA+	REYNOLDS NO. ROD* COBRA+
12	9G	418.43	309.26	297.04	295.47	77.67 74.18	19769.8 20237.0
12	11E	436.34	314.75	297.08	296.58	55.79 54.23	19690.2 20136.4
	AVE	427.39	312.01	297.06	296.52	66.73 64.21	19730.0 20186.7
24	8N	717.63	325.66	302.82	301.89	70.20 67.45	19453.0 19629.0
24	8K	679.16	321.40	302.59	301.69	80.91 77.25	19516.8 19520.7
	AVE	698.39	323.53	302.70	301.79	75.55 72.35	19484.9 19574.8
39	9G	1141.08	350.63	315.42	313.24	70.15 66.15	18927.8 19204.3
39	11G	1124.55	344.23	315.54	312.71	85.70 78.13	19016.6 19329.7
	AVE	1132.81	347.53	315.48	312.98	77.93 72.14	18972.2 19267.0
48	2H	1347.31	367.23	325.79	323.12	69.47 65.35	18566.7 19239.3
48	5J	1362.76	360.48	326.33	322.54	85.65 77.24	18649.6 18499.5
48	8H	1203.22	365.11	323.12	322.45	61.44 60.47	18630.6 19911.2
48	8K	1306.23	362.88	325.92	323.29	75.74 70.80	18623.2 18917.6
48	8N	1347.21	370.66	326.57	323.86	65.24 61.40	18509.5 19163.5
48	12D	1318.17	371.77	326.89	322.58	62.49 57.17	18492.1 18981.0
48	8E	1333.25	372.61	326.23	323.69	60.91 57.83	18487.0 18777.8
	AVE	1316.88	367.28	325.85	323.07	68.71 64.32	18565.5 18912.5
60	10M	1609.01	390.18	342.31	339.11	67.87 65.60	18052.1 19300.3
60	7G	1539.41	394.87	341.61	336.82	59.91 55.12	18001.4 18516.2
60	9I	1535.46	392.70	341.26	336.09	61.98 56.49	18033.4 18568.3
	AVE	1561.30	392.58	341.73	337.34	63.92 59.07	18029.0 19461.6

* ROD-CENTERED SUBCHANNEL ENERGY BALANCE
 + COBRA-IV-I ANALYSIS

A-19

TABLE A-9b (cont)

CALCULATED RESULTS AT VARIOUS THERMOCOUPLE LOCATIONS FOR EIGHT STEAM COOLING TESTS

RUN 36261

MASS FLOW = .65LBM/SEC

INLET VAPOR TEMP = 287.0 DEG F

TOTAL POWER = 40.67 BTU/SEC

Z (IN)	ROD LOCATION	HEAT FLUX (BTU/HR-SQFT)	WALL SURFACE TEMP DEG F	VAPOR TEMP (DEG F) ROD*	COBRA+	NU /PR** .33 RJD* COBRA+	REYNOLDS NO. ROD* COBRA+
12	9G	339.46	301.59	292.04	291.47	81.33 76.72	16135.2 16533.6
12	11E	353.99	305.82	292.08	291.58	58.77 56.67	16084.9 16468.3
	AVE	346.72	303.70	292.06	291.52	70.05 66.70	16110.0 16500.9
24	8N	562.18	320.18	297.82	296.88	58.60 56.23	15851.0 16318.7
24	8K	550.98	315.91	297.59	296.69	67.88 64.71	15903.1 15927.1
	AVE	566.58	318.04	297.70	296.78	63.24 60.47	15877.0 15972.9
39	9G	925.71	342.07	310.42	308.22	64.30 60.17	15458.8 15710.1
39	11G	912.30	334.40	310.54	307.69	84.49 75.58	15543.6 15824.8
	AVE	919.01	338.23	310.48	307.96	74.39 67.88	15501.2 15767.5
48	2H	1093.02	359.64	320.80	318.10	60.66 56.79	15150.0 15726.3
48	5J	1105.55	353.04	321.35	317.53	75.52 67.53	15216.2 15106.2
48	8H	976.13	357.41	318.13	317.43	53.76 52.81	15203.6 15461.3
48	8K	1059.69	356.39	320.93	319.26	64.57 60.12	15184.2 15452.9
48	9N	1092.94	363.73	321.58	318.84	55.84 52.38	15096.0 15657.7
48	12D	1069.38	360.70	321.89	317.56	59.31 53.49	15126.7 15466.8
48	8E	1081.61	362.98	321.74	318.67	55.72 52.55	15109.0 15375.1
	AVE	1068.33	359.13	320.86	318.06	60.77 56.52	15155.1 15463.7
60	10M	1305.33	380.64	337.84	334.11	63.31 59.01	14748.7 14967.6
60	11G	1319.42	372.27	339.18	332.25	84.10 69.84	14817.4 15514.1
60	7G	1248.87	384.05	336.64	331.79	55.21 50.23	14720.4 15159.4
60	9I	1245.66	382.90	336.29	331.06	56.07 50.57	14736.0 15190.1
	AVE	1279.82	379.97	337.36	332.30	64.67 57.41	14755.6 15207.6

* RJD-CENTERED SUBCHANNEL ENERGY BALANCE
+ COBRA-IV-I ANALYSIS

TABLE A-9b (cont)

CALCULATED RESULTS AT VARIOUS THERMOCOUPLE LOCATIONS FOR EIGHT STEAM COOLING TESTS

RUN 36362

MASS FLOW = .40LBM/SEC

INLET VAPOR TEMP =280.0 DEG F

TOTAL POWER =25.05 BTU/SEC

Z (IN)	ROD LOCATION	HEAT FLUX (BTU/HR-SQFT)	WALL SURFACE TEMP DEG F	VAPOR TEMP (DEG F) ROD*	COBRA+	NU /PR** .33 ROD* COBRA+	REYNOLDS NO.1 ROD* COBRA+
12	6J	218.43	298.43	285.22	284.50	38.09 36.13	9925.5 10012.9
12	9G	209.07	294.27	285.06	284.48	52.43 49.34	9956.9 10229.5
12	11E	218.02	298.54	285.10	284.59	37.37 35.99	9925.6 10191.3
	AVE	215.17	297.08	285.13	284.53	42.63 40.49	9936.0 10144.6
24	8N	358.56	310.38	290.85	289.90	41.81 39.85	9798.9 9739.1
24	8K	329.34	307.32	290.83	289.71	46.38 43.96	9822.5 9868.5
	AVE	348.95	308.85	290.75	289.80	44.09 41.90	9810.7 9903.8
39	6J	578.65	332.20	304.29	301.40	46.07 41.81	9550.7 9585.7
39	9G	570.14	331.21	303.52	301.26	45.81 42.39	9562.9 9755.2
39	11G	561.88	325.71	303.64	300.72	56.84 50.28	9600.3 9910.2
	AVE	570.23	329.71	303.82	301.13	49.57 44.83	9571.3 9717.0
48	2H	673.18	349.88	313.95	311.17	40.86 37.97	9363.4 9761.4
48	5J	660.90	346.01	314.50	310.61	47.23 42.13	9385.9 9336.5
48	8H	661.19	346.60	311.27	310.47	37.25 36.43	9403.8 9504.7
48	8K	652.66	346.55	314.08	311.31	43.92 40.52	9385.1 9592.6
48	8N	673.14	352.08	314.83	311.91	39.33 36.52	9342.6 9732.2
48	12D	658.62	350.98	315.04	310.63	39.90 35.62	9348.5 9590.8
48	8E	666.16	350.98	314.89	311.72	39.66 37.01	9353.0 9559.0
	AVE	657.98	349.01	314.01	311.12	41.16 38.03	9368.9 9596.7
60	10M	803.94	367.44	330.57	327.25	46.44 42.67	9136.1 9294.6
60	11G	812.62	360.07	332.42	325.32	62.84 50.21	9172.2 9639.6
60	6J	849.73	367.47	333.87	327.08	53.69 44.86	9114.2 9332.4
60	9I	767.19	368.71	329.52	324.14	41.68 36.77	9134.7 9438.9
	AVE	806.37	365.93	331.60	325.95	51.16 43.63	9139.8 9426.1

* ROD-CENTERED SUBCHANNEL ENERGY BALANCE
 + COBRA-IV-I ANALYSIS

A-21

TABLE A-9b (cont)

CALCULATED RESULTS AT VARIOUS THERMOCOUPLE
LOCATIONS FOR EIGHT STEAM COOLING TESTS

RUN 36463

MASS FLOW = .24 LBM/SEC

INLET VAPOR TEMP = 273.0 DEG F

TOTAL POWER = 15.06 BTU/SEC

Z (IN)	ROD LOCATION	HEAT FLUX (BTU/HR-SQFT)	WALL SURFACE TEMP DEG F	VAPOR TEMP (DEG F)		NU / PR**		REYNOLDS NO.†	
				ROD*	COBRA+	ROD*	COBRA+	ROD*	COBRA+
12	6J	131.33	289.46	278.14	277.43	26.99	25.40	6100.8	6166.1
12	9G	125.70	286.55	277.98	277.41	34.19	32.05	6114.4	6298.9
12	11E	121.08	290.85	278.02	277.52	23.76	22.85	6095.1	6276.5
	AVE	129.37	288.96	278.05	277.45	28.31	26.77	6103.4	6247.2
24	8N	215.58	298.43	283.70	282.72	33.74	31.65	6036.5	6146.1
24	8K	204.02	296.23	283.47	282.54	36.92	34.42	6047.2	6095.1
	AVE	209.90	297.33	283.58	282.63	35.33	33.04	6041.8	6120.6
39	6J	347.91	319.71	296.92	294.04	34.39	30.57	5886.5	5923.4
39	9G	342.79	320.29	296.17	293.88	32.02	29.27	5887.2	6027.9
39	11G	337.82	316.98	296.29	293.36	36.84	32.32	5900.9	6051.3
	AVE	342.84	318.99	296.46	293.76	34.42	30.72	5891.5	6000.9
48	2H	404.74	335.63	306.44	303.63	30.70	28.04	5778.6	6050.7
48	5J	409.36	333.34	306.99	303.10	34.43	30.07	5785.9	5766.3
48	8H	361.46	334.55	303.80	302.93	26.09	25.37	5794.2	5943.4
48	8K	392.40	332.37	306.57	303.75	33.74	30.45	5791.7	5945.3
48	8N	404.71	336.77	307.32	304.35	30.38	27.64	5770.2	6037.8
48	12D	395.99	336.80	307.52	303.11	29.90	26.04	5769.2	5938.6
48	8E	400.52	336.77	306.88	304.16	29.63	27.19	5772.0	5924.6
	AVE	395.60	335.17	306.50	303.58	30.69	27.83	5780.2	5943.8
60	10M	483.36	353.24	322.83	319.48	34.37	31.01	5638.3	5751.2
60	11G	488.58	347.74	324.66	317.51	45.89	35.19	5653.2	5960.9
60	6J	510.89	351.03	326.08	319.29	44.24	34.92	5634.0	5783.2
60	7G	462.45	353.25	322.14	317.10	32.16	27.76	5641.1	5936.3
60	9I	461.26	353.16	321.79	316.38	31.82	27.23	5642.8	5943.5
	AVE	461.31	351.68	323.50	317.95	37.70	31.22	5641.9	5935.0

* ROD-CENTERED SUBCHANNEL ENERGY BALANCE

+ COBRA-IV-I ANALYSIS

A-22

TABLE A-9b (cont)

CALCULATED RESULTS AT VARIOUS THERMOCOUPLE
LOCATIONS FOR EIGHT STEAM COOLING TESTS

RUN 36564

MASS FLOW = .18LBM/SEC

INLET VAPOR TEMP = 271.0 DEG F

TOTAL POWER = 11.92 BTU/SEC

Z (IN)	ROD LOCATION	HEAT FLUX (BTU/HR-SQFT)	WALL SURFACE TEMP DEG F	VAPOR TEMP ROD*	(DEG F) COBRA+	NU /PR** .33 ROD* COBRA+	REYNOLDS NO. ROD* COBRA+
12	6J	103.97	286.56	276.25	275.54	23.55 22.03	4736.4 4829.3
12	9G	99.52	284.46	276.09	275.52	27.78 26.01	4744.3 4945.9
12	11E	103.78	287.66	276.13	275.62	21.00 20.11	4733.1 4939.4
	AVE	102.42	286.23	276.16	275.56	24.11 22.71	4737.9 4904.9
24	8N	170.68	295.14	281.93	280.90	29.89 27.73	4687.4 4846.3
24	8K	161.53	293.07	281.70	280.79	32.89 30.47	4695.3 4770.5
	AVE	166.11	294.11	281.81	280.85	31.39 29.10	4691.4 4808.4
39	6J	275.45	315.91	295.45	292.34	30.44 26.46	4571.7 4682.0
39	9G	271.39	317.04	294.68	292.13	27.43 24.65	4570.5 4902.2
39	11G	267.46	314.33	294.80	291.63	31.00 26.71	4579.1 4927.2
	AVE	271.43	315.76	294.98	292.03	29.62 25.94	4573.7 4770.5
48	2H	320.44	331.32	305.19	302.00	27.24 24.32	4488.7 4729.7
48	5J	324.12	330.19	305.74	301.82	29.47 25.45	4490.6 4452.1
48	8H	266.17	331.25	302.48	301.48	22.15 21.40	4497.8 4526.6
48	8K	310.67	328.21	305.32	302.31	30.22 26.75	4498.5 4634.0
48	8N	320.42	332.61	306.08	302.73	26.80 23.84	4481.7 4719.4
48	12D	313.51	332.46	306.29	301.50	26.58 22.53	4481.5 4636.2
48	8E	317.10	332.62	305.63	302.70	26.08 23.56	4483.1 4618.4
	AVE	313.21	331.24	305.25	302.08	26.93 23.98	4488.8 4630.9
60	10M	362.69	349.47	321.95	318.33	30.16 26.71	4376.7 4510.4
60	11G	366.82	346.67	323.82	316.34	36.74 27.81	4379.7 4652.8
60	6J	404.48	347.77	325.27	318.22	33.96 29.79	4371.7 4508.8
60	7G	366.13	350.06	321.94	316.02	27.56 23.41	4377.1 4521.7
60	9I	365.19	348.70	320.88	315.33	23.51 23.85	4382.6 4531.9
	AVE	361.06	348.53	322.63	316.85	32.39 26.31	4377.6 4545.1

* ROD-CENTERED SUBCHANNEL ENERGY BALANCE

+ COBRA-IV-I ANALYSIS

TABLE A-9b (cont)

CALCULATED RESULTS AT VARIOUS THERMOCOUPLE LOCATIONS FOR EIGHT STEAM COOLING TESTS

RUN 36766

MASS FLOW = .12LBM/SEC

INLET VAPOR TEMP = 267.0 DEG F

TOTAL POWER = 7.61 BTU/SEC

Z (IN)	ROD LOCATION	HEAT FLUX (BTU/HR-SQFT)	WALL SURFACE TEMP DEG F	VAPOR TEMP (DEG F) ROD*	(DEG F) COBRA+	NU /PR** .33 ROD* COBRA+	REYNOLDS NO. ROD*	NO. COBRA+	
12	6J	66.40	281.94	272.24	271.08	16.07	14.35	3042.3	3144.5
12	9G	63.55	281.27	272.09	270.85	16.23	14.33	3044.2	3275.1
12	11E	66.27	282.30	272.12	270.98	15.28	13.74	3041.8	3265.5
	AVE	65.41	281.84	272.15	270.97	15.86	14.14	3042.8	3225.7
24	8N	108.99	288.76	277.90	276.04	23.39	19.98	3014.8	3137.7
24	8K	103.15	287.69	277.67	275.99	23.98	20.55	3017.7	3091.4
24	8E	111.92	289.86	277.77	276.06	21.54	18.89	3012.7	3086.0
	AVE	108.02	288.77	277.78	276.03	22.97	19.81	3015.0	3105.0
39	6J	175.90	308.24	291.39	287.85	23.79	19.70	2943.1	2991.1
39	9G	173.31	309.34	290.52	287.42	21.09	18.04	2942.4	3054.5
39	11G	170.80	308.03	290.74	286.99	22.53	18.55	2945.0	3062.1
	AVE	173.34	308.54	290.92	287.42	22.47	18.76	2943.5	3035.9
48	2H	204.63	321.32	301.11	297.29	22.71	19.14	2894.6	3085.7
48	5J	206.98	322.53	301.56	297.20	22.23	18.36	2890.9	2891.5
48	8H	182.75	322.14	298.41	296.60	17.30	16.08	2898.6	3020.2
48	8K	158.39	319.23	301.24	297.47	24.77	20.52	2898.8	3023.5
48	8N	204.62	322.76	302.00	298.00	22.08	18.55	2889.8	3079.2
48	12D	200.21	323.12	302.21	296.99	21.44	17.21	2888.5	3016.6
48	9E	202.50	324.73	301.55	297.80	19.55	16.86	2886.5	3011.1
	AVE	200.01	322.26	301.17	297.34	21.44	18.10	2892.5	3018.3
60	10M	244.38	340.59	317.84	313.67	23.51	19.91	2820.0	2927.2
60	11G	247.02	339.26	319.71	311.46	27.64	19.54	2818.9	3019.3
60	6J	258.30	339.38	321.16	313.39	30.98	21.83	2815.7	2925.9
60	9I	233.21	339.22	316.78	310.51	22.77	17.88	2825.0	2942.8
	AVE	245.73	339.61	318.87	312.26	26.23	19.79	2819.9	2954.1

* ROD-CENTERED SUBCHANNEL ENERGY BALANCE
+ COBRA-IV-I ANALYSIS

A-24

TABLE A-9b (cont)

CALCULATED RESULTS AT VARIOUS THERMOCOUPLE LOCATIONS FOR EIGHT STEAM COOLING TESTS

RUN 36867

MASS FLOW = .11LBM/SEC

INLET VAPOR TEMP = 267.0 DEG F

TOTAL POWER = 6.35 BTU/SEC

Z (IN)	ROD LOCATION	HEAT FLUX (BTU/HR-SQFT)	WALL SURFACE TEMP DEG F	VAPOR TEMP (DEG F) ROD*	COBRA+	NU /PR** .33 ROD* COBRA+	REYNOLDS NO. ROD* COBRA+
12	6J	55.41	279.54	271.48	270.09	16.18 13.80	2973.1 3135.7
12	9G	53.03	279.05	271.84	269.95	16.20 13.72	2974.5 3250.0
12	11E	55.30	280.25	271.3*	270.05	14.66 12.75	2971.8 3251.8
	AVE	54.58	279.61	271.40	270.03	15.68 13.42	2973.1 3212.5
24	8N	50.95	286.57	276.93	274.45	20.74 17.54	2947.5 3110.4
24	8K	66.08	285.54	276.13	274.37	21.37 18.02	2950.2 3045.3
24	8E	93.39	286.54	276.21	274.45	21.11 18.04	2947.8 3044.1
	AVE	90.14	286.21	276.22	274.42	21.07 17.87	2948.5 3066.6
39	6J	146.78	302.35	287.85	284.27	23.21 18.64	2889.4 2979.6
39	9G	144.62	302.78	287.19	283.96	21.28 17.65	2889.9 3064.4
39	11G	142.53	301.65	287.80	283.70	22.79 18.26	2892.0 3079.1
	AVE	144.65	302.26	287.45	283.97	22.43 18.18	2890.4 3060.7
48	2H	170.76	313.62	296.15	292.44	22.12 18.28	2848.4 3038.8
48	5J	172.72	314.01	296.62	292.35	22.45 18.07	2846.6 2944.9
48	8H	152.50	313.84	293.84	291.87	17.28 15.74	2852.8 2966.9
48	8K	165.56	311.57	296.25	292.62	24.49 19.83	2852.5 2971.4
48	8N	170.75	314.95	296.90	292.98	21.39 17.61	2844.1 3033.4
48	12D	167.07	315.09	297.08	292.09	20.96 16.45	2843.4 2972.8
48	8E	168.98	315.94	296.52	292.88	19.66 16.58	2842.8 2962.1
	AVE	166.91	314.15	296.20	292.46	21.19 17.51	2847.2 2970.0
60	10M	203.93	329.98	310.41	306.43	23.10 19.23	2785.7 2896.4
60	11G	206.13	325.83	312.00	304.67	33.10 21.72	2790.9 2992.3
60	6J	215.55	327.02	313.24	306.13	34.67 22.97	2785.9 2999.6
60	9I	194.61	328.00	309.51	303.82	23.36 17.93	2791.5 2909.1
	AVE	205.06	327.71	311.29	305.26	28.56 20.46	2788.5 2924.1

* ROD-CENTERED SUBCHANNEL ENERGY BALANCE

+ COBRA-IV-I ANALYSIS

A-25

APPENDIX B

ERROR ANALYSIS OF CALCULATED HEAT TRANSFER RESULTS FOR EIGHT STEAM COOLING TESTS

In this appendix, a simple error analysis is performed for the calculated Nusselt and Reynolds numbers (based on COBRA-IV-I calculated vapor temperatures), using specified instrumentation errors. It will be recalled that the Nusselt and Reynolds numbers were calculated using the following:

- Wall surface temperatures calculated from measured cladding inner surface temperatures by an inverse conduction method
- Rod heat flux calculated from measured power and individual rod resistances
- Subchannel vapor temperatures calculated by the COBRA-IV-I code

The following assumptions are made when performing the error analysis:

- Error in wall surface temperature is equal to error in the measured cladding inner surface temperature; that is, errors due to inverse conduction calculations are neglected.
- Error in rod heat flux is equal to error in the measured power; errors due to individual rod resistances and axial power steps are neglected.
- Error in vapor temperature calculated by the COBRA-IV-I code is due to the input rod power, mass flow, and inlet vapor temperature; errors due to calculations and assumptions made in the COBRA-IV-I code are neglected.
- Error due to evaluation of vapor physical properties is neglected.
- Error due to rod bundle physical dimensions is neglected.

With the above assumptions, the relative errors⁽¹⁾ of the calculated Nusselt and Reynolds numbers can be obtained from equations (3-1), (3-2), and (3-3):

$$\frac{\Delta Re}{Re} = \frac{\Delta \dot{M}_V}{\dot{M}_V} \quad (B-1)$$

$$\frac{\Delta Nu}{Nu} = \frac{\Delta P}{P} + \frac{\Delta(T_W - T_V)}{(T_W - T_V)} \quad (B-2)$$

where

Re = Reynolds number

Nu = Nusselt number

\dot{M}_V = Bundle stream flow rate (kg/sec)

P = Bundle power (kw)

T_W = Wall surface temperature (°C)

T_V = Vapor temperature (°C)

The error in the wall and vapor temperature difference is expressed as

$$\Delta (T_W - T_V) = \sqrt{(\Delta T_W)^2 + (\Delta T_V)^2} \quad (B-3)$$

1. Young, H. D., *Statistical Treatment of Experimental Data*, McGraw-Hill, New York, 1962.

The error in vapor temperature is due to the error in the measured inlet vapor temperature and the calculated vapor temperature rise:

$$(\Delta T_v)^2 = [\Delta T_o]^2 + [\Delta (T_v - T_o)]^2 \quad (B-4)$$

where

$$T_o = \text{inlet vapor temperature (}^\circ\text{C)}$$

The error due to the calculated vapor temperature rise can be estimated from an energy balance equation as in equation (3-11):

$$[\Delta (T_v - T_o)]^2 = (T_v - T_o)^2 \left[\left(\frac{\Delta P}{P} \right)^2 + \left(\frac{\Delta \dot{M}_v}{\dot{M}_v} \right)^2 \right] \quad (B-5)$$

Substituting equations (B-3), (B-4), and (B-5) into equation (B-2) produces

$$\frac{\Delta Nu}{Nu} = \frac{\Delta P}{P} + (T_w - T_v)^{-1} \sqrt{(\Delta T_w)^2 + (\Delta T_o)^2 + (T_v - T_o)^2 \left[\left(\frac{\Delta P}{P} \right)^2 + \left(\frac{\Delta \dot{M}_v}{\dot{M}_v} \right)^2 \right]} \quad (B-6)$$

The manufacturer's specified instrumentation errors are as follows:

$$\Delta T_w = \pm 1.39^\circ\text{C}$$

$$\Delta T_o = \pm 1.34^\circ\text{C}$$

$$\Delta \dot{M}_v = \pm 0.0009 \text{ kg/sec}$$

$$\Delta P = \pm (0.001 P + 0.03 \text{ kw})$$

The calculated errors for the eight steam cooling tests are shown in table B-1. It should be noted that, because of the small wall-to-vapor temperature difference, the relative errors in the Nusselt numbers calculated by equation (B-6) are quite large, especially for lower elevations [below 0.61 m (24 in.)].

The large errors (more than 20 percent) reported in table B-1 are mostly from lower elevations [less than 0.61 m (24 in.)] and account for about 19.4 percent of the total data; 81.6 percent of the total data has a calculated error of less than 20 percent and are mostly obtained from elevations greater than 0.61 m (24 in.).

TABLE B-1

ESTIMATED ERRORS FOR CALCULATED NUSSELT AND
REYNOLDS NUMBERS FOR EIGHT STEAM COOLING TESTS

DIN 32753

MASS FLOW = .3429 KG/SEC (6.800 LPM/SEC)

TOTAL POWER = 58.26 KW (55.22 BTU/SEC)

ERROR IN MASS FLOW = .25 PERCENT

ERROR IN TOTAL POWER = .151 PERCENT

Z M (IN)	RND LOCATION	NU NO. / (PR NO.)**0.33	ERROR IN NU NO. (PERCENT)
.30 (12)	6J	47.53	15.71
.30 (12)	9G	45.39	15.67
	AVE	46.46	15.69
.61 (24)	8N	55.08	11.26
.61 (24)	12F	60.61	13.72
	AVE	57.84	12.49
.99 (39)	6J	60.89	7.97
.99 (39)	9G	53.98	7.21
.99 (39)	5E	56.88	7.64
	AVE	57.25	7.60
1.22 (48)	2H	57.84	6.65
1.22 (48)	5J	58.53	6.66
1.22 (48)	8H	50.33	6.50
1.22 (48)	8K	62.99	7.45
1.22 (48)	8N	59.85	6.88
1.22 (48)	12D	71.04	8.39
	AVE	60.25	7.69
1.52 (60)	4J	65.30	6.31
1.52 (60)	11G	62.44	6.14
1.52 (60)	6J	64.97	6.11
1.52 (60)	10H	61.75	6.11
1.52 (60)	7G	57.18	5.93
1.52 (60)	9I	58.81	6.12
1.52 (60)	11I	67.44	6.44
1.52 (60)	11F	59.82	5.95
1.52 (60)	10G	56.37	5.83
1.52 (60)	7J	66.68	6.73
	AVE	62.64	6.17

TABLE B-1 (cont)

ESTIMATED ERRORS FOR CALCULATED NUSSELT AND REYNOLDS NUMBERS FOR EIGHT STEAM COOLING TESTS

RIIN 36160

MASS FLOW = .3674 KG/SEC (.810 LBM/SEC)

TOTAL POWER = 52.89 KW (50.13 BTU/SEC)

ERROR IN MASS FLOW = .24 PERCENT

ERROR IN TOTAL POWER = .157 PERCENT

Z M (IN)	POD LOCATION	NU NO. / (PR NO.) ** .33	ERROR IN NU NO. (PERCENT)
.30 (12)	QC	74.18	27.42
.30 (12)	11F	54.23	19.74
	AVE	64.21	23.38
.61 (24)	8N	67.45	14.82
.61 (24)	8K	77.25	17.85
	AVE	72.35	16.34
.99 (39)	QC	66.15	9.43
.99 (39)	11C	78.13	11.22
	AVE	72.14	10.33
1.22 (48)	2H	65.35	8.06
1.22 (48)	FJ	77.24	9.35
1.22 (48)	8H	69.47	8.33
1.22 (48)	8K	70.80	8.97
1.22 (48)	8N	61.40	7.61
1.22 (48)	12D	57.17	7.25
1.22 (48)	8E	57.83	7.26
	AVE	64.32	8.12
1.52 (60)	10M	65.60	6.99
1.52 (60)	7C	55.12	6.17
1.52 (60)	9T	66.49	6.32
	AVE	59.07	6.49

TABLE B-1 (cont)

ESTIMATED ERRORS FOR CALCULATED NUSSELT AND REYNOLDS NUMBERS FOR EIGHT STEAM COOLING TESTS

PIIN 34261

MASS FLOW = .2971 KG/SEC (.655 LB/SEC)

TOTAL POWER = 42.91 KW (40.67 BTU/SEC)

ERROR IN MASS FLOW = .30 PERCENT

ERROR IN TOTAL POWER = .170 PERCENT

M	Z (IN)	PRO LOCATION	NU NO. / (PR NO.)** .33	ERROR IN NU NO. (PERCENT)
.30	(12)	9G	76.72	34.63
.30	(12)	11F	56.67	24.65
		AVE	66.70	29.64
.61	(24)	8N	56.23	15.14
.61	(24)	8K	64.71	18.31
		AVE	60.47	16.72
.99	(39)	9C	69.17	10.47
.99	(39)	11C	75.58	13.23
		AVE	67.88	11.85
1.22	(48)	2H	56.79	8.57
1.22	(48)	5J	67.53	9.99
1.22	(48)	8H	52.81	8.89
1.22	(48)	8K	60.12	9.32
1.22	(48)	8N	52.38	7.94
1.22	(48)	12D	53.49	8.26
1.22	(48)	8E	52.55	8.04
		AVE	56.52	8.72
1.52	(60)	10M	59.11	7.67
1.52	(60)	11C	69.84	8.89
1.52	(60)	7G	50.23	6.85
1.52	(60)	9T	53.57	6.90
		AVE	57.41	7.58

TABLE B-1 (cont)

ESTIMATED ERRORS FOR CALCULATED NUSSLELT AND REYNOLDS NUMBERS FOR EIGHT STEAM COOLING TESTS

PIIN 36362

MASS FLOW = .1814 KG/SEC (.400 LBM/SEC)

TOTAL POWER = 26.43 KW (25.05 BTU/SEC)

ERROR IN MASS FLOW = .50 PERCENT

ERROR IN TOTAL POWER = .214 PERCENT

Z M (IN)	ROD LOCATION	NU NO. / (PR NO.)**0.33	ERROR IN NU NO. (PERCENT)
.30 (12)	6J	26.13	25.26
.30 (12)	9C	49.74	35.85
.30 (12)	11F	35.69	25.22
	AVE	40.49	28.77
.61 (24)	8N	39.85	17.24
.61 (24)	8K	43.96	20.01
	AVE	41.90	18.63
.99 (39)	6J	41.81	11.54
.99 (39)	9C	42.39	11.86
.99 (39)	11G	50.78	14.17
	AVE	44.83	12.53
1.22 (48)	2H	37.07	9.23
1.22 (48)	5J	42.13	10.67
1.22 (48)	PH	36.43	9.87
1.22 (48)	8K	40.52	10.12
1.22 (48)	8N	36.52	8.90
1.22 (48)	12D	35.62	8.86
1.22 (48)	8F	37.01	9.16
	AVE	38.63	9.45
1.52 (60)	10M	42.67	8.91
1.52 (60)	11G	50.71	10.27
1.52 (60)	6J	44.86	8.87
1.52 (60)	9I	36.77	8.66
	AVE	43.63	9.63

B-8

TABLE B-1 (cont)

ESTIMATED ERRORS FOR CALCULATED NUSSELT AND REYNOLDS NUMBERS FOR EIGHT STEAM COOLING TESTS

RUN 36463

MASS FLOW = .1102 KG/SEC (1.243 LPM/SEC)

TOTAL POWER = 15.89 KW (15.06 BTU/SEC)

ERROR IN MASS FLOW = .02 PERCENT

ERROR IN TOTAL POWER = .289 PERCENT

M	Z (IN)	PRO LOCATION	NU NO. / (PR NO.)**0.33	ERROR IN NU NO. (PERCENT)
.30	(12)	6J	25.40	29.27
.30	(12)	9C	32.05	38.41
.30	(12)	11E	22.85	26.44
		AVE	26.77	31.37
.61	(24)	8N	31.65	22.50
.61	(24)	9K	34.42	25.77
		AVE	33.04	24.14
.99	(30)	6J	30.57	13.89
.99	(30)	9C	29.27	13.51
.99	(30)	11C	32.32	15.06
		AVE	30.72	14.16
1.22	(48)	2H	28.04	11.22
1.22	(48)	6J	30.07	11.85
1.22	(48)	8H	25.37	11.35
1.22	(48)	9K	30.45	12.51
1.22	(48)	8N	27.64	11.08
1.22	(48)	12D	26.04	10.67
1.22	(48)	8E	27.10	11.01
		AVE	27.83	11.38
1.52	(60)	10M	31.01	10.68
1.52	(60)	11C	35.19	11.90
1.52	(60)	6J	34.92	11.35
1.52	(60)	7C	27.76	9.99
1.52	(60)	9I	27.23	9.83
		AVE	31.22	10.75

TABLE B-1 (cont)

ESTIMATED ERRORS FOR CALCULATED NUSSLELT AND REYNOLDS NUMBERS FOR EIGHT STEAM COOLING TESTS

RHM 26564

MASS FLOW = .0853 KG/SEC (1.188 LPM/SEC)

TOTAL POWER = 12.58 KW (11.92 BTU/SEC)

ERROR IN MASS FLOW = 1.06 PERCENT

ERROR IN TOTAL POWER = .338 PERCENT

Z R (IN)	RND LOCATION	NU NO. / (PR NO.) ** .33	ERROR IN NU NO. (PERCENT)
.30 (12)	6J	22.03	31.98
.30 (12)	9G	26.61	39.32
.30 (12)	11E	20.11	29.30
	AVE	22.71	33.54
.61 (24)	8N	27.73	24.84
.61 (24)	8K	30.47	28.74
	AVE	29.16	26.79
.99 (39)	6J	26.46	15.17
.99 (39)	9G	24.65	14.37
.99 (39)	11G	26.71	15.73
	AVE	25.04	15.69
1.22 (48)	2H	24.32	12.29
1.22 (48)	5J	25.45	12.69
1.22 (48)	8H	21.40	12.10
1.22 (48)	8K	26.75	13.87
1.22 (48)	8N	23.84	12.07
1.22 (48)	12D	22.53	11.66
1.22 (48)	RE	23.56	12.65
	AVE	23.98	12.39
1.52 (60)	10M	26.71	11.66
1.52 (60)	11G	27.81	11.96
1.52 (60)	6J	29.79	12.27
1.52 (60)	7G	23.41	10.69
1.52 (60)	9I	23.88	10.89
	AVE	26.31	11.49

B-10

TABLE B-1 (cont)

ESTIMATED ERRORS FOR CALCULATED NUSSELT AND REYNOLDS NUMBERS FOR EIGHT STEAM COOLING TESTS

RUN 26766

MASS FLOW = .0544 KG/SEC (.120 LB/SEC)

TOTAL POWER = 8.03 KW (7.61 BTU/SEC)

ERROR IN MASS FLOW = 1.66 PERCENT

ERROR IN TOTAL POWER = .473 PERCENT

Z	FOR LOCATION	NU NO. / (PR NO.)**0.33	ERROR IN NU NO. (PERCENT)
.30 (12)	6J	14.35	32.57
.30 (12)	9G	14.33	33.94
.30 (12)	11E	17.74	31.27
	AVE	14.14	32.59
.61 (24)	8N	19.98	27.92
.61 (24)	8K	20.55	30.29
.61 (24)	8E	18.89	25.77
	AVE	19.81	27.99
.99 (39)	6J	19.70	17.67
.99 (39)	9G	18.04	16.46
.99 (39)	11E	18.55	17.13
	AVE	18.76	17.09
1.22 (48)	2H	19.14	15.15
1.22 (48)	7J	18.34	14.40
1.22 (48)	8H	16.08	14.27
1.22 (48)	8K	20.52	16.68
1.22 (48)	8N	18.55	14.72
1.22 (48)	12D	17.21	13.97
1.22 (48)	8E	16.84	13.57
	AVE	18.10	14.68
1.52 (60)	10M	19.91	13.77
1.52 (60)	11G	19.54	13.32
1.52 (60)	6J	21.83	14.24
1.52 (60)	9I	17.88	12.90
	AVE	19.79	13.56

TABLE B-1 (cont)

ESTIMATED ERRORS FOR CALCULATED NUSSELT AND REYNOLDS NUMBERS FOR EIGHT STEAM COOLING TESTS

RIIN 26867

MASS FLOW = .0531 KG/SEC (.117 LBM/SEC)

TOTAL POWER = 6.70 KW (6.35 BTU/SEC)

ERROR IN MASS FLOW = 1.79 PERCENT

ERROR IN TOTAL POWER = .547 PERCENT

M (TN)	POD LOCATION	NU NO. / (PP NO.)** .33	ERROR IN NU NO. (PERCENT)
.30 (12)	6J	13.80	37.45
.30 (12)	9C	13.72	38.86
.30 (12)	11F	12.75	34.71
	AVE	13.42	37.01
.61 (24)	8N	17.54	29.35
.61 (24)	8K	18.02	31.79
.61 (24)	8F	18.04	29.40
	AVE	17.87	30.18
.99 (30)	6J	18.64	19.90
.99 (30)	9C	17.65	19.14
.99 (30)	11G	18.26	20.64
	AVE	18.18	19.70
1.22 (48)	2M	18.28	17.15
1.22 (48)	5J	18.07	16.78
1.22 (48)	8H	15.74	16.55
1.22 (48)	8K	19.83	19.11
1.22 (48)	8A	17.61	16.57
1.22 (48)	12D	16.45	15.83
1.22 (48)	8E	16.58	15.80
	AVE	17.51	16.83
1.52 (60)	10M	19.23	15.65
1.52 (60)	11G	21.72	17.33
1.52 (60)	6J	22.97	17.57
1.52 (60)	9I	17.93	15.22
	AVE	20.46	16.65

B-12

APPENDIX C

SUMMARY OF DRYOUT TIMES FOR BOILOFF TESTS

This appendix presents the calculated dryout time at various instrumentation locations. The average dryout times listed are the average of the times at the respective elevation.

TABLE C-1
CALCULATED DRYOUT TIMES AT VARIOUS
THERMOCOUPLE LOCATIONS FOR BOILOFF TESTS

Elevation [m (in.)]	Rod	Dryout Time (sec)	Average Dryout Time (sec)
Run 35557 ^(a)			
0.991 (39)	6J	-125.60	-127.93
	9G	-124.60	
	11G	-133.60	
1.22 (48)	5J	-170.60	-168.10
	8H	-170.60	
	8K	-166.60	
1.52 (60)	12D	-164.60	-191.60
	10M	-184.60	
	11G	-196.60	
	6J	-187.60	
	7G	-198.60	
1.70 (67)	9I	-196.60	-202.20
	7J	-185.60	
	9J	-200.60	
	6J	-202.60	
	9G	-202.60	
1.83 (72)	11G	-202.60	-206.76
	10G	-202.60	
	7H	-210.60	
	5I	-207.60	
	7K	-207.60	
	9F	-207.60	
	4L	-206.60	
	12F	-206.60	
	6C	-206.60	
	7J	-207.60	
	6L	-209.60	
	11D	-207.60	
	9K	-192.60	
	12D	-206.60	
	8G	-206.60	
	8E	-207.60	
	8F	-206.60	
9D	-209.60		
8K	-207.60		
9E	-206.60		
7G	-206.60		

a. Beginning of test = -270 sec

TABLE C-1 (cont)
CALCULATED DRYOUT TIMES AT VARIOUS
THERMOCOUPLE LOCATIONS FOR BOILOFF TESTS

Elevation [m (in.)]	Rod	Dryout Time (sec)	Average Dryout Time (sec)		
Run 35557 (cont)					
1.98 (78)	9F	-213.60	-212.52		
	11F	-204.60			
	7F	-214.60			
	8C	-213.60			
	5I	-214.60			
	10D	-213.60			
	7H	-214.60			
	9E	-214.60			
	6L	-212.60			
	8K	-205.60			
	12D	-213.60			
	12F	-214.60			
	2.13 (84)	7H		-217.60	-215.04
		11F		-214.60	
9C		-214.60			
8E		-215.60			
9G		-213.60			
9F		-218.60			
9J		-213.60			
13G		-212.60			
7E		-214.60			
2.29 (90)		9J	-220.60	-218.24	
	8J	-217.60			
	9F	-218.60			
	9G	-217.60			
	7D	-217.60			
	7M	-218.60			
	8D	-217.60			
	8C	-218.60			
	11E	-217.60			
	6D	-218.60			
2.44 (96)	7H	-217.60	-219.16		
	8I	-219.60			
	4L	-216.60			
	9F	-220.60			
	8E	-220.60			
	7M	-218.60			
	7H	-220.60			

TABLE C-1 (cont)
CALCULATED DRYOUT TIMES AT VARIOUS
THERMOCOUPLE LOCATIONS FOR BOILOFF TESTS

Elevation [m (in.)]	Rod	Dryout Time (sec)	Average Dryout Time (sec)
Run 35557 (cont)			
2.59 (102)	11D	-222.60	-214.73
	8K	-217.60	
	7E	-215.60	
	8J	-212.60	
	9L	-215.60	
	8D	-210.60	
	6D	-217.60	
	7E	-214.60	
	5J	-211.60	
	4L	-218.60	
2.82 (111)	8E	-216.60	-222.24
	8G	-219.60	
	11D	-224.60	
	9F	-223.60	
	6J	-223.60	
	7D	-220.60	
	7M	-221.60	
	9C	-221.60	
	11G	-222.60	
	11E	-223.60	
3.05 (120)	8C	-223.60	-223.10
	9G	-219.60	
	6E	-224.60	
	4L	-222.60	
	8J	-222.60	
	8H	-222.60	
	8K	-223.60	
	8D	-222.60	
Run 35658(b)			
0.991 (39)	6J	-142.20	-141.20
	9G	-139.20	
	11G	-142.20	
1.22 (48)	5J	-172.20	-172.70
	8H	-175.20	

b. Beginning of test = -260 sec

TABLE C-1 (cont)
CALCULATED DRYOUT TIMES AT VARIOUS
THERMOCOUPLE LOCATIONS FOR BOILOFF TESTS

Elevation [m (in.)]	Rod	Dryout Time (sec)	Average Dryout Time (sec)
Run 35658 (cont)			
1.52 (60)	8K	-172.20	-202.20
	12D	-171.20	
	10M	-187.20	
	11G	-204.20	
	6J	-206.20	
	7G	-205.20	
	9I	-204.20	
1.70 (67)	7J	-206.20	-206.40
	9J	-206.20	
	6J	-208.20	
	9G	-206.20	
	11G	-205.20	
1.83 (72)	10G	-206.20	-208.88
	7H	-212.20	
	5I	-208.20	
	7K	-211.20	
	9F	-214.20	
	4L	-209.20	
	12F	-208.20	
	6C	-208.20	
	7J	-209.20	
	6L	-210.20	
	11D	-209.20	
	9K	-204.20	
	12D	-208.20	
	8G	-209.20	
	8E	-203.20	
	8F	-208.20	
	9D	-210.20	
	8K	-209.20	
	9E	-207.20	
	1.98 (78)	7G	
9F		-212.20	
11F		-208.20	
7K		-215.20	
8C		-216.20	
5I		-215.20	
10D		-212.20	
7H		-216.20	

TABLE C-1 (cont)
CALCULATED DRYOUT TIMES AT VARIOUS
THERMOCOUPLE LOCATIONS FOR BOILOFF TESTS

Elevation [m (in.)]	Rod	Dryout Time (sec)	Average Dryout Time (sec)
Run 35658 (cont)			
2.13 (84)	9E 6L 8K 12D 12F 7H 11F 9C 8E 9G 9F 9J 13G	-216.20 -208.20 -213.20 -213.20 -214.20 -214.20 -210.20 -208.20 -211.20 -209.20 -210.20 -208.20 -207.20	-209.76
2.29 (90)	7E 9J 8J 9F 9G 7D 7M 8D 8C 11E 6D	-209.20 -214.20 -217.20 -216.20 -215.20 -212.20 -216.20 -215.20 -217.20 -214.20 -216.20	-215.75
2.44 (96)	7H 8I 4L 9F 8E 7M 7H 11D	-219.20 -212.20 -211.20 -220.20 -220.20 -217.20 -221.20 -222.20	-217.42
2.59 (102)	8K 7E 8J 9L 8D 6D 7E	-219.20 -213.20 -221.20 -211.20 -220.20 -218.20 -217.20	-216.45

TABLE C-1 (cont)
CALCULATED DRYOUT TIMES AT VARIOUS
THERMOCOUPLE LOCATIONS FOR BOILOFF TESTS

Elevation [m (in.)]	Rod	Dryout Time (sec)	Average Dryout Time (sec)		
Run 35658 (cont)					
2.82 (111)	5J	-210.20	-219.29		
	4L	-212.20			
	8E	-221.20			
	8G	-224.20			
	11D	-217.20			
	9F	-219.20			
	6J	-212.20			
	7D	-219.20			
	7M	-218.20			
	9C	-219.20			
	11G	-222.20			
	11E	-222.20			
	8C	-219.20			
	9G	-219.20			
3.05 (120)	6E	-218.20	-215.37		
	4L	-210.20			
	8J	-213.20			
	8H	-220.20			
	8K	-213.20			
	8D	-217.20			
	Run 35759(c)				
	0.991 (39)	6J		-135.50	-136.83
9G		-137.50			
1.22 (48)	11G	-137.50	-175.00		
	5J	-176.50			
	8H	-176.50			
1.52 (60)	8K	-172.50	-193.33		
	12D	-174.50			
	10M	-189.50			
	11G	-186.50			
	6J	-186.50			
	7G	-201.50			
	9I	-194.50			
7J	-201.50				

c. Beginning of test = -280 sec

TABLE C-1 (cont)
CALCULATED DRYOUT TIMES AT VARIOUS
THERMOCOUPLE LOCATIONS FOR BOILOFF TESTS

Elevation [m (in.)]	Rod	Dryout Time (sec)	Average Dryout Time (sec)
Run 35759 (cont)			
1.70 (67)	9J	-202.50	-202.90
	6J	-205.50	
	9G	-202.50	
	11G	-201.50	
	10G	-202.50	
1.83 (72)	7H	-209.50	-207.50
	5I	-209.50	
	7K	-209.50	
	9F	-208.50	
	4L	-208.50	
	12F	-206.50	
	6C	-208.50	
	7J	-208.50	
	6L	-209.50	
	11D	-208.50	
	9K	-196.50	
	12D	-208.50	
	8G	-208.50	
	8E	-203.50	
	8F	-208.50	
	9D	-209.50	
	8K	-202.50	
9E	-208.50		
1.98 (78)	7G	-209.50	-213.50
	9F	-213.50	
	11F	-204.50	
	7K	-216.50	
	8C	-216.50	
	5I	-215.50	
	10D	-215.50	
	7H	-216.50	
	9E	-210.50	
	6L	-212.50	
2.13 (84)	8K	-214.50	-216.06
	12D	-216.50	
	12F	-209.50	
	7H	-219.50	
	11F	-216.50	
	9C	-213.50	

TABLE C-1 (cont)
CALCULATED DRYOUT TIMES AT VARIOUS
THERMOCOUPLE LOCATIONS FOR BOILOFF TESTS

Elevation [m (in.)]	Rod	Dryout Time (sec)	Average Dryout Time (sec)		
Run 35759 (cont)					
2.29 (90)	8E	-218.50	-220.05		
	9G	-214.50			
	9F	-217.50			
	9J	-214.50			
	13G	-212.50			
	7E	-217.50			
	9J	-219.50			
	8J	-219.50			
	9F	-220.50			
	9G	-219.50			
	7D	-218.50			
	7M	-215.50			
	8D	-220.50			
	8C	-220.50			
2.44 (96)	11E	-220.50	-222.39		
	6D	-223.50			
	7H	-222.50			
	8I	-219.50			
	4L	-219.50			
	9F	-226.50			
	8E	-224.50			
	7M	-224.50			
	7H	-225.50			
	11D	-224.50			
	8K	-221.50			
	7E	-215.50			
	8J	-209.50			
	9L	-211.50			
2.59 (102)	8D	-212.50	-213.00		
	6D	-215.50			
	7E	-210.50			
	5J	-206.50			
	4L	-220.50			
	8E	-217.50			
	8G	-223.50			
	11D	-222.50			
	9F	-222.50			
	6J	-222.50			
	7D	-220.50			
	2.82 (111)				-221.23

TABLE C-1 (cont)
CALCULATED DRYOUT TIMES AT VARIOUS
THERMOCOUPLE LOCATIONS FOR BOILOFF TESTS

Elevation [m (in.)]	Rod	Dryout Time (sec)	Average Dryout Time (sec)
Run 35759 (cont) 3.05 (120)	7M	-218.50	-223.33
	9C	-221.50	
	11G	-220.50	
	11E	-219.50	
	8C	-220.50	
	9G	-221.50	
	6E	-224.50	
	4L	-222.50	
	8J	-223.50	
	8H	-223.50	
	8K	-222.50	
	8D	-223.50	

**NRC/EPRI/WESTINGHOUSE REPORT NO. 8
EXTERNAL DISTRIBUTION**

Dr. L. S. Tong, Assistant Director
Water Reactor Safety Research
Division of Reactor Safety Research
U.S. Nuclear Regulatory Commission
Washington, DC 20555

Dr. H. Sullivan
Division of Reactor Safety Research
U. S. Nuclear Regulatory Commission
Washington, DC 20555

A. L. M. Hon
Separate Effects Research Branch
U. S. Nuclear Regulatory Commission
Washington, DC 20555

K. V. Morton, Chief
Research Contracts Branch
Division of Contracts
U. S. Nuclear Regulatory Commission
Washington, DC 20555

D. E. Solberg
U. S. Nuclear Regulatory Commission
Washington, DC 20555

Mr. Wayne Hodges
U. S. Nuclear Regulatory Commission
DSS
Washington, DC 20555

Mr. L. Phillips
NRR
U. S. Nuclear Regulatory Commission
Washington, DC 20555

Mr. Harry Balukjan
NRR
U. S. Nuclear Regulatory Commission
Washington, DC 20555

Dr. D. Ross
NRR
U. S. Nuclear Regulatory Commission
Washington, DC 20555

Dr. W. Johnston
Core Performance Branch
U. S. Nuclear Regulatory Commission
Washington, DC 20555

Dr. B. Bingham
Babcock & Wilcox Company
P. O. Box 1206
Lynchburg, VA 24505

Mr. N. H. Shah
Babcock & Wilcox Co. (NPGD)
P.O. Box 1260
Lynchburg, VA 24505

Mr. W. Kayser
Exxon Nuclear
2101 Horn Rapids Road
Richland, WA 99352

Mr. G. E. Wilson (TSB)
EG&G Idaho, Inc.
P. O. Box 1625
Idaho Falls, ID 83401

J. A. Dearien
EG&G Idaho, Inc.
P. O. Box 1625
Idaho Falls, ID 83401

P. North
EG&G Idaho, Inc.
P. O. Box 1625
Idaho Falls, ID 83401

Mr. G. Sozzi
General Electric Co.
175 Curtner Avenue
San Jose, CA 95125

Dr. P. Griffith
Dept. of Mechanical Engineering
MIT
Cambridge, MA 02139

Dr. P. A. Lottes
Argonne National Laboratory
9700 South Cass Avenue
Argonne, IL 60439

Mr. G. Ofey
Sandia National Laboratory
P.O. Box 5800
Albuquerque, NM 87185

Dr. F. Mynatt
Engineering Technology Division
Oak Ridge National Laboratory
Box 7
Oak Ridge, TN 37830

Mr. R. Jensen
Intermountain Technology
Box 1604
Idaho Falls, ID 83401

Mr. F. D. Lang
Energy Incorporated
P. O. Box 763
Idaho Falls, ID 83401

Dr. J. Chen
Lehigh University
Dept. of Mechanical Engineering
Bethlehem, PA 18015

Dr. K. H. Sun (5 copies)
Nuclear Power Division
Electric Power Research Institute
P. O. Box 10412
Palo Alto, CA 94303

Dr. J. J. Cudlin
Power Generation Group
Babcock & Wilcox
P. O. Box 1260
Lynchburg, VA 24505

Mr. J. Longo, Jr.
Combustion Engineering
P. O. Box 500
Windsor, CT 06095

Mr. J. Blaisdell
Combustion Engineering
P.O. Box 500
Windsor, CT 06095

Mr. Ken Moore
Energy, Inc.
P. O. Box 736
Idaho Falls, ID 83401

Dr. K. P. Galbraith
Nuclear Safety Engineering
Exxon Nuclear Company
2101 Horn Rapids Road
Richland, WA 99352

Dr. J. A. Block
Create Inc.
Hanover, NH 03755

Dr. W. Hancox
Whiteshell Nuclear Laboratory
Atomic Energy of Canada
Pinawa, Manitoba
Canada ROE 1LO

Professor T. Theofanous
Department of Nuclear Energy
Purdue University
West Lafayette, IN 47907

Professor I. Catton
Dept. of Chemical, Nuclear, and
Thermal Engineering
University of California
Los Angeles, CA 90024

Dr. Max W. Carbon
Nuclear Engineering Department
The University of Wisconsin
Madison, WI 53706

Professor R. A. Seban
Dept. of Mechanical Engineering
University of California
Berkeley, CA 94720

Professor W. Y. Chon
Dept. of Engineering Science,
Aerospace Engineering, and
Nuclear Engineering
State University of New York
Buffalo, NY 14214

Dr. R. R. Gay
Nuclear Engineering Department
Rensselaer Polytechnic Institute
Troy, NY 12181

Dr. Owen Jones
Brookhaven National Laboratory
Building 820
Upton, NY 11973

Professor E. V. McAssey, Jr.
Dept. of Mechanical Engineering
Villanova University
Villanova, PA 19085

Professor S. C. Yao
Dept. of Mechanical Engineering
Carnegie-Mellon University
Pittsburgh, PA 15213

Dr. S. J. Board
CEGB
Berkeley Nuclear Laboratory
Berkeley
Gloucestershire, England

Prof. T. Wu
California Institute of Technology
Pasadena, CA 91109

Dr. S. Levy
S. Levy, Inc.
1901 S. Bascom Ave. Suite 275
Campbell, CA 95008

Dr. D. A. Prelewicz
NUS Corporation
4 Research Place
Rockville, MD 20850

Professor A. Tapucu
Ecole Polytechnique,
Universite de Montreal
Institut de Genie Nucleaire
Casier Postale 6079
Succursal "A,"
Montreal, Quebec H3C 3A7

for NRC (360 copies)
Distribution Services Branch
Nuclear Regulatory Commission
7920 Norfolk Avenue
Bethesda, MD 20555

Ms. Nora Schofield
EG&G Idaho, Inc.
P. O. Box 1625
Idaho Falls, ID 83401



